AN ABSTRACT OF THE THESIS OF

Tsai-Chen Wang for the degree of Doctor of Philosophy in Chemical Engineering

presented on September 18, 1996

Title : High Temperature Fluidized-Bed Nitridation of 316 Stainless Steel Powder

Abstract approved: Redacted for Privacy

Shoichi Kimura

The nitridation of 316 stainless steel powder, 70 μm of average particle size and 4.5 cm/sec of minimum fluidization velocity, was carried out at temperatures from 450 to 800 °C in two different gas systems: NH_3/ H_2 and N_2/ H_2. The process was operated in a high-temperature fluidized bed system equipped with a 55 mm I.D. quartz reactor tube. The fluidizing-gas velocity in this study was fixed at 8.3 cm/sec, based on the empty bed and operating temperature at all temperatures, however it was raised to 16.6 cm/sec at 800 °C. LECO nitrogen analysis, Kjeldahl chemical nitrogen analysis, X-ray diffraction (XRD), color metallography, optical microscopy, scanning electron microscopy (SEM), and scanning electron microprobe analysis (EMPA) were employed for studying the mechanism of nitrogen-addition process.

In this study, the main focus is the process using NH_3/ H_2 gas system because extremely high nitrogen contents of product powder could be achieved. The nitridation rate was increased with the processing temperature due to an increase in the concentration of free nitrogen from NH_3 dissociation. The NH_3 concentration had pronounced effects on the progress of nitridation while the effect of H_2 was minor. On the other hand, an increase in the processing temperature reduced the saturated level of nitrogen content. Nitrogen contents ranging from 0.1 % to 10 % by mass were obtained, dependent on lengths of processing time, processing temperatures, and gas mixtures used.

The process of nitrogen addition could be divided in three stages: initial induction, enhanced nitridation, and final saturation stages. The nitridation after the induction stage proceeded by forming a CrN shell progressing from the particle exterior surface inward, followed by the uniform precipitation of Fe_4N throughout the CrN shell when temperature was low.

A mathematical model was proposed to describe the progress of nitridation in the enhanced nitridation stage. The reaction-controlled shrinking unreacted core model was used for the CrN shell formation, and the pseudo-homogeneous model was applied to the Fe_4N precipitation in the shell.

High Temperature Fluidized-Bed Nitridation of 316 Stainless Steel Powder

by

Tsai-Chen Wang

A THESIS

submitted to

Oregon State University

in partial fulfillment of
the requirements for the
degree of

Doctor of Philosophy

Completed September 18, 1996

Commencement June 1997

Doctor of Philosophy thesis of Tsai-Chen Wang presented on September 18, 1996

APPROVED:

Redacted for Privacy

Major Professor, representing Chemical Engineering

Redacted for Privacy

Head of Department of Chemical Engineering

Redacted for Privacy

Dean of Graduate School

I understand that my thesis will become part of the permanent collection of Oregon State University libraries. My signature below authorizes release of my thesis to any reader upon request.

Redacted for Privacy

Tsai-Chen Wang, Author

ACKNOWLEDGMENT

It is my pleasure to record my thanks to all those who have helped me in many ways in this study.

First, I like to thank Dr. Kimura for his incalculable guidance through my graduate study. His wisdom and impeccable attitude in studying research have always implanted in my mind.

I also want to express my appreciation to Dr. J. Dunning and Dr. James Rawers, Bureau of Mines at Albany, who brought in this project.

Thanks to my committee members, Dr. James Frederick, Dr. Goran Jovanovic and Dr. Ronald Miner, for their valuable help and suggestions in this thesis.

To Mr. Keith Collins, Mr. John Siple and Mr. Rick Krabbe, Bureau of Mines at Albany, for their contribution in SEM pictures, nitrogen analysis, and experiment support.

To Dr. Seung-Tae Hong and Dr. Pat Woodward in Chemistry Department at OSU who unselfishly provide their help in XRD analysis.

To Mr. Yao-Dian Liu for his generosity in helping me in the preliminary experiment to make my further study less difficult.

To Mr. Hirofumi Honda, Fuji Silysia Chemical Ltd., Aichi-Ken, Japan, for his fervor assistance in BET surface area analysis.

To my colleagues, Dr. Dah-Cheng Lin, Chia-Chang Hsu, Utami Setiowati, Kaj Wåg and Enrique Arriola, for their helpful suggestions and encouragement in years of my study here.

Finally, I like to express my deep thanks my wife, Shih-Yi Chang, for her help in so many ways. Also, to my families for their financial support to make my study possible.

TABLE OF CONTENTS

	Page
Chapter 1 Introduction	1
Chapter 2 Literature Survey and Current Studies	3
2-1 Stainless Steels	3
2-1-1 Structure of Metals	3
2-1-2 Classification	5
2-1-2-1 Ferritic Stainless Steels	5
2-1-2-2 Martensitic Stainless Steels	5
2-1-2-3 Austenitic Stainless Steels	5
2-1-2-4 Duplex (Ferritic-Austenitic) Stainless Steels	6
2-1-2-5 Precipitaion-Hardening Stainless Steels	6
2-2 High Nitrogen Stainless Steels	7
2-3 Current Techniques	7
2-4 Solid-State Nitrogen Addition	9
Chapter 3 Experimentals	11
3-1 Characterization of 316 Stainless Steel Powder	11
3-2 Apparatus and Procedures	16
3-2-1 Nitridation Process	16
3-2-2 Ammonia Dissociation	19
3-3 Analysis Methods	20
Chapter 4 Results and Discussion	23
4-1 NH_3 Dissociation	23
4-1-1 Background	24
4-1-2 Study of Thermal Decomposition	26
4-1-2-1 Development of Rate Equation	26

TABLE OF CONTENTS (Continued)

	Page
4-1-2-2 Experimental Results	29
4-1-2-3 Study of Entrance Region	34
4-1-3 Study of Catalytic Reaction	39
4-1-4 Estimated Overall Rate Equation	42
4-2 Nitridation in NH_3/ H_2/ Ar System	46
4-2-1 Effect of Temperature	46
4-2-2 Effects of Ammonia and Hydrogen	53
4-3 Nitridation in N_2/ H_2/ Ar System	57
4-3-1 Effect of Temperature	61
4-3-2 Effect of Gas Composition	63
4-4 Microstructural Change	63
Chapter 5 Nitridation Mechanism	78
5-1 Induction Stage	78
5-2 Enhanced Nitridation Stage	83
5-2-1 High Temperature Nitridation	84
5-2-1-1 Shrinking Un-reacted Core Model (SCM)	84
5-2-1-2 Model Inspection	90
5-2-2 Low Temperature Nitridation	95
5-2-2-1 Assumptions in Mathematical Model	101
5-2-2-2 CrN Formation	104
5-2-2-3 Fe_4N Formation	105
5-2-3 Model Evaluation	109
5-2-3-1 Effects of NH_3 and H_2 on CrN Formation	112
5-2-3-2 Effects of NH_3 and H_2 on Fe_4N Formation	116
5-2-3-3 Fitting with Experimental Data	119

TABLE OF CONTENTS (Continued)

	Page
5-2-3-4 Effect of Particle Size	121
5-2-3-5 Apparent Activation Energy	123
5-2-3-6 Effect of Gas on Induction Period	124
5-3 Final Saturation Stage	124
Chapter 6 Summary of Results	128
Chapter 7 Recommendations for Future Work	132
Bibliography	133
Appendices	139
Appendix A Calculating Concentrations of NH_3 and H_2	140
Appendix B Integration of Equations (5.11) from Equation (5.5)	147
Appendix C Manipulation of Integration from Equations (5.29) to (5.32)	150
Appendix D Calculation of Model Predication	152

LIST OF FIGURES

Figure		Page
2.1	(a) Body-centered cubic unit of structure (b) Face-centered cubic unit of structure	4
3.1	SEM images of 316 stainless steel particles	12
3.2	Log-particle size distribution of the powder used in the present study	14
3.3	X-ray diffraction chart of 316 stainless steel particles used in this study	15
3.4	Schematic diagram of the fluidized-bed reactor system	17
3.5	Minimum fluidization velocity of 316 stainless steel powder in N_2 gas at room temperature.	18
4.1	Fractions of NH_3 dissociated before entering the distributor	30
4.2	Fractions of NH_3 dissociated after leaving the empty bed	31
4.3	Log-log plot of average reaction rates against NH_3 concentration in the empty bed	33
4.4	Plot of $\ln(k_{homog})$ v.s. 1/T for NH_3 dissociation in the empty bed	36
4.5	Temperature gradients in the entrance region at different operating temperatures	37
4.6	Fractions of NH_3 dissociated by the fluidizing bed of 316 stainless steel	40
4.7	Plot of $\ln(k'_{cat})$ v.s. 1/T evaluated at the beginning and steady states	44
4.8	Effect of temperature on 316 stainless steel nitridation in the NH_3/ H_2 system	47
4.9	Close-up of the initial nitridation of 316 stainless steel in the NH_3/ H_2 system	48
4.10	BSE image of a cross-sectioned particle, nitrided in the feed gas of 90% NH_3 and 10% H_2 at 550 °C for 90 min.	49

LIST OF FIGURES (Continued)

Figure		Page
4.11	Comparison of nitridation at 550 and 650 °C in the feed gas of 90% NH_3 and 10% H_2	50
4.12	X-ray diffraction charts of final nitrided powder at T = 550, 700, and 750 °C	52
4.13	The effect of H_2 on the nitridation process at 550 °C at a fixed fraction of NH_3	55
4.14	The effect of NH_3 on the nitridation process at a fixed fraction of H_2 in the feed gas	56
4.15	Effect of temperature on 316 stainless steel nitridation in the N_2/ H_2 system	58
4.16	Close-up of the initial nitridation of 316 stainless steel in the N_2/ H_2 system	59
4.17	X-ray diffraction spectra of nitrided powder at 800 °C in the feed gas of 90% N_2 and 10% H_2 for 24 hours	60
4.18	Effect of gas composition on 316 stainless steel nitridation in the N_2/ H_2/ Ar system	62
4.19	XRD charts of 316 stainless steel powder nitrided for different lengths of time in the feed of 50% NH_3 and 50% H_2 gas at 550 °C	64
4.20	Optical images of cross-sectioned particles, nitrided in the feed of 50% NH_3 and 50% H_2 at 550 °C for (a) 120 min. and (b) 300 min.	66
4.21	Optical image of a cross-sectioned particle, nitrided in the feed of 50% NH_3 and 50% H_2 at 550 °C for 540 min.	67
4.22	BSE image of a cross-sectioned particles, nitrided in the feed of 50% NH_3 and 50% H_2 at 550 °C for 120 min.	68
4.23	The distribution of nitrogen in the cross-sectioned particle shown in Figure 4.20 (b)	69
4.24	The distribution of nitrogen in the cross-sectioned particle nitrided for 9 hours	70

LIST OF FIGURES (Continued)

Figure		Page
4.25	Comparison of nitridation process and ammonia dissociation for the feed gas of 100% NH_3 at 550 °C	72
4.26	Comparison of nitridation process and ammonia dissociation for the feed gas of 100% NH_3 at 600 °C	73
4.27	Comparison of nitridation process and ammonia dissociation for the feed gas of 100% NH_3 at 650 °C	74
4.28	Comparison of nitridation process and ammonia dissociation for the feed gas of 100% NH_3 at 750 °C	75
5.1	BSE image of a cross-sectioned particle, nitrided in the feed of 50% NH_3 and 50% H_2 at 550 °C for 30 min.	81
5.2	The comparison of the surface morphology images of (a) an original stainless steel particle, and (b) a nitrided particle for 60 min.	82
5.3	BSE image of a cross-sectioned particle, nitrided in the feed of 90% NH_3 and 10% H_2 at 750 °C for 180 min.	85
5.4	The distribution of nitrogen content in the cross-sectioned particle shown in Figure 5.3	86
5.5	Shrinking core model prediction compared with experimental data for Cr conversion v.s. time obtained at 750 °C in the feed of 50% NH_3 and 50% H_2	93
5.6	The linearity test of the SCM prediction using data obtained at 750 °C in the feed of 50% NH_3 and 50% H_2	94
5.7	Shrinking core model prediction compared with experimental data for Cr conversion v.s. time obtained at 750 °C in the feed of 70% NH_3, 10% H_2, and 20% Ar	96
5.8	The linearity test of the SCM prediction using data obtained at 750 °C in the feed of 70% NH_3, 10% H_2, and 20% Ar	97
5.9	Overall nitrogen contents and the amount of nitrogen used to form CrN in products obtained in the feed gas of 50% NH_3 and 50% H_2 at 550 °C	99

LIST OF FIGURES (Continued)

Figure		Page
5.10	SCM prediction compared with Cr nitridation data obtained at 550 °C in the feed of 50% NH_3 and 50% H_2	102
5.11	The linearity test of the SCM prediction using data obtained at 550 °C in the feed of 50% NH_3 and 50% H_2	103
5.12	Comparison of calculated results with the experimental data obtained at 550 °C in the feed of 50% NH_3 and 50% H_2	111
5.13	Effect of H_2 concentration on the rate of CrN precipitation	114
5.14	Effect of NH_3 concentration on the rate of CrN precipitation	115
5.15	Effect of H_2 concentration on the rate of Fe_4N formation	117
5.16	Effect of NH_3 concentration on the rate of Fe_4N formation	118
5.17	Comparison of calculated results with the experimental data obtained at 550 °C at different gas compositions	120
5.18	Effect of particle size on the nitridation process	122
6.1	An overall view of studies	129

LIST OF TABLES

Table		Page
3.1	Chemical and Physical Properties of 316 Stainless Steel Powder	13
4.1	Differential flow analysis of ammonia thermal dissociation at 550 °C	32
4.2	Calculation of k_{homog} values at different temperatures	35
4.3	Calculation of k'_{cat} values from the overall reaction data, Equation (4.15)	43
4.4	Feed gas and estimated average gas composition in bed at 550 °C	54
4.5	Estimated nitrogen concentration of surface shell at 550 °C in the feed gas of 50% NH_3/ 50% H_2	77
5.1	Nitrogen diffusivities in fcc and bcc-Fe measured by Grieveson *et al.* [1964]	79
5.2	The comparison of nitrogen contents by the LECO analysis and Kjeldahl's methods of samples obtained at 550 °C with the feed of 50% NH_3 and 50% H_2	98
5.3	Nitridation rates evaluated at 3 wt % nitrogen-addition from data obtained with different NH_3 and H_2 mixtures at 550 °C	113
5.4	The estimated induction periods for different gas mixtures at 550 °C	125
5.5	Estimated saturated nitrogen contents of nitrided products obtained with different temperatures and gas composition	127

NOMENCLATURE

b	stoichiometric constant
C_A	ammonia gas concentration
C_{Fe}	apparent iron concentration in a stainless steel particle
D_{eff}	effective diffusivity of nitrogen through product layer
$f(C_A)$	the dependency of reaction rate on the gas concentration in the formation of CrN
$f'(C_A)$	the dependency of reaction rate on the gas concentration in the formation of Fe_4N
f_{inert}	volume fraction of inert gas to ammonia
F_A	molar feed rate of ammonia
k, k'	rate constant of NH_3 dissociation
k'', k'''	rate constant of gas solid reaction
k_g	mass transfer coefficient of gas reactant
$K(C_A)$	defined by Equation (5.30)
m	power order of gaseous concentration for NH_3 concentration
n	power order of gaseous concentration for H_2 concentration, or reaction order of NH_3 dissociation.
N	molar amount of reactant
P	system pressure
r_C	radius of un-reacted core
$-r_A$	NH_3 dissociation rate, based on volume of voids in the reactor
$-r_s$	reaction rate, based on the unit volume of stainless steel
$-r'_A$	NH_3 dissociation rate, based on weight of catalyst powder
R	radius of a spherical particle, or gas constant
R^2	coefficient of multiple determination
S_{ex}	unchanging exterior surface area of a particle
t	time
T	temperature

V	volume of voids in the reactor
V_s	volume of surface layer in a stainless steel particle
W	mass of catalyst
w_N	mass fraction of nitrogen in the nitrided stainless steel powder
W_N	mass of nitrogen added per unit mass of stainless steel powder
X	conversion of the solid reactant, or the extent of NH_3 dissociation
X_N	the fraction of overall nitrogen addition in the stainless steel powder

Greek symbols

ε	fraction change in volume of the system, defined by Equation (4.6)
τ	time needed for complete conversion of Cr in a stainless steel particle
θ	X-ray diffraction angle
ρ	molar density
ϕ	volumetric fraction of surface shell in a particle
Ψ	defined by Equation (5.35)
ω	τ_{dff} / τ_{oval}, defined by Equation (5.11)

Subscript

AVG	average value
B	solid reactant B
c	critical point where Fe_4N starts to form
cat	catalytic NH_3 dissociation
Cr	for the formation of CrN
dff	diffusion resistant control
entc	in entrance region
f or fin	final state, or saturation state
Fe	for the formation of Fe_4N

NOMENCLATURE (Continued)

g	gas phase
homog	homogeneous NH_3 dissociation
i or ini	initial state
0	standard state
ovl	overall resistant, including diffusion and chemical reaction
overall	overall NH_3 dissociation
rxn	chemical reaction control
s	surface layer in a stainless steel particle
sln	solid solution
void	void volume of the bed in the fluidizing 316 stainless steel powder

HIGH TEMPERATURE FLUIDIZED-BED NITRIDATION OF 316 STAINLESS STEEL POWDER

Chapter 1
Introduction

Over the past 30 years, nitrogen has become a very attractive alloying element in the steel industry. It has been recognized that adding nitrogen into stainless steel improves its mechanical and physical properties, including tensile and yield strengths, corrosion and wear resistance, etc..

However, the current commercial method for nitrogen-alloying is predominately carried out by melting iron alloys in a nitrogen rich environment at atmospheric pressure, resulting in low nitrogen contents due to the gas-liquid equilibrium limitation. Applying high nitrogen pressure in the system is an alternative way to increase nitrogen content. However, the increase in nitrogen content is still limited, and high-pressure use becomes impractical commercially.

Therefore, a process for solid-state nitrogen addition has gained people's attention because of high nitrogen solubility in solid stainless steel. However, fine stainless steel powder is needed to reduce the processing time, owing to slow nitrogen diffusion in solid. As a result, an application of a fluidized bed system, which can provide temperature uniformity and good gas-solid contact, has been proposed to promote the process of nitrogenization.

The main purpose of this research is to study the process of nitrogen addition to 316 stainless steel powder in a fluidized bed using NH_3/ H_2 and N_2/ H_2 systems at temperatures between 450 °C and 800 °C. It has been found that the nitridation process may be divided into three stages: initial induction, enhanced nitridation, and final saturation stages. An effort has been made to develop a model to describe the nitridation process in the enhanced nitridation stage.

This thesis is divided into 7 chapters to present a complete view of findings and development in this study.

Chapter 2 describes the literature survey of relevant studies in the area of high nitrogen stainless steels, which provides the background for this study.

Chapter 3 illustrates the experimental set-up, the detailed procedure of operating a high temperature fluidized-bed reactor, and the experimental study of ammonia dissociation. In addition, all analytical techniques that have been used in this study are also briefly explained in this chapter.

Chapter 4 presents the experimental results that basically include two systems of gas mixtures: NH_3/ H_2 and N_2/ H_2. The NH_3/ H_2 system, which is the main focus of this work, is divided into two parts: NH_3 dissociation in the bed and nitridation of stainless steel powder. A kinetic rate equation has been proposed, with which the average NH_3 and H_2 contents in the bed may be evaluated. Based on experimental results, the nitrogen addition process is addressed qualitatively, and later is extended to model development.

In Chapter 5, a mathematical model is developed to predict the process of nitrogen addition of 316 stainless steel powder in the enhanced nitridation stage in NH_3 and H_2 mixtures. A comparison of experimental data with the prediction by the proposed model is also shown here.

Conclusions of the present study are summarized in Chapter 6. Finally, Chapter 7 suggests recommended work for further investigation.

Chapter 2
Literature Survey and Current Studies

In the past century, steels have played a manifest role as one of key materials in the development of modern technology [Steel, 1992]. Steels, a large family of iron-based alloys, are relatively cheap and can be applied in a variety of areas. Among the family of steels, stainless steels have been used in a wide range of industrial services ever since they were developed in the 1920s [Source Book on Stainless Steels, 1976]. Without the excellent corrosion resistance of stainless steel to most chemicals, many of important commercial chemical processes would not have been feasible.

2-1 Stainless Steels

Stainless steels are generally defined as iron-base alloys with more than 10 or 12 wt% of Cr, that cover the standard composition, variations of company trade names and special alloys made for particular applications [Metals Handbook, 1990]. A wide variety of mechanical properties can be obtained from so many types of stainless steels. However, the mechanical properties and thus the use of stainless steel depend on its constitution and microstructure, i.e., its internal structure. This section introduces some basic aspects of metallic structure and the classification of stainless steels used in modern industry.

2-1-1 Structure of Metals

Solid metals are crystalline. Iron alloys generally attain two of the most common types of possible arrangements of atom. The first one is called the body-centered cubic structure (bcc), and a unit of this pattern is illustrated in Figure 2.1(a). The second structure is called the face-centered cubic structure (fcc), of which a unit of pattern is shown in Figure 2.1(b).

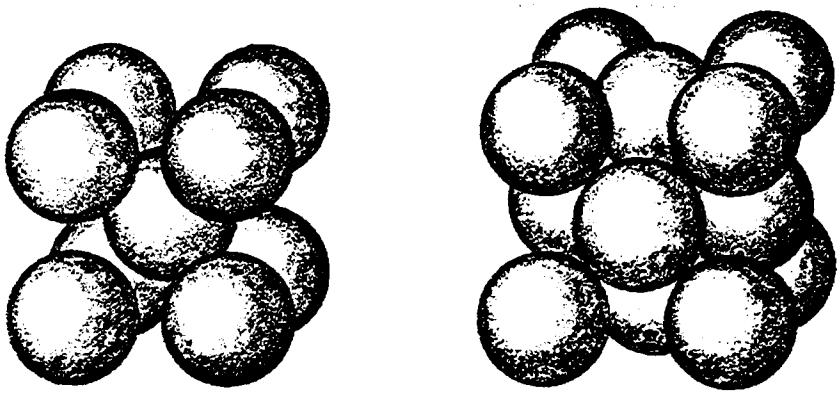

(a) (b)

Figure 2.1 (a) Body-centered cubic unit of structure. (b) Face-centered cubic unit of structure.

A single crystal of pure iron, for instance, shows the body-centered cubic structure at temperatures below 910 °C, known as α-Fe. In the range from 910 °C to 1400 °C, iron atoms rearrange into the face-centered cubic structure, called γ-Fe. From 1400 °C to its melting point, 1540 °C, iron resumes the body-centered cubic structure, called δ-Fe [Lula, 1986].

As mentioned early, stainless steel is mainly an alloyed mixture of iron and chromium, as well as other elements. Added elements in the iron-based crystal may be classified into two groups. One represents substitutional elements in the crystalline lattices such as the alloying of metal atoms like Cr, Ni, Mo etc.; the other does the interstitial elements in the crystalline lattices like carbon and nitrogen. The influences of added elements on the microstructural change of stainless steel alloys may be seen elsewhere [Metals Handbook, 1990; Source Book on Stainless Steels, 1976].

2-1-2 Classification

Many organizations have classified stainless steels based on their chemical composition and properties. However, no matter how these organizations classified them, all stainless steels can be categorized into five groups: ferritic stainless steels, martensitic stainless steels, austenitic stainless steels, duplex (ferritic-austenitic) stainless steels, and precipitation-hardening stainless steels [Source Book on Stainless Steels, 1976].

2-1-2-1 Ferritic Stainless Steels

Steels in this category have the bcc crystal structure, the same structure as pure α-iron. Chromium contents are normally between 10.5% and 30% by mass, with no nickel. In addition, a very low carbon content is found in ferritic alloys. These grades of steels are ferromagnetic. They can have good ductility, but high temperature strength is relatively poor compared to austenitic stainless steels.

2-1-2-2 Martensitic Stainless Steels

Alloys with adjusted composition of iron, chromium and carbon are classified in this class. They are ferromagnetic, hardenable, and resistant to corrosion in mild conditions. Chromium contents are generally in the range of 10.5% to 18% by mass, and carbon contents normally exceed 1.2% by mass. The hardness of martensitic stainless steel also depends on its carbon content.

2-1-2-3 Austenitic Stainless Steels

This is one of the most popular groups among all steels in the industry in terms of the amount of consumption. The crystal structure of these steels is fcc, and this

structure is maintained by using austenitizing elements such as nickel, manganese, and nitrogen. Austenitic stainless steels usually hold an excellent cryogenic properties and good high-temperature strength [Marshall, 1984].

2-1-2-4 Duplex (Ferritic-Austenitic) Stainless Steels

These steels maintain mixed structure of bcc ferrite and fcc austenite; and likewise the mechanical properties unite the properties of both steels. Hence, duplex steels has the corrosion resistance of austenitic steels and the hardness of ferritic steels.

2-1-2-5 Precipitation-Hardening Stainless Steels

Iron alloys contain chromium and nickel along with precipitation-hardening elements such as copper, aluminum, or titanium. These steels may be either austenitic or martensitic stainless steels. They attain high strength at high operating temperature due to the precipitation-hardening elements.

The advantageous properties of all stainless steels are their excellent corrosion resistance, physical properties, and mechanical properties. Nevertheless, a large number of different types of stainless steels are developed for different applications, as classified above. Therefore, selecting one type of stainless steel for certain advantageous properties may at the same time have disadvantages in other properties. For instance, although austenitic stainless steels hold excellent corrosion resistance and cryogenic properties, their mechanical properties are generally inferior to other hardening alloys, such as ferritic and martensitic types of stainless steels [Irvine *et al.*, 1979; Metals Handbook, 1990]. However, with ever increasing demands for higher yield and tensile strengths, higher wear and corrosion resistances in many applications,

further development of high performance stainless steels in most properties becomes more important.

2-2 High Nitrogen Stainless Steel

Recently, high-nitrogen stainless steels have been proposed to be potential new iron-based materials in applications that require operation at elevated temperature, high pressure and corrosion resistance [Anthamatten *et al.*, 1989; Norström, 1977; Rawers *et al.*, 1993; Degallaix *et al.*, 1986]. The advantages of adding nitrogen into stainless steels have been demonstrated by many studies, indicating that nitrogen is a strengthening element, and increases the stability of the austenite phase and corrosion resistance of a stainless steel [Hendry, 1993; Rayaprolu *et al.*, 1987]. One study, for instance, showed that an increase in nitrogen concentration from 0.04% to 0.69% by mass resulted in increasing the yield and tensile strengths of as-cast Fe-15Cr-15Ni alloy approximately linearly up to twofold [Rawers *et al.*, 1992]. The significant improvement of mechanical properties of high nitrogen stainless steel alloys has called people's attention on their development [Stein *et al.*, 1990; Lankreijer *et al.*, 1989; Rawers *et al.*, 1990].

There are two effects of nitrogen addition on the stainless steel. Nitrogen initially dissolves interstitially into the stainless steel solid solution. Depend upon alloy composition, dissipated metal nitride phases may start to form after the nitrogen content in the stainless steel achieves a certain level. It is found that both forms of nitrogen addition have improved the strength of a stainless steel [Uggowitzer *et al.*, 1990].

2-3 Current Techniques

In the 1970s, an important technique, called argon-oxygen-decarburization process (AOD), revolutionized stainless steel melting techniques, allowing major

alloying elements to be controlled more accurately [Peckner and Bernstein, 1977; Metals Handbook, 1990]. The stainless steel industry has become firmly established since then. In the AOD and related processes, the addition of nitrogen into the alloy solution is carried out by introducing nitrogen gas through melting alloy. The solubility of nitrogen in the stainless steel is hence controlled by its gas-liquid equilibrium, usually at one atmosphere. Although the solubility of nitrogen also depends upon the alloy's structure and composition [Small, 1990; Kikuchi *et al.*, 1989; Shahapurkar *et al.*, 1987; Imai *et al.*, 1967], the increase in nitrogen concentration by composition variation is still narrowly restrained. As a result, the concentration of nitrogen in the stainless steel is normally limited to less than 0.4% by mass when the process pressure is at one atmosphere of nitrogen gas. To further increase nitrogen concentration in a stainless steel, new techniques have to be developed.

The common way to overcome the limitation of nitrogen's solubility is to increase the nitrogen pressure during processing [HNS-88, 1988; HNS-90, 1990]. The solubility of nitrogen in the stainless steel can be increased by holding the molten metal in a pressurized vessel. The nitrogen concentration was found to increase proportionally to the square root of nitrogen pressure, which is known as Sievert's law [Rawers and Petty, 1993]. Nitrogen contents as high as 0.6% by mass have been recently reported by melting stainless steels under the nitrogen-argon gas atmosphere containing 75% N_2 at a pressure of 0.4 MPa [Stein et al. 1989].

Moreover, a recent technique for melting alloy in a hot-isostatic pressure (HIP) furnace, designed to sinter ceramic materials, with nitrogen as the pressurizing gas has been developed [Rawers and Petty, 1993]. Up to 6% by mass of nitrogen has been added into the melting stainless steel alloys under a pressure of 200 Mpa in this system [Rawers and Gokcen *et al.*, 1993]. However, the increased operating pressure requires the specially designed equipment, which leads to a considerable increase in cost. Therefore, nothing has been reported on the large-scale manufacture of high nitrogen-alloyed stainless steels in applications of pressurized furnaces. In addition, although the process of molten-state nitrogen addition (nitrogenization) has been well established by a considerable amount of research, some principle problems remain in the process, such as a decrease in nitrogen solubility between the melt and

solidification phases and possible nitrogen gas nucleation (bubble) in molten solution especially when high nitrogen concentration is prepared [Hendry, 1993]. These difficulties have led to search for an alternative approach that can promise high nitrogen contents at reasonable cost for equipment set-up and process operation.

2-4 Solid-State Nitrogen Addition

Because the solubility of nitrogen in solid stainless steel is greater than in liquid, solid-phase nitrogen diffusion has been proposed to increase the nitrogen concentration obtainable by liquid-phase diffusion [Kikuchi *et al.*, 1989; Lee *et al.*, 1993; Rawers *et al.*, 1995]. However, because of nitrogen's slow diffusion rate in solid, the surface layer is only nitrided while the core remains with the properties of ordinary stainless steel in most cases. To date, most methods for nitrogen-diffusion-addition to bulk stainless steel components have been designed only as the near-surface addition [Kossowsky, 1989]. In fact, high-temperature diffusion of nitrogen into solids has been used notably for surface coating of nitriding metals for a number of years. The production of hard, corrosion-resistant, wear-resistant, and fatigue-resistant surfaces on core materials has been successful [Sudarshan, 1989; Kossowsky and Singhal, 1983]. For example, cutting tools like drills, thread cutters, and milling tools are nitrided on the surface to produce high surface nitrogen concentration to improve their mechanical properties. To nitride the surface layer, high gas-phase activity of nitrogen has to be provided [Dressler, 1989]. For several decades, the nitriding process has been developed by gas nitriding or salt-bath nitriding. Recently, new techniques like ion and plasma nitriding have provided an accurate control of the surface compound zone. However, these technologies are all confined on the surface modification.

Nevertheless, with the increasing knowledge of enhanced properties of high nitrogen stainless steels, the surface nitridation of metals has been applied to extend ultra-high nitrogen stainless steels through bulk quantities. The nitrogen diffusion process may be completed in a reasonable process time if the diffusion distance is

significantly reduced by using fine powder. In this research, an attempt has been made to apply fluidization technologies to nitriding 316 stainless steel powder using NH_3 gas. Fluidized bed reactors have been employed in many gas-solid reaction systems that require good heat transfer, i.e., temperature uniformity, and good gas-solid contact [Kunii *et al.*, 1991; Jovanovic *et al.* 1994; Jaraiz *et al.* 1992; Liu *et al.* 1993; Jovanovic, 1994]. The nitrided powder can then be consolidated into a solid compact with a uniform, high nitrogen concentration. Furthermore, Henry [1993] has suggested that mixing steel powder with nitrides in some forms may give a homogeneous microstructure of required properties through the thermo-mechanical processing.

Therefore, the objective of this study is to investigate the kinetics and mechanisms of nitriding 316 stainless steel powder in a fluidized bed under NH_3/ H_2 and N_2/ H_2 systems. The attempts of this research are listed below.

(1). To determine an appropriate range of operating conditions, i.e., gas flow-rate and temperature, for the fluidized bed of 316 stainless steel powder.

(2). To determine the kinetics of ammonia dissociation in the bed of 316 stainless steel powder and to estimate the average ammonia and hydrogen contents in the bed.

(3). To investigate the effects of process temperature and gas composition on the nitridation of 316 stainless steel powder.

(4). To investigate the microstructural change of 316 stainless steel particles due to the increase in nitrogen concentration.

(5). To clarify the mechanism of nitridation and to develop a mathematical model of the nitridation process of 316 stainless steel powder.

Chapter 3
Experimentals

3-1 Characterization of 316 Stainless Steel Powder

Stainless steels are iron-base alloys containing at least 10 to 12 wt% of Cr. The powder used in this study is in the form of non-porous, dense alloy particles, designed as 316 stainless steel. Type 316 is the family of austenitic stainless steels. Scanning electron microscopy pictures, presented in Figure 3.1(a) and (b), illustrate the typical morphology of particles used in this study. Most of original stainless steel particles show a spherical shape of structure. The physical and chemical properties of the 316 stainless steel powder are summarized in Table 3.1. As one may notice, the concentration of carbon is 0.015% by mass, suggesting the powder studied has a low carbon content, known as 316L stainless steel powder. The study, however, finds no effect of carbon in the nitrogen addition process. Therefore, the powder studied is simply called as 316 stainless steel.

Furthermore, the particle size distribution of the powder was measured with a HORIBA CAPA 7000 analyzer, and an average particle size of about 70 μm was obtained. Figure 3.2 shows the log-particle size distribution of this powder, indicating roughly a log-normal size distribution. Because of the narrow size distribution of the major portion of powder between 45 μm and 120 μm, particles may be roughly approximated as a uniform size of 70 μm in the present study.

The X-ray diffraction of raw 316 stainless steel particles indicates a face-centered cubic (fcc) lattice structure and a trace of body-centered cubic (bcc) lattice structure, as shown in Figure 3.3. The fcc is the designed structure for austenitic stainless steels, as discussed in Chapter 2. As shown in Table 3.1, Cr, Ni and Mo are the major additions in 316 stainless steels to provide particular characteristics. It has been known that Fe and Cr react with nitrogen to precipitate new solid nitride phases [Rawers *et al.* 1993, Rawers *et al.* 1994]. Hence, the results in this study describe the nitridation of Fe and Cr only. The content of nitrogen is expected to be increased

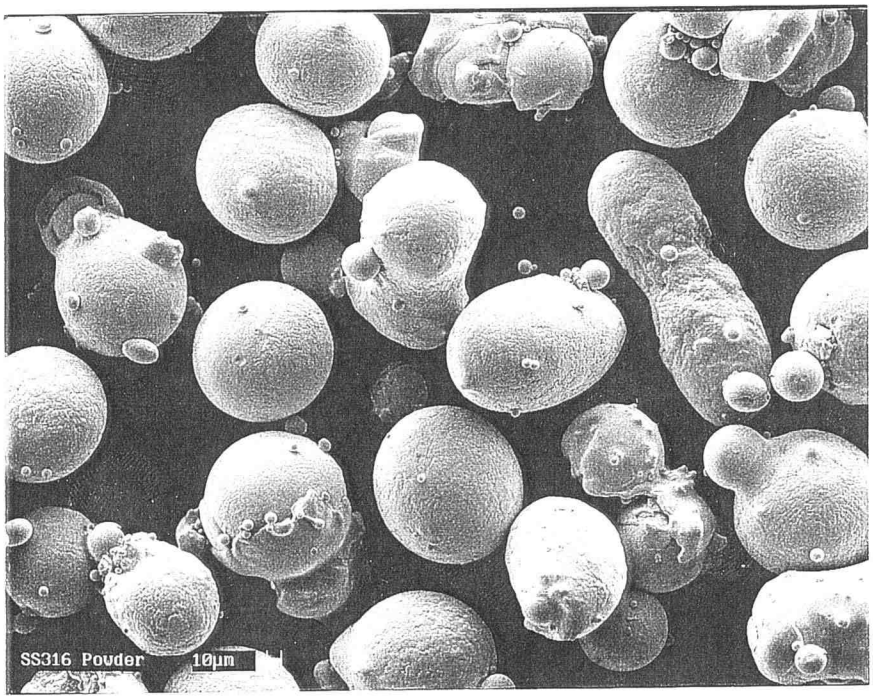

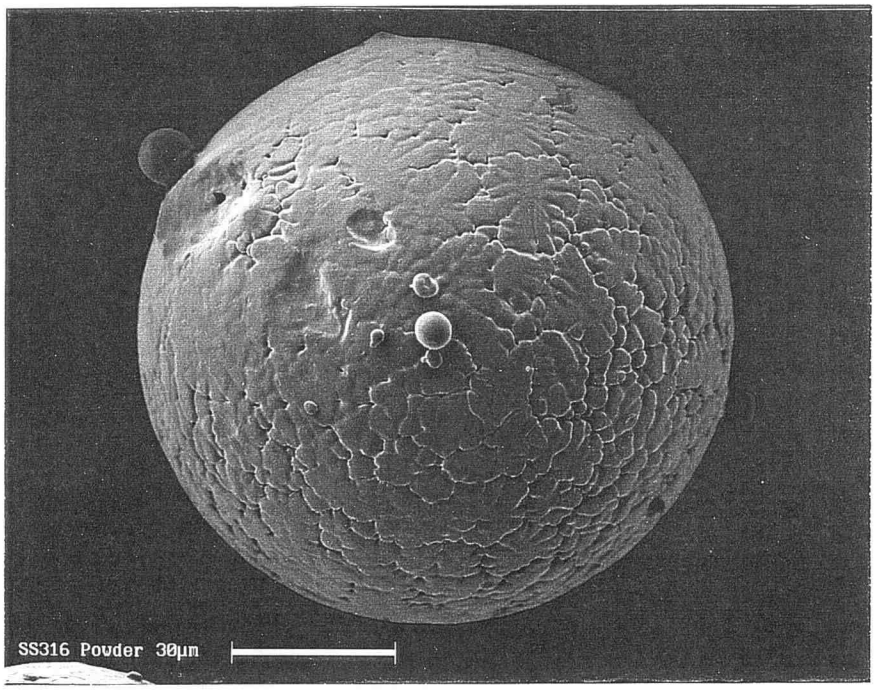

Figure 3.1 SEM images of 316 stainless steel particles

Table 3.1 Chemical and Physical Properties of 316 Stainless Steel Powder

Chemical Composition, % in mass	
Fe	66.5
Cr	16.65
Ni	13.5
Mo	2.15
Si	0.75
C	0.015
N	0.04
O	0.2
Impurities	0.195

Physical Properties	
Density, kg m^{-3}	7860
Average Particle Size, μm	70
Surface Area (BET), m^2 g^{-1}	0.06

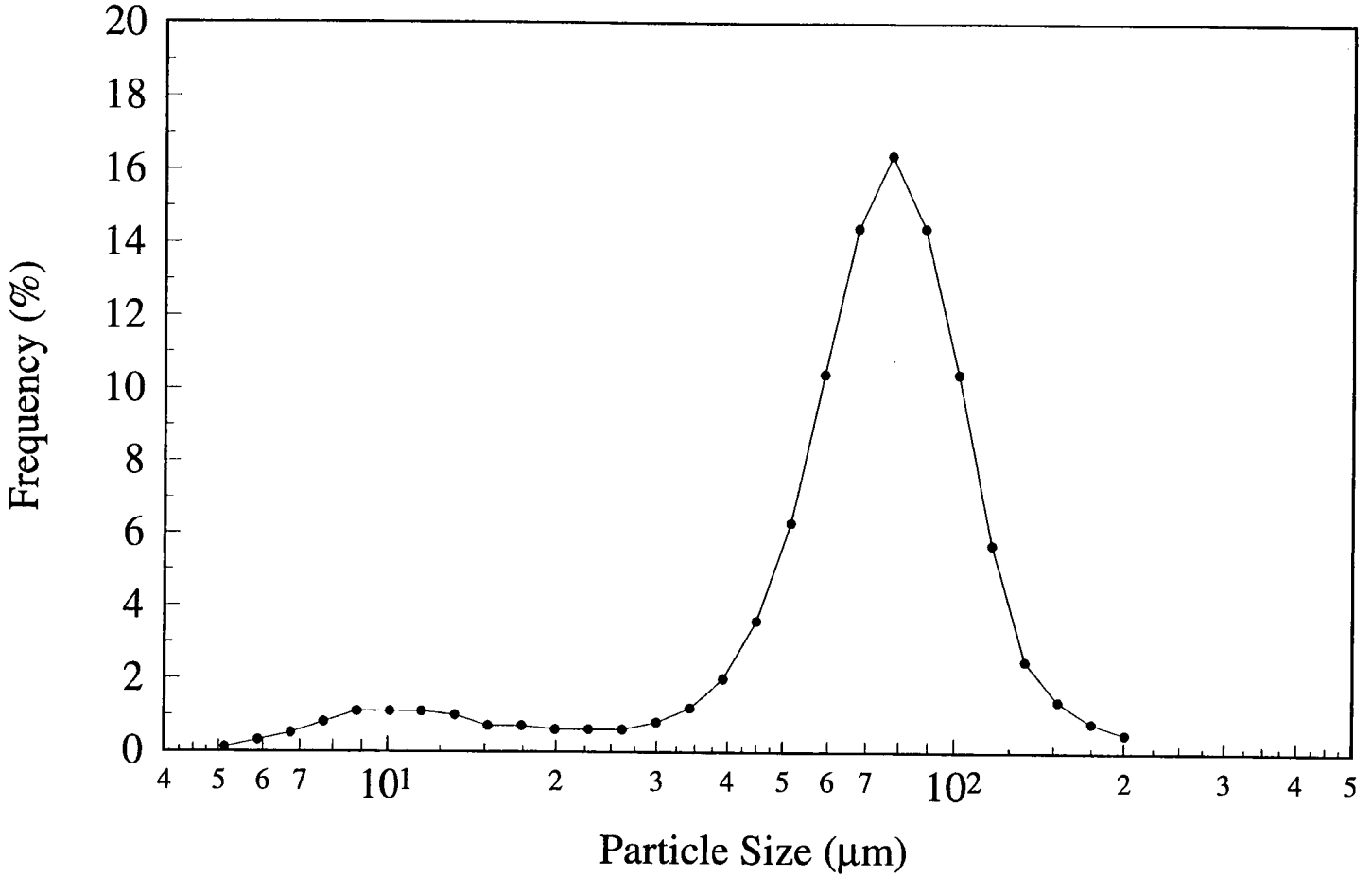

Figure 3.2 Log-particle size distribution of the powder used in the present study

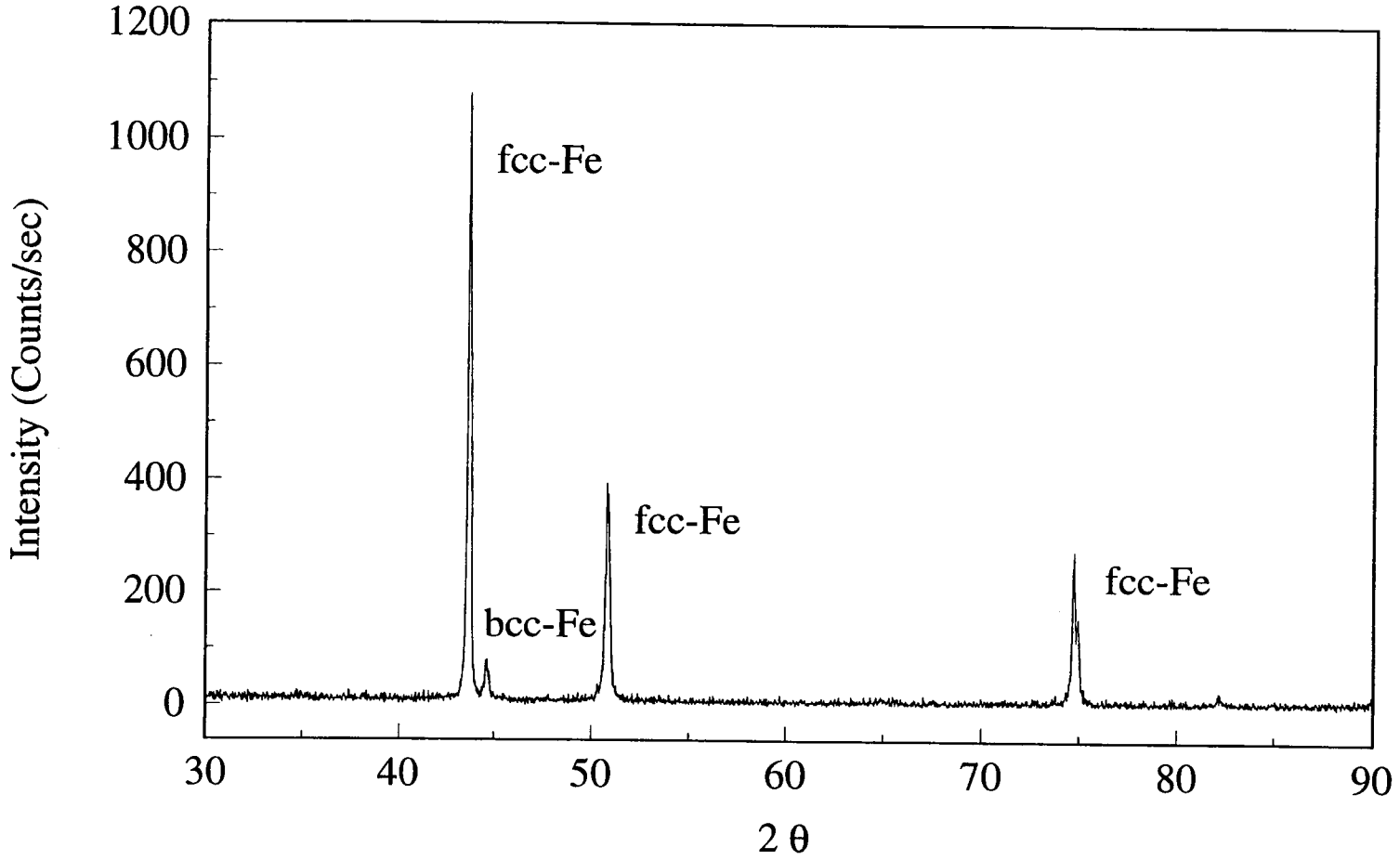

Figure 3.3 X-ray diffraction chart of 316 stainless steel particles used in this study

significantly when new nitride phases have precipitated, because more nitrogen atoms must stay in the lattice of metal atoms continuously in order to form new phases.

3-2 Apparatus and Procedures

The results of this study focus on both the gas and solid phases. Because NH_3 decomposes at high temperatures, the first part investigates the actual gas composition in the bed when NH_3 is used. The second investigation is mainly the study of the effects of gas-composition and process temperature on the increase of nitrogen content and microstructural change in 316 stainless steels particles during nitridation process.

3-2-1 Nitridation Process

Figure 3.4 illustrates schematically the experimental apparatus used for this study. A 55 mm I.D. quartz tube was used as a fluidized-bed reactor with a sintered quartz disk as its distributor. The bed was inserted into the 80 mm I.D. mullite-furnace tube of an electric furnace. Raw material-solids were pneumatically charged directly into the bed through a mullite tube. Product solids were also pneumatically discharged from the fluidizing surface through another mullite tube into a sampling flask. The composition of reactant gas mixtures was adjusted with calibrated rotameters. The pressure drop of the bed and its fluctuations were measured with a pressure transducer. The standard deviation of the pressure fluctuations was computed at an interval of 10 seconds by a data acquisition system and was used to monitor the fluidization condition of the bed [Jovanovic *et al.* 1994]. The operating pressure of the system was measured by the pressure manometer and bed pressure-drop. It was slightly higher than atmospheric pressure, that

The minimum fluidization velocity of the stainless steel powder in nitrogen was found to be about 4.5 cm s^{-1} at room temperature, as shown in Figure 3.5. The fluidizing gas velocity, U_0, in this study was normally set at 8.3 cm s^{-1} based on the

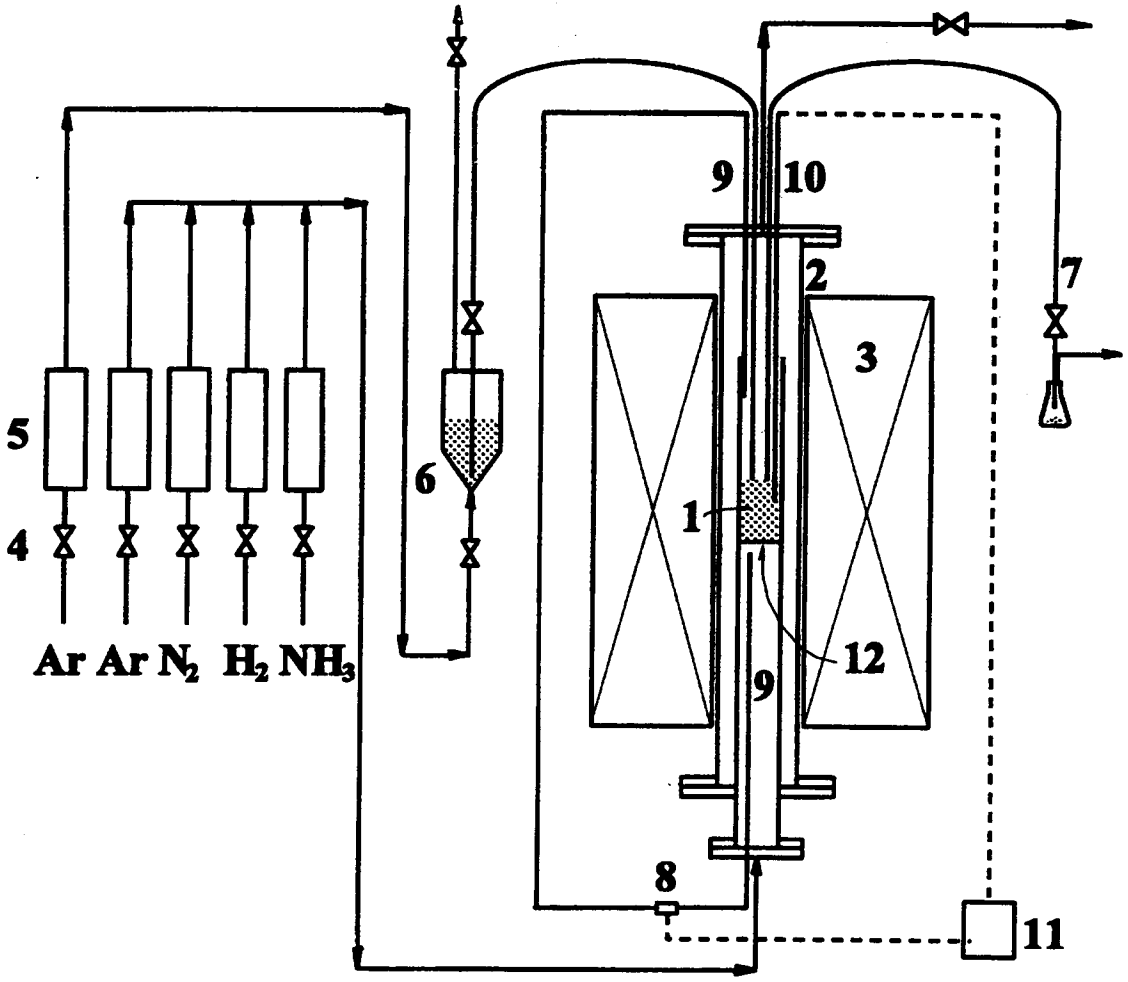

1. Fluidized-bed reactor
2. Furnace tube
3. Furnace
4. Control valves
5. Rotameters
6. Pneumatic solids charger
7. Pneumatic solids discharger
8. Pressure transducer
9. Pressure probe
10. Thermocouple
11. Data acquisition system
12. Distributor

Figure 3.4 Schematic diagram of the fluidized-bed reactor system

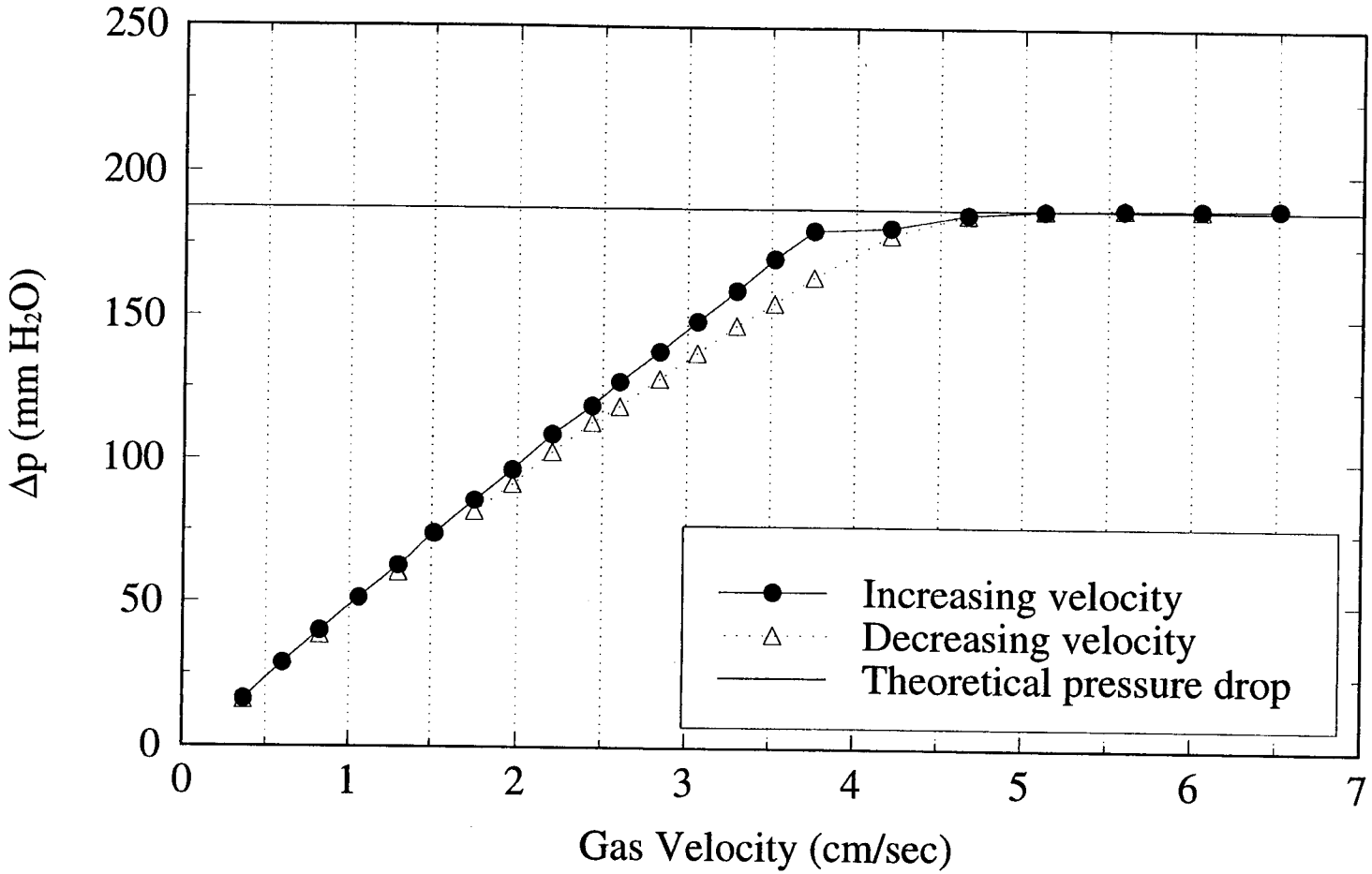

Figure 3.5 Minimum fluidization velocity of 316 stainless steel powder in N_2 gas at room temperature

empty column and operating temperatures. When the bed was operated at 800 °C, the fluidizing-gas velocity was raised to 16.6 cm s^{-1} to prevent the fluidized bed from collapsing into a packed bed. The empty bed was first heated to a prescribed operation temperature and then raw material stainless steel powder of about 0.5 kg was pneumatically charged into the bed using argon as a carrier gas, while argon gas was introduced into the bed through the distributor at a designed gas velocity. After the bed temperature reached the set point, from a temperature lowered due to the supply of cold powder, the argon stream was switched to a mixture of 50% H_2 and 50% Ar with the gas velocity kept unchanged. The stainless steel powder was then pre-treated for one hour in this gas mixture to remove surface oxide.

The process of nitridation was initiated by supplying a reactant-gas mixture with designed composition. Two different systems were used in this study: NH_3/ H_2/ Ar and N_2/ H_2/ Ar. The operating temperature covered a range of 450-750 °C for the NH_3/ H_2/ Ar system and 650-800 °C for the N_2/ H_2/ Ar system. Samples of nitrided powder were occasionally removed from the bed for analysis. The fluidizing-gas velocity was kept unchanged throughout the course of each run.

3-2-2 Ammonia Dissociation

NH_3 easily decomposes at high temperatures. When NH_3 is used as a nitriding gas, knowing its concentration in the bed is essential for the kinetic analysis of the nitriding process. In this study, the concentration of NH_3 was measured under actual operating conditions. Two 3.9 mm I.D. alumina tubes were inserted into the fluidized-bed reactor, one directly underneath the distributor and the other about 9 cm above the distributor of the bed, and part of fluidizing gas was withdrawn through the tubes for NH_3 analysis. The velocity of the gas stream through each sampling tube was adjusted fast enough so that the dissociation of NH_3 in the sampling tube was negligibly small.

In the dissociation of NH_3 in the bed, there are two ways: thermal and catalyzed dissociations. The thermal dissociation of NH_3 in the bed was first

investigated using the empty bed. A kinetic rate equation for the NH_3 thermal dissociation was developed from experimental data. The overall NH_3 dissociation was then measured in the fluidized bed of stainless steel powder. By subtracting the thermal NH_3 dissociation from the measured overall NH_3 dissociation, the rate of catalytic dissociation was then determined. The detailed description of this procedure will be presented in the next chapter.

3-3 Analysis Methods

Several analytical methods were applied in this study, mainly used for the solid phase determination. A titration method was also used to estimate the gas composition in the bed.

The concentration of nitrogen in the stainless steel powder was measured with a LECO TC-436 nitrogen-oxygen analyzer. An empty graphite crucible was first placed between the two electrodes in the furnace. A high electric current was then passed through the crucible to drive off all possible gases from the graphite, and thus gases were purged out the system by highly pure helium gas (called outgassing). A measured amount of sample powder, loaded in a tin crucible or a nickel capsule, was thus dropped into the empty graphite crucible. A high electric current through the crucible heated up the sample to drive off gases in the sample. All nitrogen, interstitial as well as in metal nitrides, was liberated. Helium was then introduced to carry all the liberated nitrogen through a thermal conductivity cell for nitrogen detection. In the present analysis of nitrogen content in stainless steel powder, three different standard reagents were used: titanium nitride (NIST SRM 367) containing 0.168% nitrogen by mass, nitrided Mn (ICRM F29) containing 5.43% nitrogen by mass, and titanium nitride containing 22.4% nitrogen by mass, depending on the level of nitrogen content in sample powder. The nitrogen content in sample powder was determined from the calibration of standard reagents. In this system, the power was supplied at a ramp rate of about 80 Watts per second with a minimum of 1200 Watts and a maximum of about 5000 Watts.

The Kjeldahl method [Hargis, 1988] was also used to determine nitrogen interstitial content in 316 stainless steel powder. Unlike the LECO analyzer, the Kjeldahl method is based on chemical analysis and can release all nitrogen in metal but CrN. Sample powder was oxidized with hot, concentrated sulfuric acid in a long-necked Kjeldahl flask, in which nitrogen in solid solution and iron nitride would dissolve and convert into ammonium ion. It normally required more than one hour to complete the oxidation. After the oxidation was completed, a concentrated sodium hydroxide solution was added into the solution to yield ammonia gas by the following reaction.

$$NH_4^+ + OH^- \rightarrow NH_3\,(g) + H_2O \qquad \textbf{(3.1)}$$

The NH_3 was then evaporated and collected in excess standard acid that was back-titrated with standard base, such as NaOH solution, to determine the amount of liberated ammonia. The insoluble residue remaining in the sulfuric acid solution was identified to be CrN precipitate by using X-ray diffraction. Hence, the amount of nitrogen in CrN could also be measured.

X-ray diffraction (XRD) was used to determine the solid phase structure of sample powder. The XRD analysis was performed by using a solid detector (Si, Li) SIEMENS D5000 diffraktometer with CuK_α radiation and a scan rate of 30 s/degree. The penetration depth of X-ray into the powder particle was estimated with its software (SIEMENS DIFFRAC AT) to be 1.6 - 4.8 μm, depending on the diffraction angle.

To determine the phase structures of both particle surface and interior, sample-powder particles impregnated in epoxy were cross-sectioned. An optical microscopy was then used to observe etching patterns and colors which developed for different phases [Beraha and Shpigler, 1977]. Selected nitrided-samples were also analyzed using a scanning electron microscopy (SEM) instrument. A pointed electron beam scanned over an area of the specimen surface, causing several types of energetic emission: backscattered electrons, secondary electrons, Auger electrons, continuous X-rays, and characteristic X-rays. Secondary electron images identified surface features,

such as the structure of fracture faceting, morphology of crystals, and pores ... etc. On the other hand, backscattered electron images were used to obtain contrast based on the average atomic number of the region or phase examined, which differentiated between materials in a composite. Details of SEM characteristics may be found elsewhere [Goldstein *et al.*, 1981; Reimer, 1985]. Images from backscattered electrons (BSE) and secondary electrons (SE) were observed to study the morphology of solid phase in this study.

The cross-sectioned particles were also used to measure the concentration profile of nitrogen in the individual particles by the scanning electron microprobe analysis (EMPA) with a probe beam diameter of about 1μm. Images of backscattered electrons (BSE) were also taken over the cross-section of particles to compare with the results of EMPA analysis for understanding the distribution of nitrogen content in different phases.

Gaseous samples withdrawn from the fluidized-bed reactor were bubbled through an aqueous HCl solution in two flasks in series. The amount of NH_3 in each sample was determined by the amount of HCl consumed to form NH_4Cl. Also, the amount of dissociation products N_2 and H_2, that remained unabsorbed by the HCl solution, was measured by a soap-film flow meter to determine the amount of NH_3 dissociated. The flow rate was corrected by taking into consideration the saturated vapor pressure of water at room temperature. The detailed process of titration and equipment set-up may be seen in elsewhere [Lin, 1995].

Chapter 4
Results and Discussion

This chapter is divided into three sections: the dissociation of ammonia, the nitridation of 316 stainless steel powder in the NH_3/ H_2/ Ar system, and the nitridation of 316 stainless steel powder in the N_2/ H_2/ Ar system.

Because the actual amount of NH_3 in the bed depends on the dissociation rate of ammonia in the system, it is necessary to study the dissociation of ammonia, that may be affected by the operating temperature and the surface of 316 stainless steel powder. Hence, before studying the nitridation process in the NH_3/ H_2/ Ar system, it is required to investigate the dissociation of ammonia in the fluidized bed of 316 stainless steel powder.

As mentioned earlier, the nitridation process was studied using two systems: NH_3/ H_2/ Ar and N_2/ H_2/ Ar. A higher nitridation rate was found in the ammonia system at lower operating temperatures while the nitridation process was slower in the nitrogen system even at higher operating temperatures, as described later. It is suggested that dissociated ammonia provides high nitrogen chemical potential that drives nitrogen into solid solution [Shohoji *et al.*, 1990; Katsura, 1992]. Hence, this study will concentrate mainly on the ammonia-nitridation process.

The stainless steel alloy composition varies for different applications. Fe, Cr, Ni, and Mo are the four major elements of 316 stainless steel. Fe and Cr may react with nitrogen to form new solid nitride phases. The following hence describes the results regarding the nitridation of Fe and Cr, as well as nitrogen in solid solution of the nitrided powder.

4-1 NH_3 Dissociation

It is hard to evaluate the dissociation of ammonia in the fluidized bed of 316 stainless steel powder because of the lack of information regarding the actual

mechanism of dissociation. Besides, there are gas and metal phases being involved in the reaction, that makes the process even more complex. However, an effort is made here to estimate the average NH_3 concentration in the bed during the process. The ammonia dissociation possible in two paths is dealt with: gas-phase homogeneous reaction and catalytic heterogeneous reaction.

4-1-1 Background

It has been well known that metals enhance the dissociation of NH_3, leading to a catalytic reaction [Temkin *et al.*, 1940; Logan *et al.*, 1958; Al-Shammeri and Saleh, 1986; Vajo *et al.* 1986; Bozso *et al.* 1977; Löffler and Schmidt, 1976]. The mechanism of ammonia dissociation on different metals have been widely studied [Löffler and Schmidt, 1976; Lotz and Sebba, 1957; Nandy and Lenz, 1984]. However, there is no sufficient information regarding the NH_3 dissociation on 316 stainless steel. Because iron is the major element in 316 stainless steel, as shown in Table 3.1, the process of ammonia dissociation on stainless steel may be very similar to that on iron.

The mechanism of ammonia dissociation on iron is basically referred to as [Ertl and Huber, 1980]:

$$NH_{3,\,(g)} \rightleftarrows NH_{3,\,ad} \rightleftarrows NH_{2,\,ad} + H_{ad} \rightleftarrows NH_{ad} + 2\,H_{ad} \rightleftarrows N_s + 3\,H_{ad}$$

For desorption,

$$2\,H_{ad} \rightleftarrows H_{2\,(g)}$$

$$2\,N_s \rightleftarrows N_{2\,(g)}$$

N_s represents the surface nitride phase, a form of adsorbed or dissolved nitrogen near the surface. It has been found that an iron-nitride phase that has formed in the bulk of iron is thermodynamically stable only at temperatures below about 1000 K [Fast, 1965]. However, a surface nitride phase may be established even before the bulk nitride phase is stabilized [Löffler and Schmidt, 1976]. Ertl and Huber [1980] found the desorption of nitrogen into the gas phase was the slowest step in the process at low temperatures (< 710 K). The kinetics of nitrogen desorption was ascribed to the decomposition of surface nitride, the reaction rate of which would follow the first order with respect to the concentration of N_s.

However, when the operating temperature is high enough, the surface adsorption of NH_3 becomes difficult, and limits the process of dissociation, which suggests that the process is controlled by the adsorption of NH_3 onto the surface of iron [Ertl and Huber, 1980]. The apparent reaction rate may be proportional to ammonia concentration in the gas phase.

Based upon the mechanism of ammonia dissociation on the surface of iron described above, one may expect a similar mechanism for the NH_3 dissociation on 316 stainless steel. The operating temperature in this system is high enough so that the limiting step of ammonia dissociation may be the adsorption of NH_3 onto the surface of stainless steel. The rate expression for the catalytic NH_3 dissociation in this study is then expected to be the first order with respect to the gas-phase ammonia concentration in the bed.

In the fluidized bed of 316 stainless steel powder, the fluidizing-gas superficial velocity is low enough so that the thermal dissociation of NH_3 in the system is in considerable quantity. The dissociation of ammonia in this study is considered to take place through two paths: the thermal reaction and the catalytic reaction. Ammonia is dissociated not only on the surface of stainless steel powder, but also in the gas phase of the reactor. In this study, the two paths of ammonia dissociation are assumed to be independent of each other. In the following sections, the thermal dissociation of ammonia is first investigated without stainless steel powder. A kinetic equation obtained for the thermal dissociation is then applied to the overall dissociation of ammonia to find the kinetic rate constant for the catalytic dissociation of ammonia

when stainless steel powder is fluidized. A final overall rate equation for the ammonia dissociation will then be proposed.

4-1-2 Study of Thermal Dissociation

The thermal dissociation of NH_3 is defined as the dissociation of ammonia in the bed without the presence of stainless steel powder. As one may expect, the sintered-silica distributor of the bed may also provide a place for the dissociation of ammonia, which may be different from the gas-phase thermal dissociation. However, because of the very small volume of distributor in the bed, this part of dissociation will be included in the gas-phase study.

4-1-2-1 Development of Rate Equation

A plug flow reactor is assumed to study the kinetics of homogeneous ammonia dissociation. At steady state, the performance equation for gas phase reaction is expressed as [Levenspiel, 1972]:

$$\frac{V}{F_A} = \int_{X_{Ai}}^{X_{Af}} \frac{dX_A}{-r_A} \qquad (4.1)$$

Here, subscript A represents ammonia. X_A represents the extent of conversion of ammonia dissociation; X_{Ai} and X_{Af} are the inlet and outlet fractions of dissociated ammonia in the bed, respectively. F_A is the molar feed rate of ammonia, and V is the volume of the empty reactor. The dissociation rate is presumed to be a function of ammonia concentration only. Assuming a power law gives

$$-r_A = k_{homog}\, C_A^{\,n} \tag{4.2}$$

where k_{homog} represents the rate constant for the homogeneous thermal dissociation of ammonia.

Substituting Equation (4.2) into Equation (4.1) yields two unknown parameters, n and k_{homog}. The reaction rate constant, k_{homog}, is a function of operating temperature while reaction order, n, may be assumed to be constant when the range of temperature is not large. In addition, if the amount of NH_3 dissociation is small, the concentration of ammonia may be assumed roughly constant along the direction of flow. The reaction rate can then be assumed to be uniform, according to Equation (4.2). Therefore, Equation (4.1) can be easily integrated and rearranged to yield

$$-r_{A,\,AVG} = \frac{X_{Af} - X_{Ai}}{\left(\frac{V}{F_A}\right)} \tag{4.3}$$

This is called the differential-flow reactor analysis, which may be applied to any reaction with low extents of conversion (practically less than 10%).

From a series of runs using different ammonia inlet concentrations (adjusted by inert gas, such as Ar) at a fixed low temperature, a set of rate v.s. concentration data can be obtained from Equation (4.3). Rearranging Equation (4.2) gives the relationship between the reaction rate and concentration as

$$\ln\left(-r_{A,\,AVG}\right) = \ln\left(k_{homog}\right) + n \ln\left(C_{A,\,AVG}\right) \tag{4.4}$$

Hence, the reaction order may easily be determined by the slope of log-log plot of average rates against average concentration data.

However, this method is appropriate only when the conversion is low. If the conversion is high, Equation (4.1) has to be directly integrated. Thus, after the reaction order is determined from the low extent conversion data at low operating temperatures, the rate equation is applied to high conversion data to evaluate the rate constant k_{homog} at high temperatures directly through the integration of Equations (4.1) and (4.2).

Because of the volume expansion due to ammonia dissociation, the fractional change in the system volume (ε_A) has to be considered. According to the stoichiometry of ammonia dissociation, there is an increase of one mole of gas per mole of ammonia dissociated.

$$NH_3 \rightleftharpoons \frac{1}{2} N_2 + \frac{3}{2} H_2 \tag{4.5}$$

The volume change may be proportional to molar change, according to the ideal gas law. The fractional change in volume of the system can be calculated as

$$\epsilon_A = \frac{(f_{inert} + 2) - (f_{inert} + 1)}{(f_{inert} + 1)} = \frac{1}{(f_{inert} + 1)} \tag{4.6}$$

where f_{inert} means the volume ratio of inert gas to ammonia in the inlet stream.

The concentration term may then be expressed, with the consideration of volume change, as

$$C_A = C_{A0} \left(\frac{1 - X_A}{1 + \epsilon_A X_A} \right) \tag{4.7}$$

Hence, the rate expression of Equation (4.2) can be rearranged as,

$$- r_A = k_{homog} C_A^n = k_{homog} C_{A0}^n \left(\frac{1 - X_A}{1 + \epsilon_A X_A} \right)^n \quad (4.8)$$

where C_{A0} is the concentration of ammonia introduced into the system. Substituting Equation (4.8) into Equation (4.1) and rearranging yield,

$$k_{homog} = \frac{F_A}{V C_{A0}^n} \int_{X_{Ai}}^{X_{Af}} \left(\frac{1 + \epsilon_A X_A}{1 - X_A} \right)^n dX_A \quad (4.9)$$

Therefore, reaction rate constant k_{homog} can be evaluated from Equation (4.9) at different operating temperatures. The apparent activation energy of reaction can be determined by the plot of $\ln(k_{homog})$ versus 1/T. The next section will illustrate measured results.

4-1-2-2 Experimental Results

Figure 4.1 shows the fractional NH_3 dissociation right before entering the fluidized bed, when 100% of NH_3 was supplied. Even when pure NH_3 was supplied into the reactor, the actual fluidizing gas was no longer pure NH_3 because of its partial dissociation in the entrance region before entering the bed. However, the amount of ammonia dissociation seems to be uniform at each operating temperature. Figure 4.2 presents the extents of ammonia dissociation in the empty bed, 9 cm above the distributor, at different operating temperatures. A stable dissociation rate is also observed at each temperature. Hence, a constant value of the extent of ammonia dissociation at each temperature is obtained by averaging the measured results. Table 4.1 shows a series of runs with different ammonia inlet concentrations at an operating

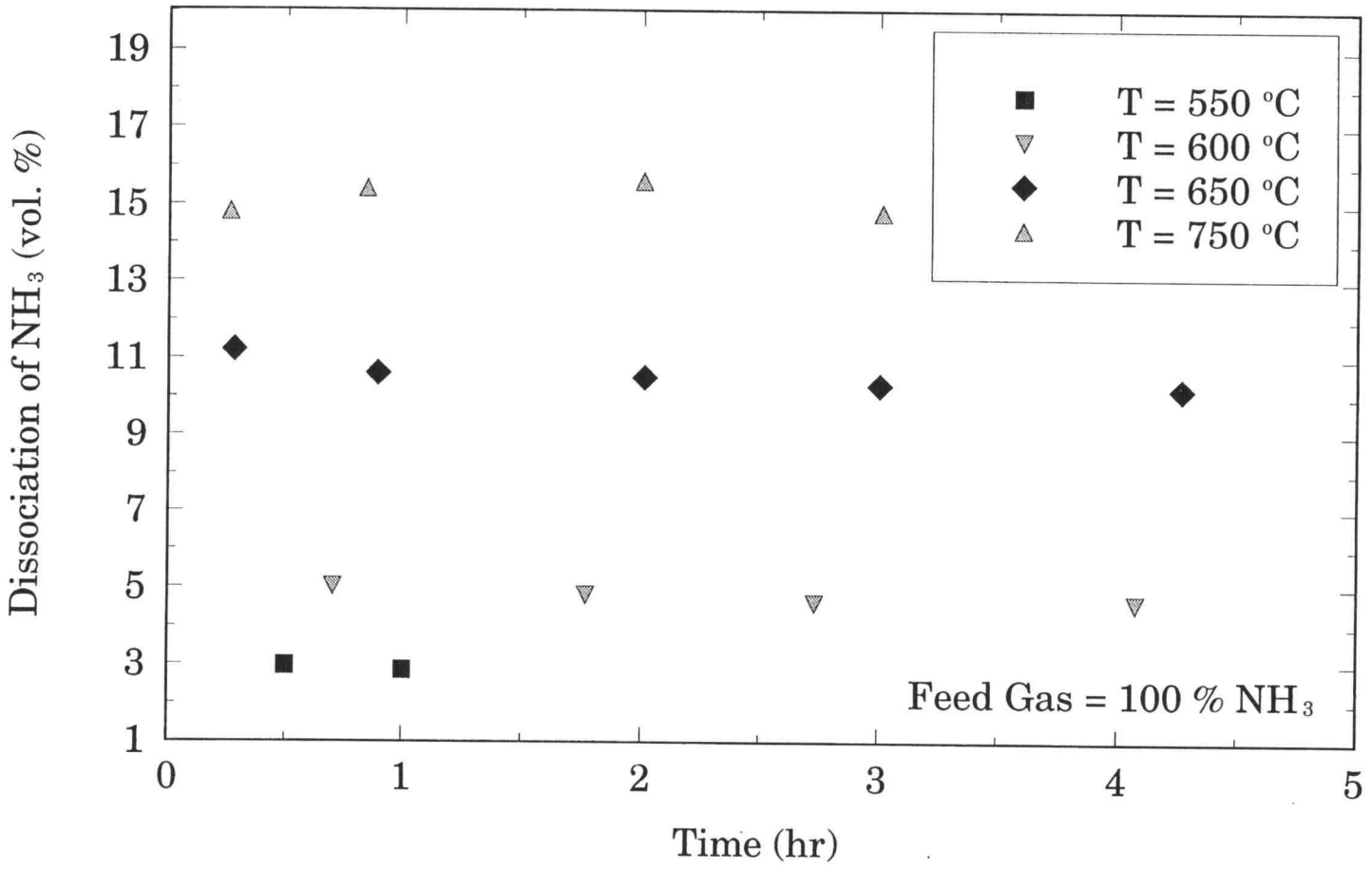

Figure 4.1 Fractions of NH_3 dissociated before entering the distributor

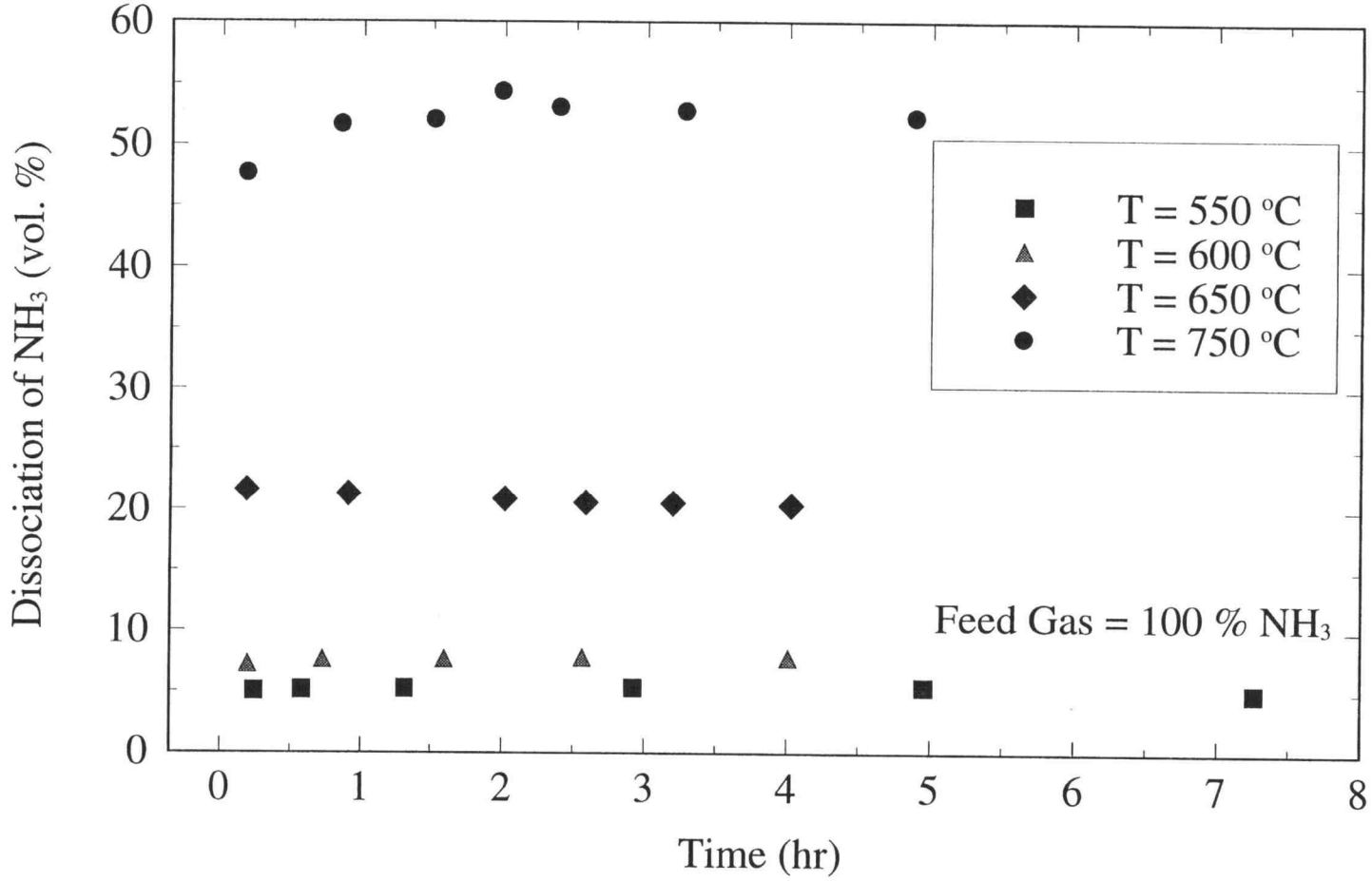

Figure 4.2 Fractions of NH_3 dissociated after leaving the empty bed

Table 4.1 Differential flow analysis of ammonia thermal dissociation at 550 °C

$(NH_3)_0$ $(cm^3/min)^{\#}$	Ar $(cm^3/min)^{\#}$	X_{Ai}^{*}	$X_{Af}^{\&}$	P (mm-Hg)	$-r_{A, AVG}$ $(mol/cm^3/min)$	$C_{A, AVG}$ (mol/cm^3)
4216	0	0.029	0.052	806.1	1.86 E-05	1.37 E-05
2433	1663	0.0294	0.0592	819.4	1.42 E-05	8.33 E-06
1464	2525	0.0431	0.0797	825.3	1.05 E-05	5.11 E-06
701	3280	0.0543	0.1083	830.2	7.49 E-06	2.43 E-06

: Based on room temperature.

* : The extent of ammonia dissociation before entering the bed (right before reaching the distributor).

& : The extent of ammonia dissociation measured at 9 cm above the distributor.

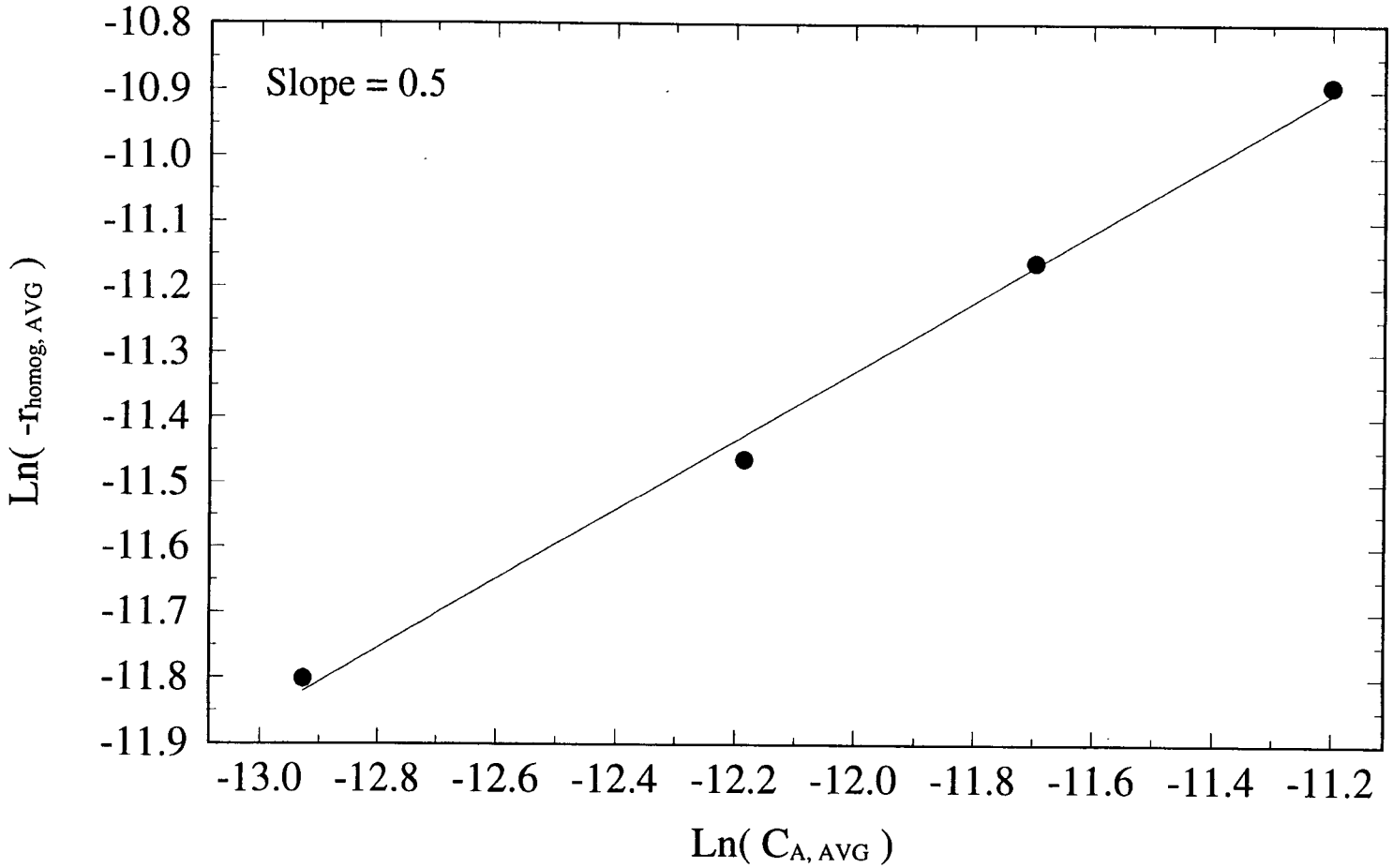

Figure 4.3 Log-log plot of average reaction rates against NH_3 concentration in the empty bed

temperature of 550 °C. One should be aware that the amount of ammonia dissociation is small enough for each case. Equations (4.3) and (4.4) may be applied here to determine the reaction order for the thermal dissociation. Figure 4.3 suggests that the reaction order is approximately 0.5 at 550 °C. The reaction order smaller than one implies that the process in the quartz tube is not the simple thermal decomposition of ammonia, which should be proportional to the ammonia concentration. Some intermediate products may be involved in the process. However, to understand the actual mechanism is beyond the purpose of this study. An appropriate kinetic equation to represent the ammonia dissociation in the bed may be more practical for this research.

The rate constant k_{homog} can be calculated from Equation (4.9) at different operating temperatures in the feed gas of 100% NH_3, as shown in Table 4.2. The apparent activation energy of the ammonia thermal dissociation is evaluated to be 109.9 kJ/mol, based on the plot of $\ln(k_{homog})$ v.s. 1/T as shown in Figure 4.4. Therefore, the rate equation for ammonia thermal dissociation in the empty bed of quartz reactor tube is concluded as below:

$$-r_{homog} = 3.6\times10^4 \, e^{\left(\frac{-109.9}{RT}\right)} \, C_{A0}^{0.5} \left(\frac{1 - X_A}{1 + \epsilon_A X_A}\right)^{0.5} \left(\frac{mole}{cm^3 \, min}\right) \quad (4.10)$$

where the pre-exponential factor, 3.6×10^4, has units of $mol^{0.5}/cm^{1.5}/min$, and the gas constant R is equal to 8.314×10^{-3} kJ/mol/K. Note that ε_A is defined by Equation (4.6) and equal to 1 when 100% NH_3 is introduced.

4-1-2-3 Study of Entrance Region

Because the bed is located at the center of the furnace (see Figure 3.4), ammonia is dissociated even before entering the bed, as represented by X_{Ai}, in Table 4.1. An appropriate equation must be derived to estimate the extent of ammonia

Table 4.2 Calculation of k_{homog} values at different temperatures

Temperature (°C)	$(NH_3)_o$ (cm^3/min)	P (mm-Hg)	X_{Ai}	X_{Af}	Area# = $\int_{X_{Ai}}^{X_{Af}} (\frac{1 + X_A}{1 - X_A})^{0.5} dX_A$	k_{homog} ($mol^{0.5}/cm^{1.5}$/min)
550	4216	806.1	0.029	0.052	0.02395	0.004895
600	3916	806.6	0.046	0.0771	0.03308	0.006469
650	3665	806.6	0.104	0.2057	0.1142	0.002149
700	3435	809	0.133	0.328	0.2486	0.04510
750	3250	813.4	0.15	0.529	0.5469	0.09649

: $\varepsilon_A = 1$ with the feed of pure NH_3.

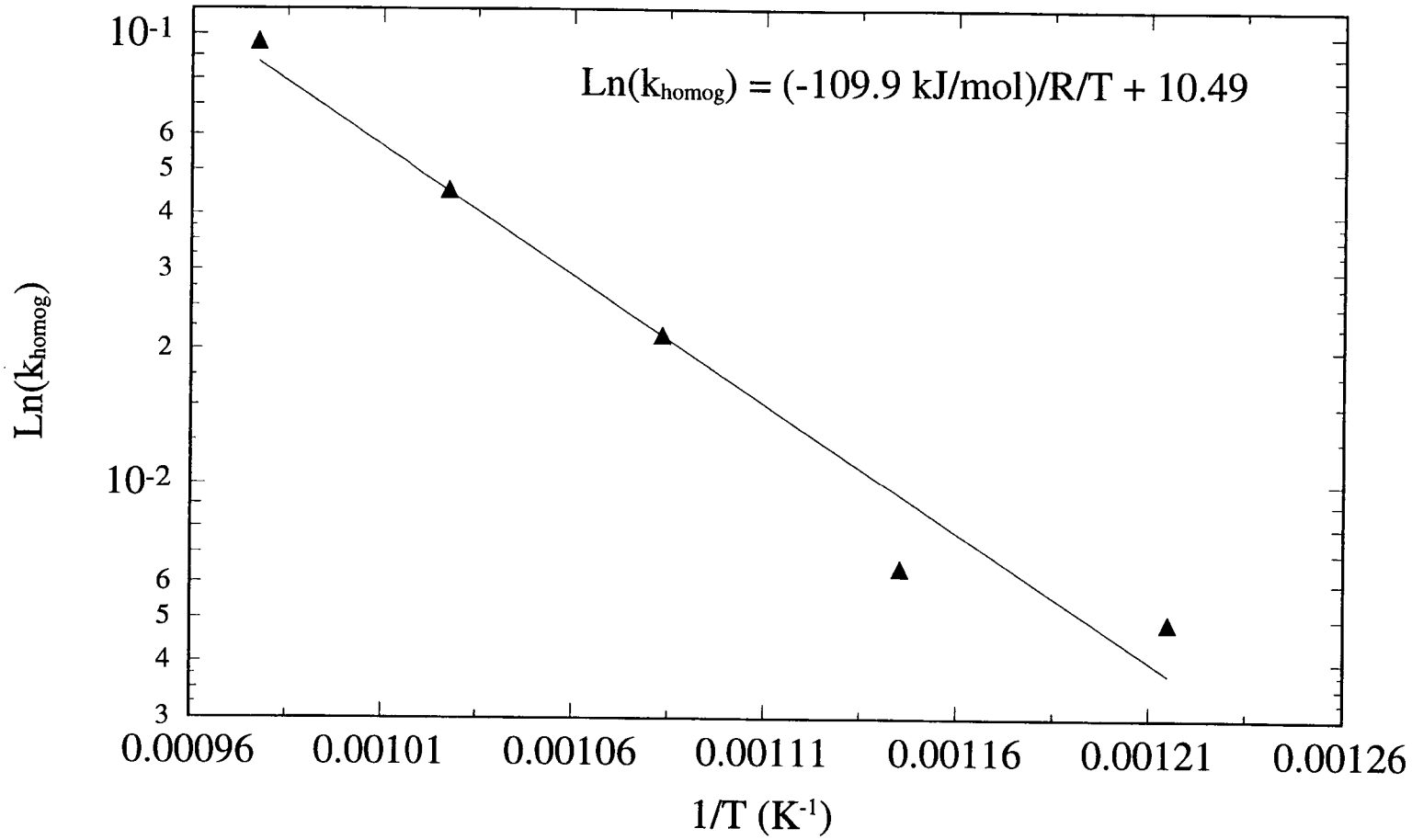

Figure 4.4 Plot of $\ln(k_{homog})$ v.s. 1/T for NH_3 dissociation in the empty bed

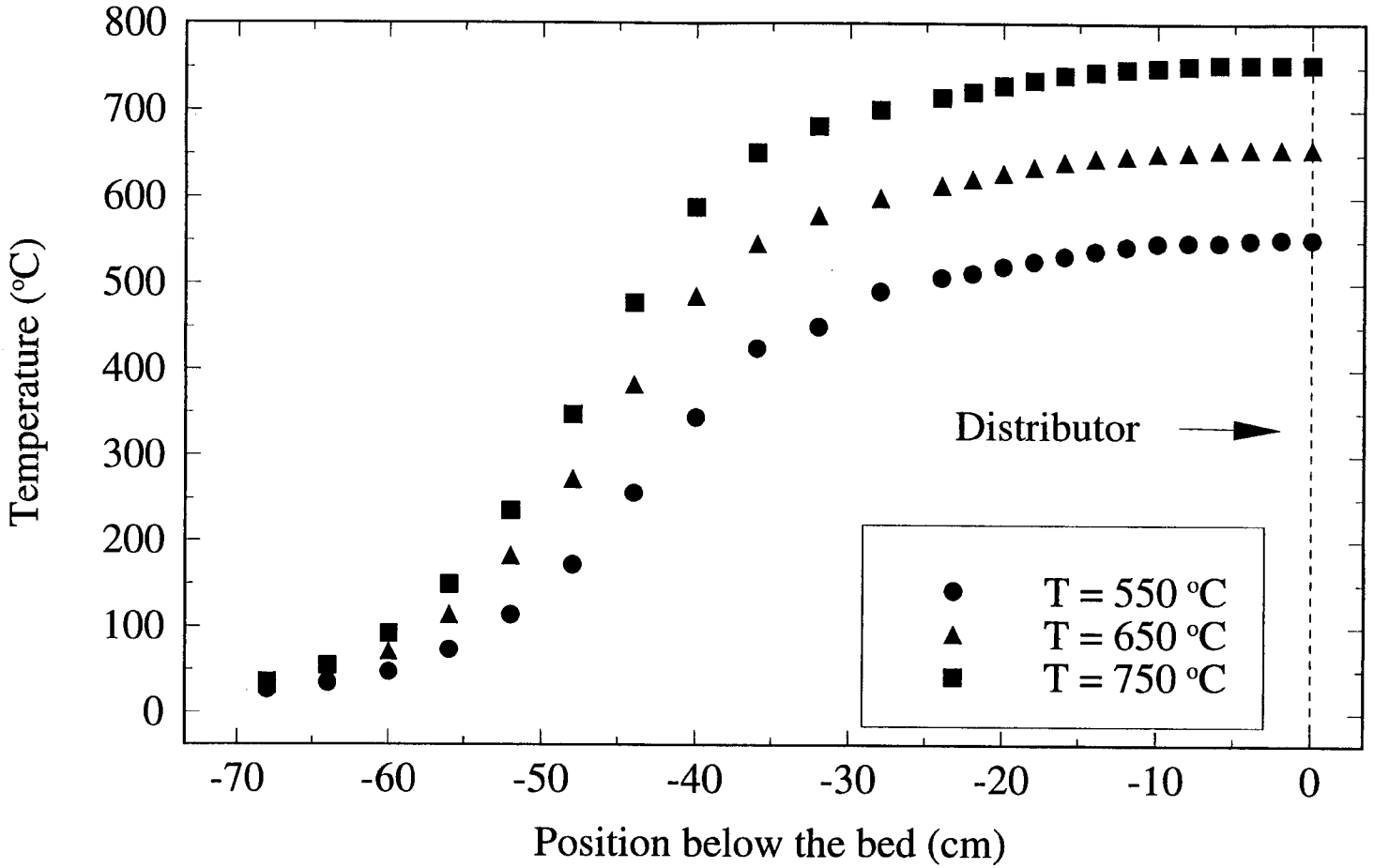

Figure 4.5 Temperature gradients in the entrance region at different operating temperatures

dissociation in the entrance region for the further calculation of gas concentration in the bed. Figure 4.5 shows the measurement of the temperature gradient in the entrance region (below the distributor). Although the dissociation of NH_3 in this region may be consequent upon the thermal dissociation as described above, the rate of reaction would vary with the location because of the temperature variation. It is hence difficult to derive an exact kinetic equation to describe the dissociation of NH_3 in this region.

Because the extents of ammonia dissociation are small in this region (according to Table 4.1), the following simple form may be derived from Equation (4.3) to estimate the dissociation of NH_3 after the entrance region, $X_{Af,\ entc}$, which is represented by X_{Ai} in the preceding section. The majority of NH_3 dissociation in the entrance region may be considered to take place in the region of about 25 cm below the distributor, where the temperature deviation is as much as about 50 °C from the set point. One may assume that no NH_3 dissociation takes place below this region because of a rapid decrease in temperature, as indicated in Figure 4.5. Therefore, the equation to express the dissociation of NH_3 in the entrance region is given as

$$X_{Af,\ entc} = (-r_{A,\ AVG}) \left(\frac{V}{F_A}\right) = k_{AVG}\ C_{A0}^{0.5} \left(\frac{V}{F_A}\right) \qquad \textbf{(4.11)}$$

where k_{AVG} is approximated by an average rate constant for the thermal dissociation of NH_3 over the temperature variation in the entrance region. The ammonia concentration in the feed gas, C_{A0}, is used here because of the low extent of NH_3 dissociation in this region. Notice that NH_3 does not dissociate before entering the entrance region. For different NH_3 inlet concentrations, the extent of NH_3 dissociation may be approximately proportional to the square root of NH_3 concentration in the feed gas and inversely proportional to the molar feed rate of NH_3 at operating temperature.

Equation (4.11) can be simply tested with experimental data given in Table 4.2. The finding of activation energy for ammonia thermal dissociation implies that the rate constant will be decreased by a factor of 2 to 3 for every decrease of 50 °C. On the

other hand, according to Figure 4.5, the reactor volume of the entrance region is about 2.6 times larger than the volume of the empty bed studied in the preceding section. By taking into account these two factors in Equation (4.11), the extent of conversion of ammonia thermal dissociation in the entrance region will be closed to that in the empty bed, if the extent of ammonia dissociation is small. Table 4.2 shows that the extent of ammonia dissociation in the bed (the difference between X_{Af} and X_{Ai}) is approximately equal to that in the entrance region (X_{Ai}) at low temperatures, at which the dissociation of ammonia is low. It is thus implied that the estimated activation energy, calculated from the preceding section, shows a consistent agreement in the entrance region. Therefore, Equation (4.11) seems to be appropriate to be used in the entrance region.

However, at temperatures above 700 °C the extent of ammonia dissociation in the bed becomes larger than that in the entrance region. It is suggested that some other factors, such as contribution of the distributor to the ammonia thermal dissociation, becomes significant with an increase in the processing temperature. However, the effect of ammonia dissociation by the distributor will not be considered in this study.

4-1-3 Study of Catalytic Reaction

The performance rate equation for the catalytic dissociation of ammonia in the bed of 316 stainless steel powder may be expressed as

$$\frac{W}{F_A} = \int_{X_{Ai}}^{X_{Af}} \frac{dX_A}{-r'_A} \qquad (4.12)$$

where W is the mass of catalyst, and the reaction rate, $-r'_A$, is based on the mass of catalyst powder, i.e., 316 stainless steel powder in the bed. In addition, as discussed

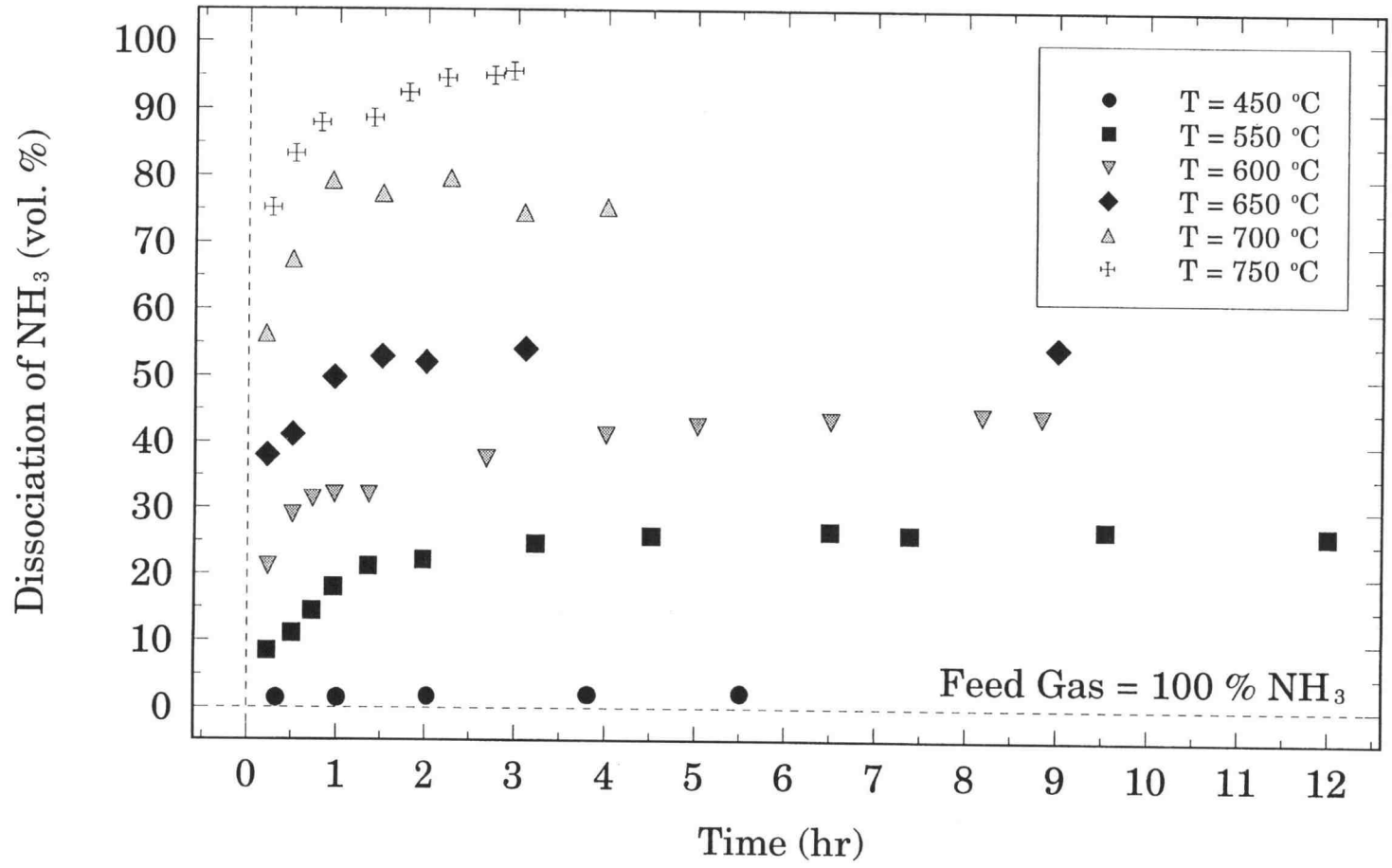

Figure 4.6 Fractions of NH_3 dissociated by the fluidizing bed of 316 stainless steel

in section 4-1-1, the reaction rate is suspected to be of the first order with respect to ammonia concentration. Thus,

$$- r_A' = k'_{cat} C_A \tag{4.13}$$

where k'_{cat} represents the catalytic rate constant based on unit catalyst mass.

Figure 4.6 illustrates fractions of NH_3 dissociation at different operating temperatures, measured at the location 9 cm above the distributor, which is estimated to be slightly above the fluidizing bed of 316 stainless steel powder. It should be mentioned that the fraction of NH_3 dissociated in the bed of stainless steel powder is time dependent initially. Because the dissociation of NH_3 in the empty bed is stable, as indicated in Figures 4.1 and 4.2, the time variation of NH_3 dissociation is attributed to its contact with stainless steel powder. The initial increase in NH_3 dissociation may be related to the surface morphological transformation of stainless steel powder in the nitridation process, that will be discussed later. Because the catalytic dissociation is always combined with thermal dissociation, the rate of the catalytic dissociation of NH_3 can not be analyzed independently in this study. Hence, an overall rate equation, combining thermal and catalytic dissociation, is introduced with the suggested reaction order for catalytic dissociation. Thus, the rate constant of catalytic rate equation may be estimated from experimental data.

The measurements shown in Figure 4.6 represent the overall NH_3 dissociation in the bed, containing both the thermal and catalytic dissociation. These two processes of NH_3 dissociation may be expressed based upon unit mass of catalyst powder in the following form [Levenspiel, 1993].

$$- r'_{overall} = (- r'_{cat}) + (\frac{V_{void}}{W_{cat}}) (- r_{homog}) \tag{4.14}$$

where V_{void} represents the void volume in the fluidized 316 stainless steel powder, and W_{cat} is the mass of powder in the bed.

The rate equation for homogeneous dissociation of NH_3 has been obtained as Equation (4.10). The performance equation for the overall reaction may be represented in the form similar to Equation (4.12).

$$\frac{W}{F_A} = \int_{X_{Ai}}^{X_{Af}} \frac{dX_A}{-r'_{A,\,overall}} \tag{4.15}$$

Combining Equations (4.10), (4.13), (4.14) and (4.15), yields the overall kinetic rate equation for ammonia dissociation in the fluidized bed of 316 stainless steel powder as

$$\frac{W}{F_A} = \int_{X_{Ai}}^{X_{Af}} \frac{dX_A}{k'_{cat} C_A + \frac{V_{void}}{W} k_{homog} C_A^{0.5}} \tag{4.16}$$

where C_A is given by Equations (4.7) and (4.6), and k_{homog} is estimated by Equation (4.10). One may notice that the only one parameter, k'_{cat}, is unknown in Equation (4.16). Therefore, the catalytic rate constant, k'_{cat}, can be obtained from experimental data by the parameter-search method.

4-1-4 Estimated Overall Rate Equation

As illustrated in Figure 4.6, there are two states of NH_3 dissociation observed in the measurements: an initial unsteady state and a final steady state. An attempt is

Table 4.3 Calculation of k'_{cat} values from the overall reaction data, Equation (4.15)

Status	Temperature (°C)	$(NH_3)_0$ (cm^3/min)	P (mm-Hg)	X_{Ai}	X_{Af}	k'_{cat} # (cm^3/g/min)
Initial State*	550	4364	813.7	0.029	0.0843	1.174
	600	4002	817.1	0.046	0.211	3.90
	650	3751	820.8	0.104	0.38	8.31
	700	3620	811	0.133	0.563	22.22
	750	3440	806.2	0.15	0.752	29.20
Steady State*	550	4364	819.6	0.029	0.263	10.83
	600	4002	824.9	0.046	0.44	21.59
	650	3751	828.9	0.104	0.541	26.45
	700	3620	830	0.133	0.75	61.81
	750	3440	832.3	0.15	0.951	141.0

* : The mass of stainless steel powder reduced from 500 g at the initial state to 450 g at the steady state.

: Calculated values.

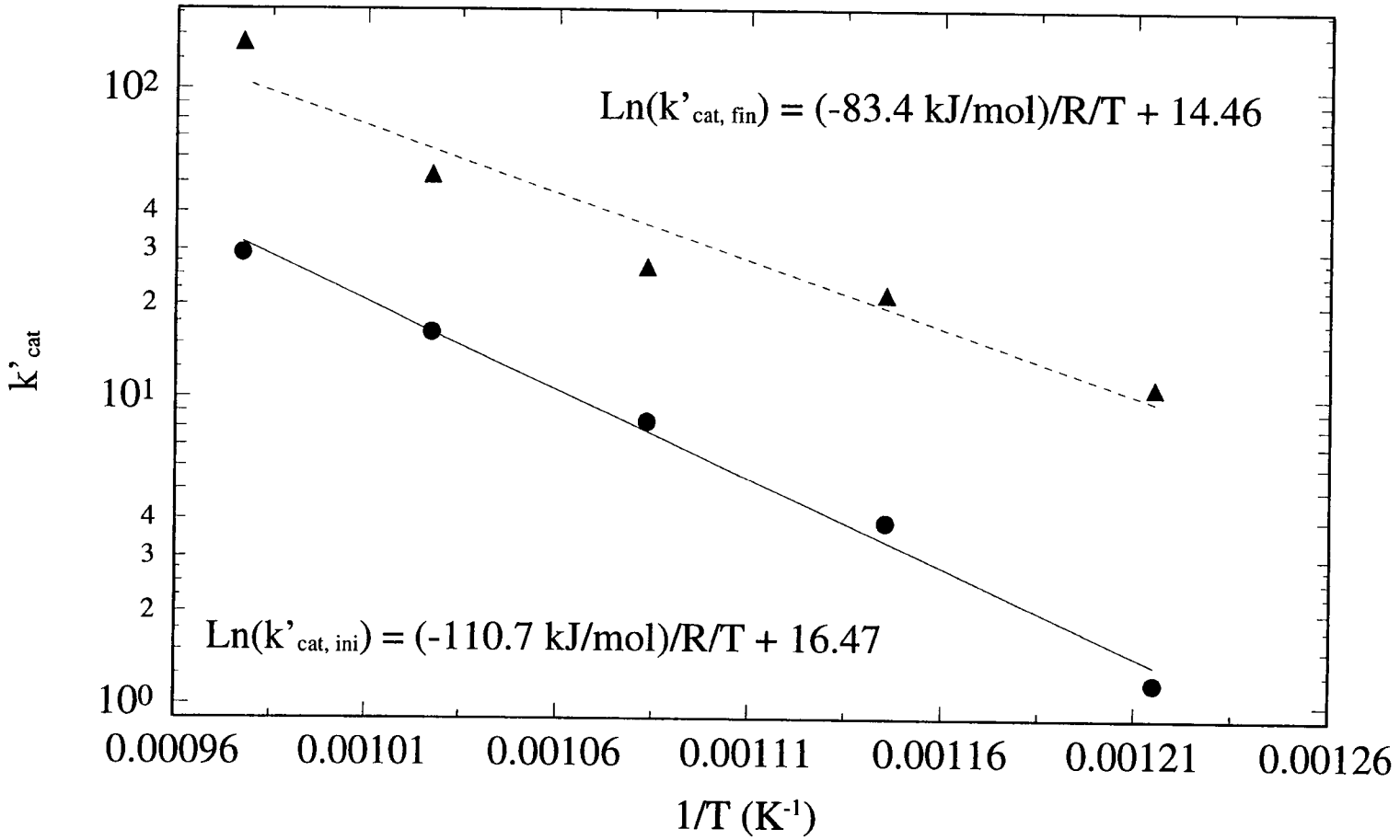

Figure 4.7 Plot of $\ln(k'_{cat})$ v.s. 1/T evaluated at the beginning and steady states

made here to determine the catalytic rate constants k'_{cat} for the very beginning state and the steady state thereafter. Table 4.3 shows the calculated results of rate constant k'_{cat} at different operating temperatures. The plot of $\ln (k'_{cat})$ v.s. 1/T, presented in Figure 4.7, gives apparent activation energies for both the beginning and steady states as 110.7 and 83.4 kJ/mol, respectively. These apparent activation energies are lower than literature values for the NH_3 dissociation at very low pressure on the metal iron surface, which lie between 146 and 209 kJ/mol [Logan *et al.* 1958; Löffler and Schmidt, 1976]. However, with an increase in temperature, the kinetics of NH_3 dissociation would change, leading to a decrease in activation energy. Ertl *et al.* [1980] have reported that the apparent activation energy may achieve zero for a well-prepared polycrystalline iron catalyst when reaction temperature reaches 800 K at a very low pressure of NH_3. Therefore, the apparent activation energies measured in this study seem to be reasonable.

Furthermore, the apparent activation energy measured in the beginning state is similar to the apparent activation energy obtained from the thermal dissociation, suggesting that the ammonia thermal dissociation may dominate the dissociation initially. The catalytic dissociation of NH_3 is enhanced in the process thereafter, showing a decrease in the apparent activation energy estimated at the steady state.

Finally, by combining the thermal and catalytic reactions, the overall NH_3 dissociation can be represented in the following two different forms.

(1) Beginning State

$$-r'_{overall,ini} = 1.43\times10^{7}\, e^{\left(-\frac{110.7}{RT}\right)} C_A + \left(\frac{V_{void}}{W_{cat}}\right) 3.6\times10^{4}\, e^{\left(-\frac{109.9}{RT}\right)} C_A^{0.5} \left(\frac{mole}{g\ \min}\right) \quad \textbf{(4.17)}$$

(2) Final Steady State

$$-r'_{overall,fin} = 3.38\times10^{6}\, e^{\left(-\frac{83.4}{RT}\right)} C_A + \left(\frac{V_{void}}{W_{cat}}\right) 3.6\times10^{4}\, e^{\left(-\frac{109.9}{RT}\right)} C_A^{0.5} \left(\frac{mole}{g\ \min}\right) \quad \textbf{(4.18)}$$

where C_A is calculated by Equations (4.7) and (4.6); V_{void} in cm^3 is the void volume in the bed, which is the difference between the reactor volume and the volume of powder; W represents the mass of 316 stainless steel powder in the fluidized bed. The apparent activation energy of ammonia thermal dissociation is 109.9 kJ/mol, while the apparent activation energies of catalytic dissociation for the beginning and steady states are 110.7 and 83.4 kJ/mol, respectively.

4-2 Nitridation in NH_3/ H_2/ Ar System

Understanding the ammonia dissociation in the fluidized bed makes it possible to study the nitridation of 316 stainless steel powder. This section will present the effects of operating temperature as well as ammonia and hydrogen average concentrations on the process.

4-2-1 Effect of Temperature

The effect of temperature on the nitridation of 316 stainless steel powder in terms of nitrogen contents varying with time is presented in Figure 4.8. Based on the observation, the nitridation progress may be divided into three stages: an induction stage, an enhanced nitridation stage, and a saturation stage.

During the induction stage (Figure 4.9), the increase in nitrogen content is approximately linear with time and independent of the operating temperature. After an

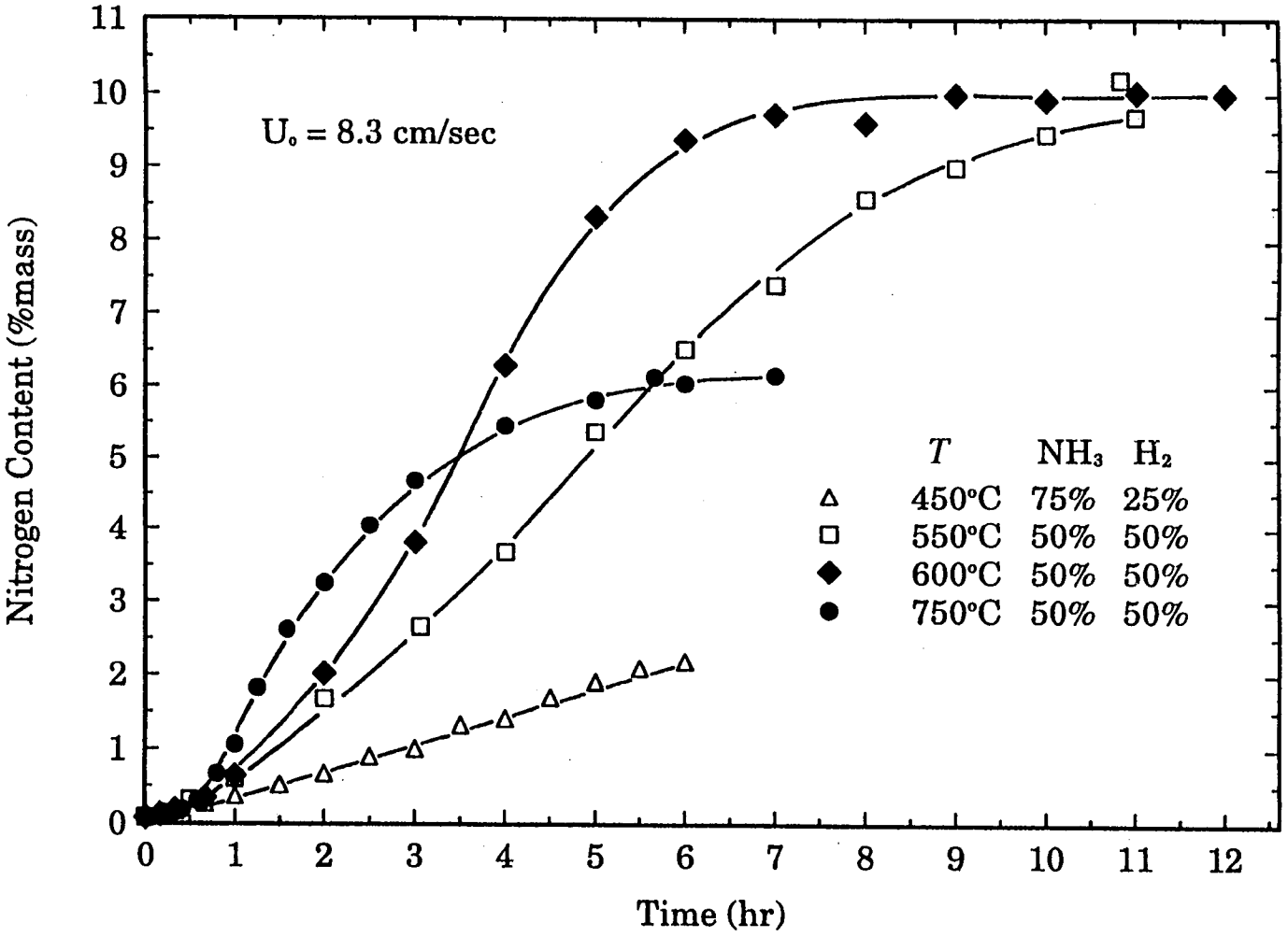

Figure 4.8 Effect of temperature on 316 stainless steel nitridation in the NH_3/ H_2 system

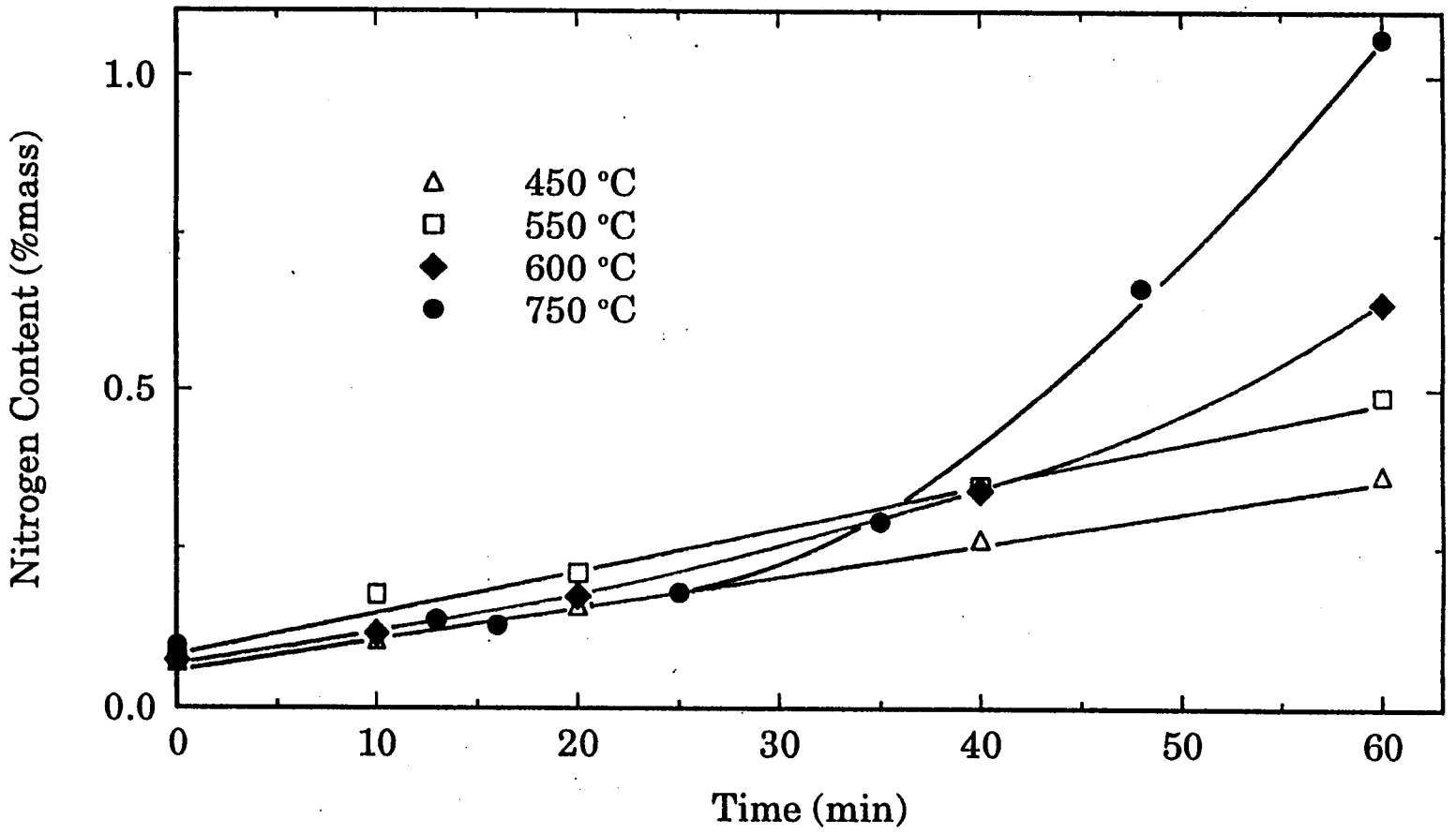

Figure 4.9 Close-up of the initial nitridation of 316 stainless steel in the NH_3/ H_2 system

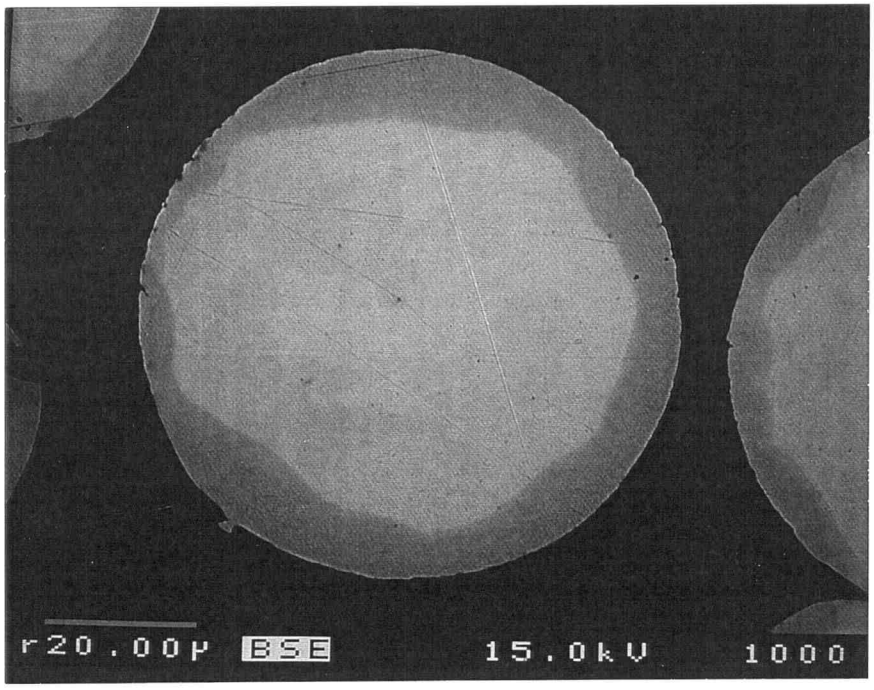

Figure 4.10 BSE image of a cross-sectioned particle, nitrided in the feed gas of 90% NH_3 and 10% H_2 at 550 °C for 90 min.

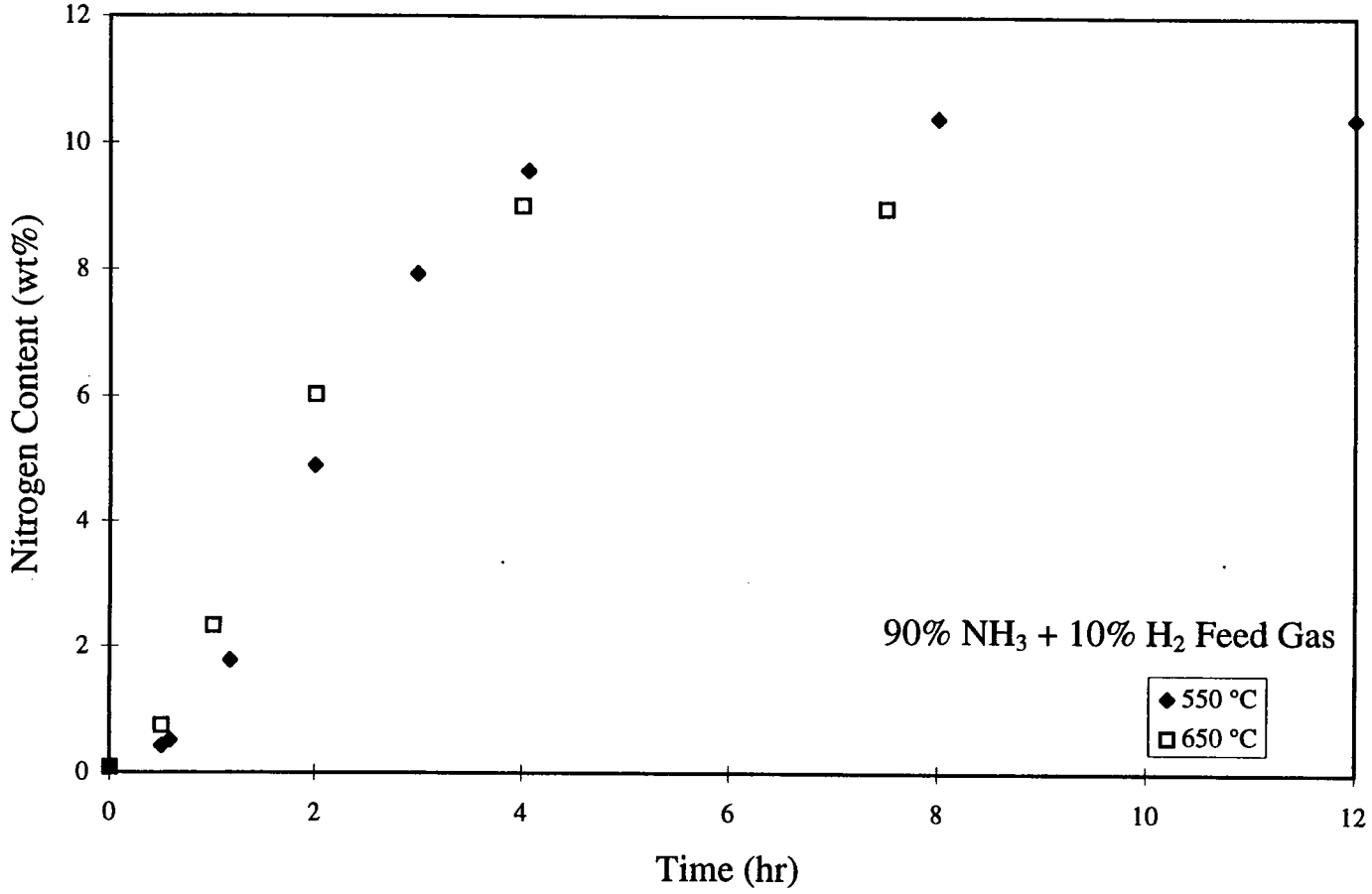

Figure 4.11 Comparison of nitridation at 550 and 650 °C in the feed gas of 90% NH_3 and 10% H_2

induction period, the nitriding process shifts to the enhanced nitridation stage. The higher the temperature, the shorter the induction period. During the early stage of nitrogen diffusion, nitrogen penetrates into the fcc-Fe as an interstitial solid solution. As soon as the concentration of nitrogen has reached a super-saturated level in the solid solution (fcc-Fe), the mechanism of nitrogen addition in the solid particle changes, leading to the formation of a new phase from the particle surface, as shown in Figure 4.10. This new phase development may lead to the enhanced nitridation stage.

As shown in Figure 4.8, an increase in the operating temperature increases the rate of nitridation during the enhanced nitridation stage. However, the level of nitrogen saturation in 316 stainless steel powder depends on the operating temperature. At 550 °C and 600 °C, the saturated nitrogen content is about 10% by mass, while at 750 °C it is about 6% by mass. It has been known that the saturated nitrogen content in stainless steel solid solution decreases with increasing operating temperature [Metals Handbook, 1973; Kikuchi *et al.* 1989]. However, the significant amount of nitrogen obtained in powder may come from the formation of new phases.

Furthermore, Figure 4.11 illustrates the nitrogen content versus processing time at temperatures of 550 °C and 650 °C in the feed gas of 90% NH_3 and 10% H_2. With an increase in NH_3 concentration, the induction period is significantly reduced, as indicated in the figure. The nitridation rate in the enhanced stage also increases with an increase in temperature. The level of saturated nitrogen content at 550 °C is found to be approximately equal to that at the temperature shown in Figure 4.8, suggesting that the final level of nitrogen content in the powder is strongly dependent on the processing temperature. In addition, the content of nitrogen in the saturation stage at 650 °C is about 9% by mass.

Figure 4.12 shows X-ray diffraction spectra of final nitrided powders obtained at three different operating temperatures of 550, 700 and 750 °C, with 100% NH_3 as the feed gas. At 550 °C, X-ray diffraction peaks indicate that Fe_4N and CrN phases are predominant in the final product. With an increase in operating temperature, the Fe_4N phase gradually decreases and eventually disappears in the product obtained at 750 °C. However, nitrogen dissolved in the interstitial fcc-Fe solid solution is still

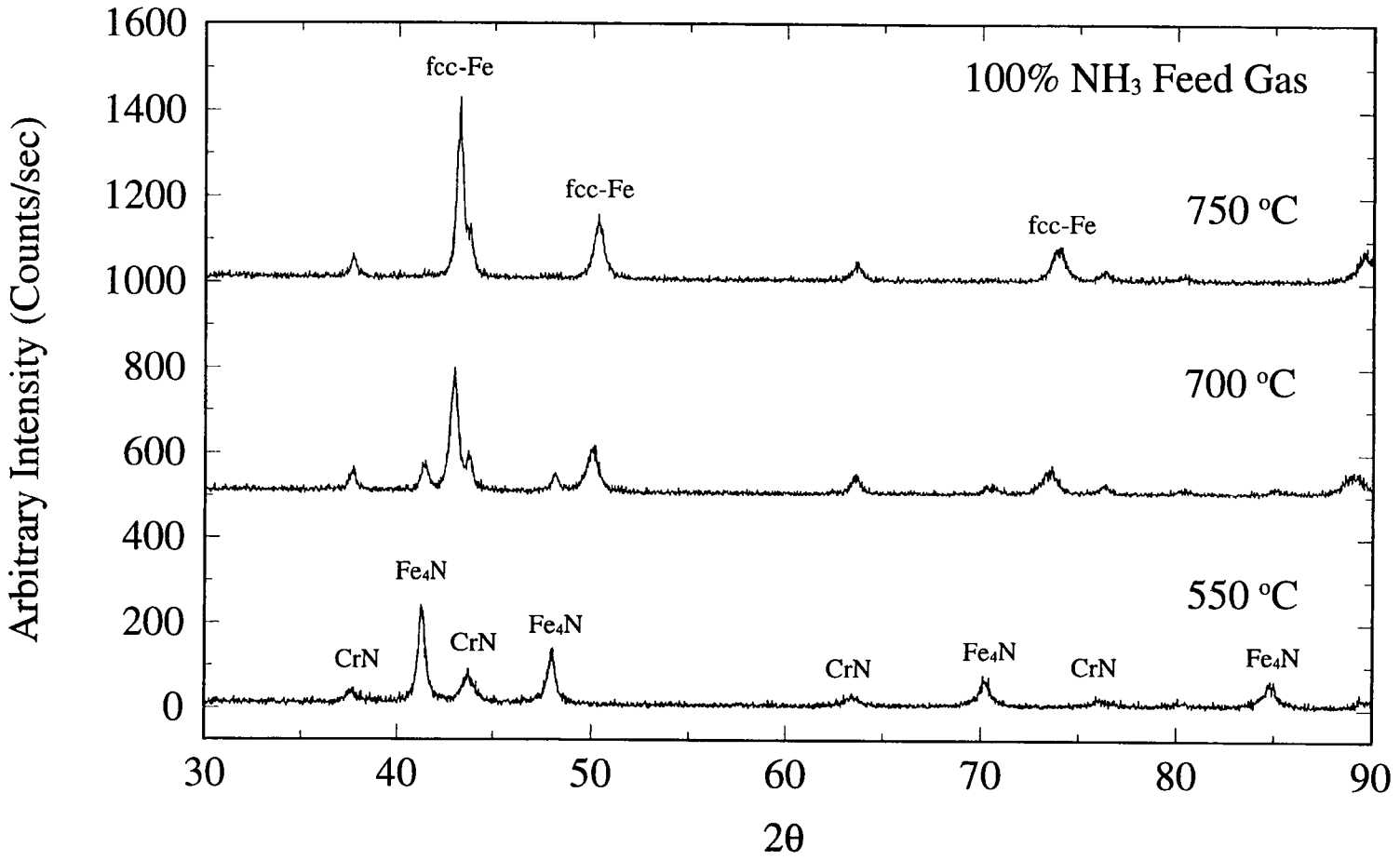

Figure 4.12 X-ray diffraction charts of final nitrided powder at T = 550, 700, and 750 °C

detected in the final powder. Hence, the Fe_4N phase in the stainless steel solid solution is unstable at temperatures higher than approximately 700 °C, as described by Fast [1965]. On the other hand, the CrN phase is found to be stable in the final nitrided powder within the range of operating temperature studied.

4-2-2 Effects of Ammonia and Hydrogen

As illustrated in section 4-1, the actual ammonia concentration in the fluidized bed can be estimated when operating conditions are known. The concentration of ammonia in the bed changes with the vertical location in the bed. However, based on the fluidizing condition monitored by the standard deviation of bed pressure-drop fluctuations, the bed is operated under the bubbling-bed condition, and hence particles are vigorously moving around in the bed. It is reasonable to assume that particles in the bed experience an average concentration of NH_3, although the gas flow is close to the plug flow with composition varying with its axial location [Kunii and Levenspiel, 1991]. One may introduce a log-mean of concentration between the inlet and outlet of the bed as an average value of NH_3 concentration in the bed [Levenspiel, 1972].

As discussed in the next section, the nitridation process in nitrogen is much slower than that in the NH_3 system even at temperatures above 750 °C. Hence, the effect of N_2 in the nitridation process is not considered in the NH_3 system, though N_2 is produced from the dissociation of NH_3.

The actual gas composition in the fluidized bed can be estimated using the procedure described in sections 4-1-3 and 4-1-4. The outlet extent of ammonia dissociation is calculated by applying the ammonia dissociation rates given by Equations (4.17) and (4.18) in Equation (4.15). After finding the inlet and outlet values of gas concentration in the bed, two slightly different log-means of gas composition may be obtained for the beginning and steady states. An arithmetic average of the calculated log-means is used to represent the estimated gas composition in the present study. The detailed process to estimate the average gas composition in the bed is shown in Appendix A. Table 4.4 shows the calculated average values of

Table 4.4 Feed gas and Estimated average gas composition in bed at 550 °C

Feed Gas	Bed*
NH_3 - H_2 - Ar*	NH_3 - H_2 -N_2 - Ar
100 - 0 - 0	80.6 - 14.6 - 4.8 - 0
90 - 10 - 0	73.2 - 22.4 - 4.4 - 0
70 - 10 - 20	58.0 - 19.9 - 3.5 - 18.6
50 - 50 - 0	42.2 - 55.3 - 2.5 - 0
50 - 30 -20	42.2 - 36.3 - 2.5 - 19.0
50 - 10 - 40	42.2 - 17.3 - 2.5 - 38.0
30 - 10 - 60	25.8 - 14.6 - 1.6 - 58.0

* : Estimated average composition.

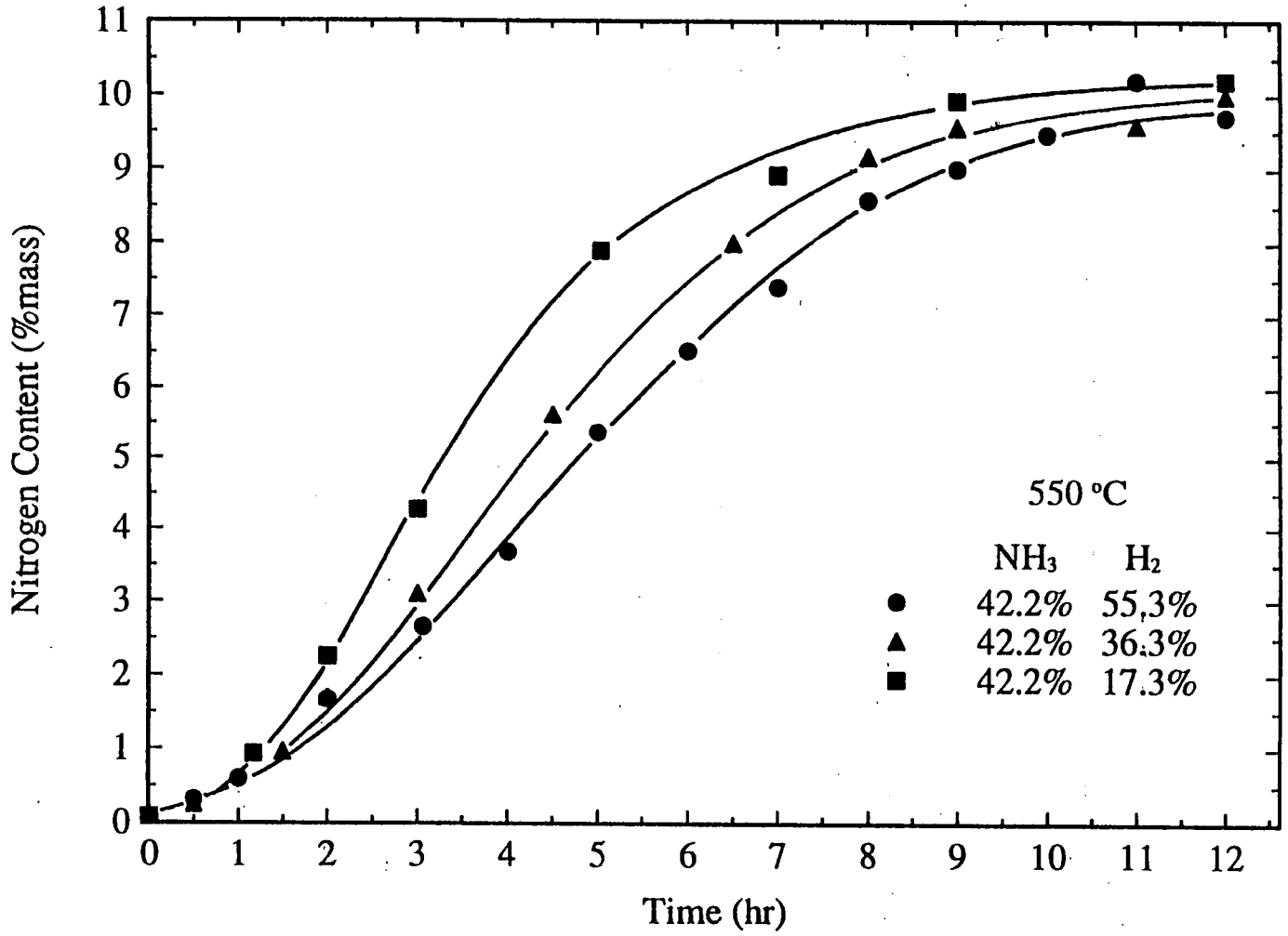

Figure 4.13 The effect of H_2 on the nitridation process at 550 °C at a fixed fraction of NH_3

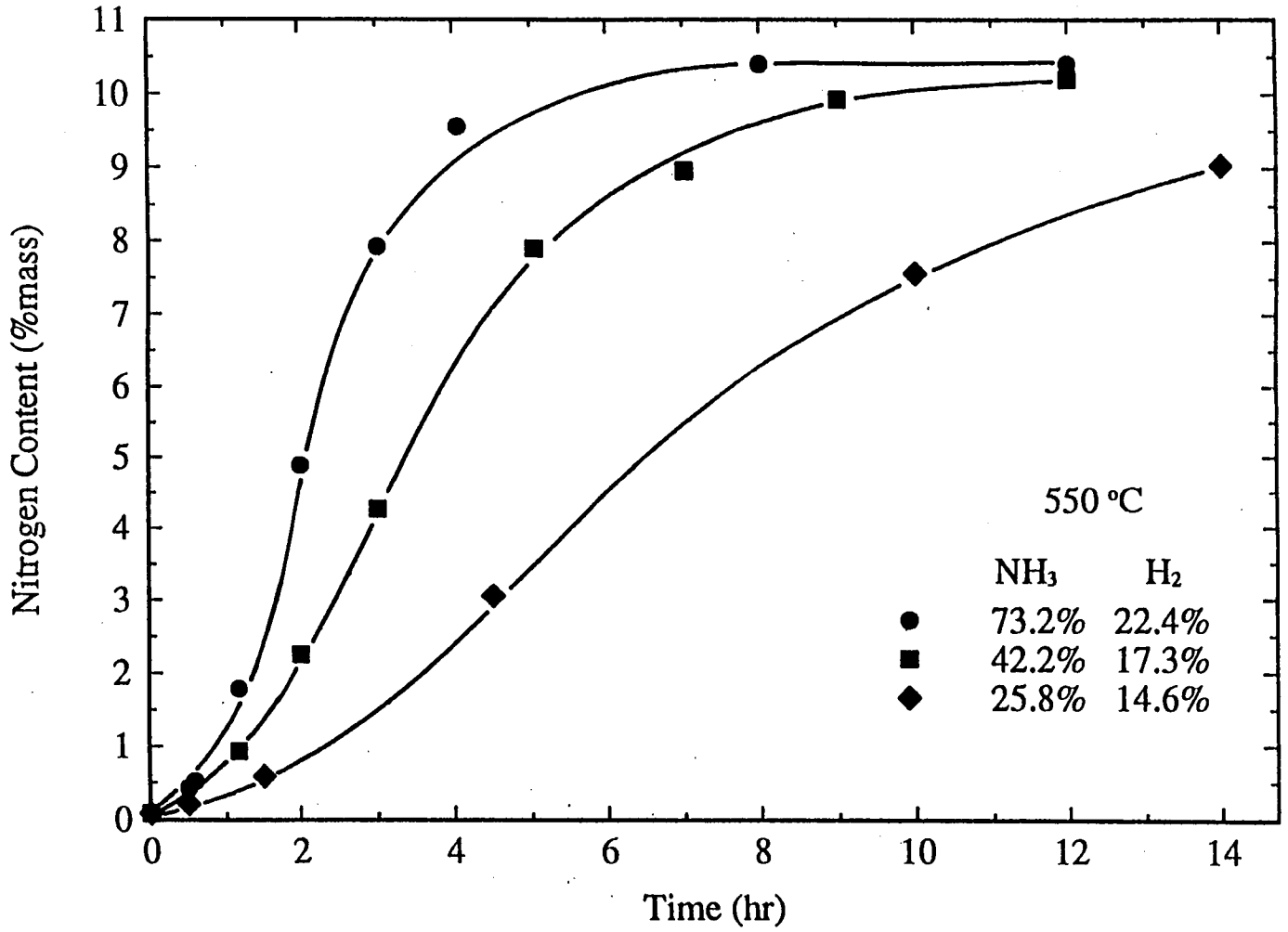

Figure 4.14 The effect of NH_3 on the nitridation process at a fixed fraction of H_2 in the feed gas

NH_3 and H_2 concentration in the fluidized bed for different values of inlet gas composition at 550 °C. Figure 4.13 shows the effect of hydrogen on the nitridation process at 550 °C when the volumetric fraction of NH_3 was fixed at 50% in the feed gas while the content of H_2 in the feed gas was changed to 50%, 30% and 10% with Ar as the balance. The corresponding estimated average hydrogen contents in the bed are 55.3%, 36.3% and 17.3% by volume while the estimated average ammonia concentration is fixed at about 42.2% by volume. It is indicated that the nitridation process is slowed by an increase in hydrogen concentration during the enhanced nitridation stage. The final nitrogen content in the stainless steel powder, however, seems not to be affected by hydrogen concentration. The higher the H_2 concentration, the longer the time for the complete nitridation. The effect of H_2 is not clear during the initial induction stage.

Figure 4.14 shows the results of nitridation when the feed H_2 concentration is fixed at 10% while the feed NH_3 contents are set at 90%, 50% and 30%, with balance Ar. The estimated average gas composition in the bed is shown in Table 4.4. Though the contents of H_2 are slightly different, the effect of this variation in the process is not important, as indicated in Figure 4.13. Hence, the nitridation process seems to be affected profoundly by NH_3 concentration, i.e., NH_3 enhances the nitridation process significantly. Figure 4.14 also shows that the initial induction time seems to decrease slightly with an increase in NH_3 concentration in the bed. Therefore, NH_3 concentration plays the major role in the nitridation process, not only in the enhanced nitridation stage but also in the initial stage. The quantitative estimation of the effect of gas composition on the initial induction period and the level of final saturated nitrogen content will be addressed in the next chapter.

4-3 Nitridation in N_2/ H_2/ Ar System

The study of nitridation process in the N_2/ H_2/ Ar system is discussed in this section. The effects of operating temperature and N_2 concentration are examined during the process. Katsura [1992] studied the reaction of iron metal with flowing

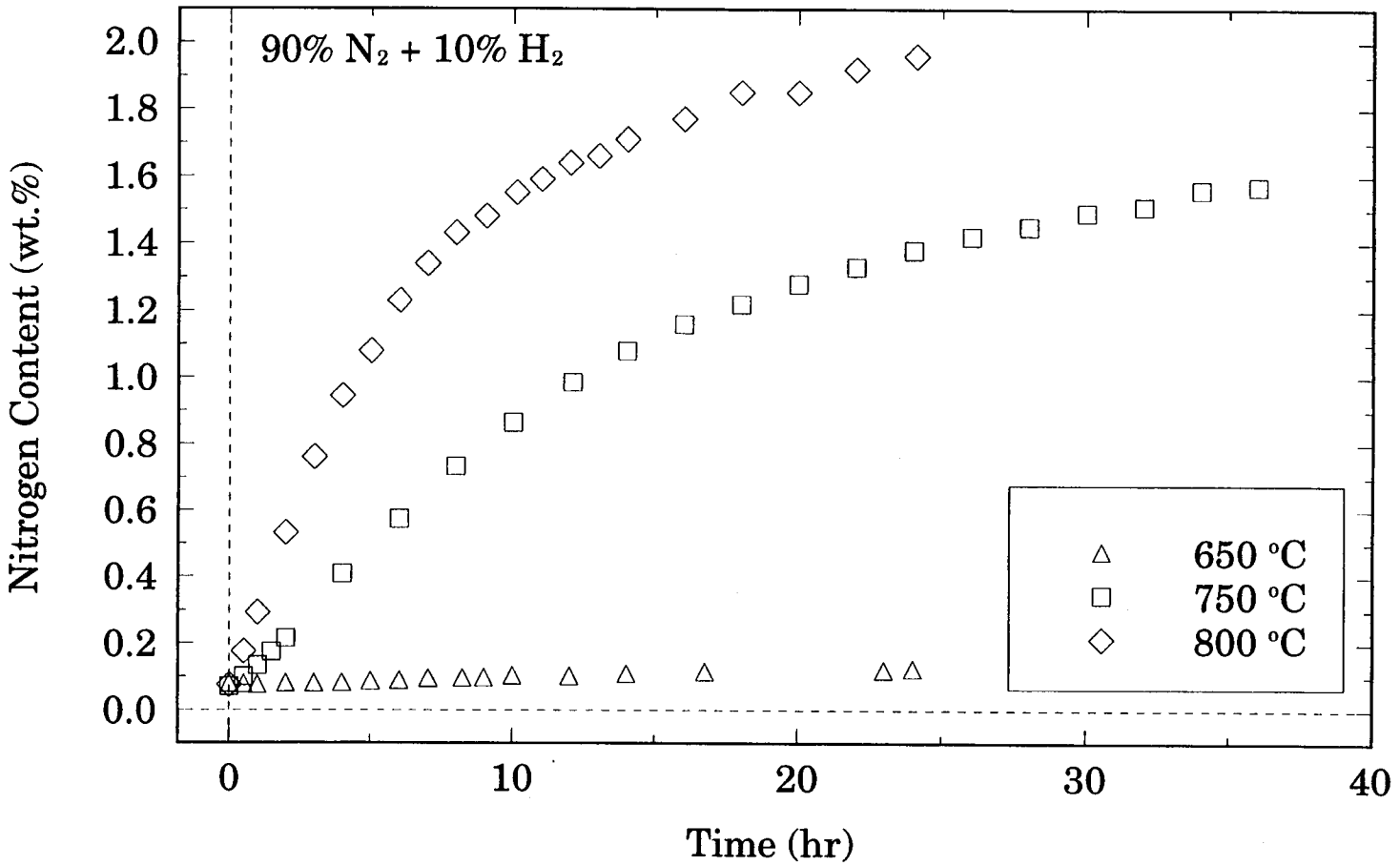

Figure 4.15 Effect of temperature on 316 stainless steel nitridation in the N_2/ H_2 system

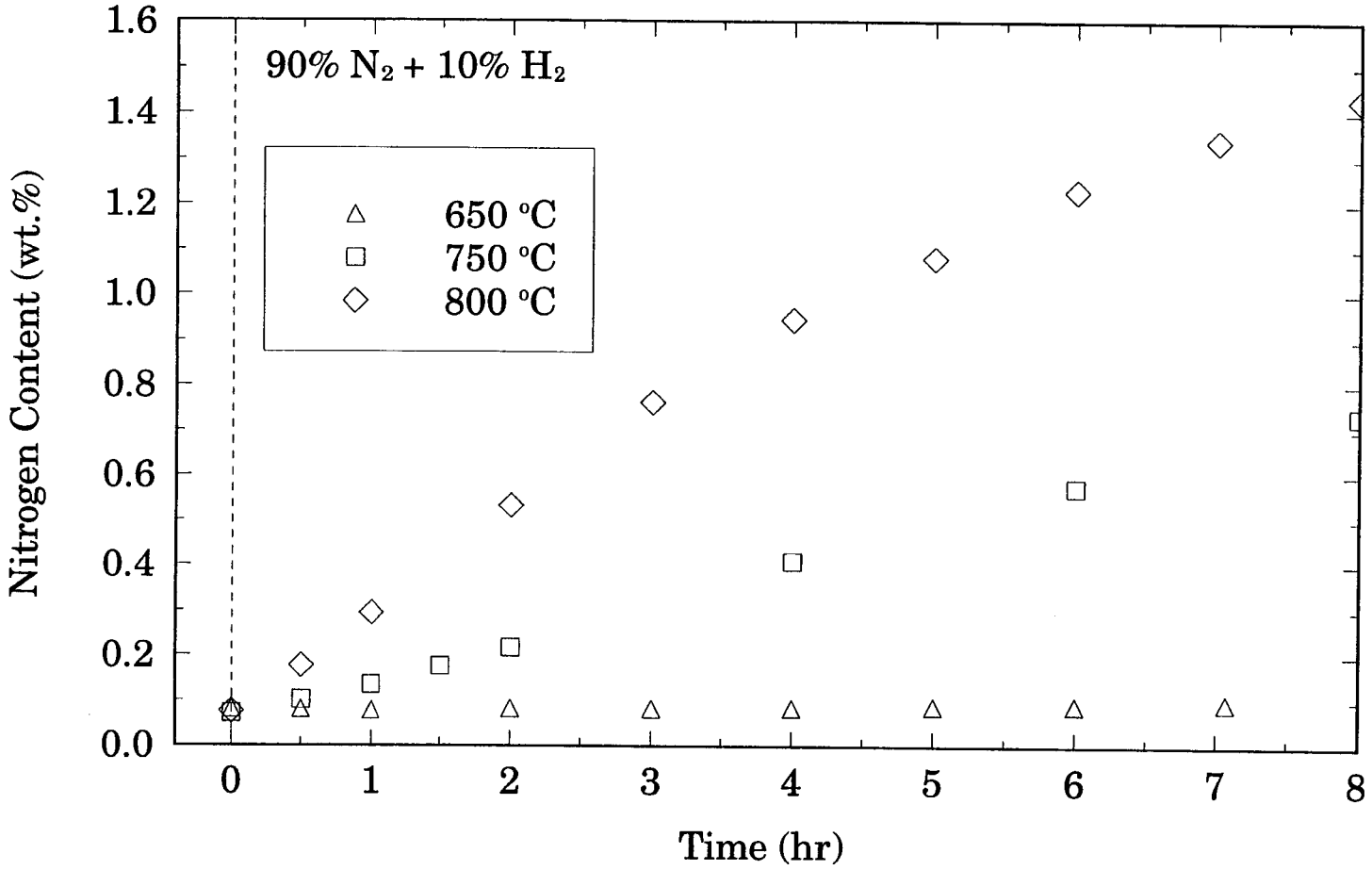

Figure 4.16 Close-up of the initial nitridation of 316 stainless steel in the N_2/ H_2 system

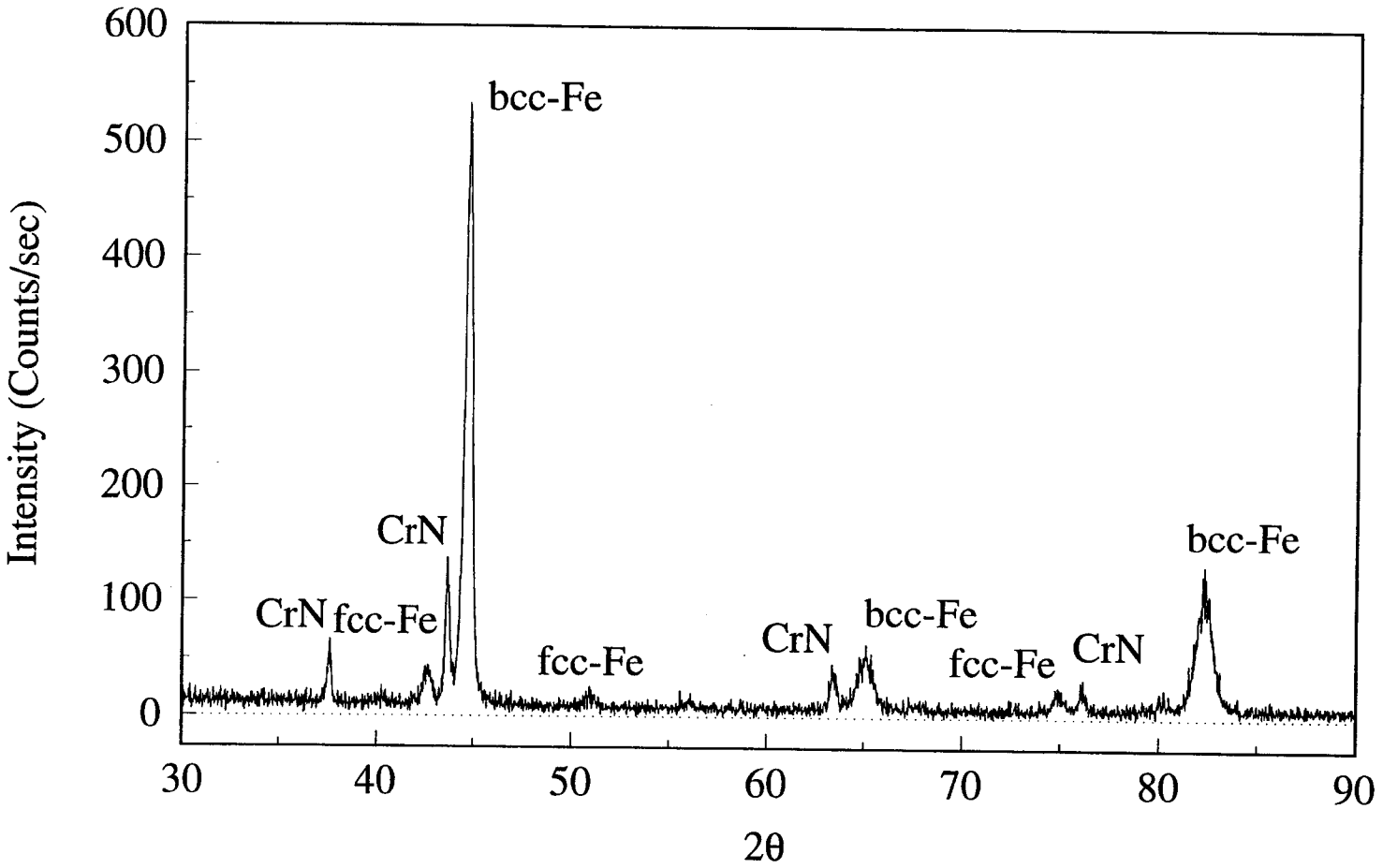

Figure 4.17 X-ray diffraction spectra of nitrided powder at 800 °C in the feed gas of 90% N_2 and 10% H_2 for 24 hours

NH_3 using thermodynamic analysis. He suggested that the use of NH_3 stream made it possible to obtain a nitrogen-rich iron nitride phase, which could not be prepared with N_2 at atmospheric pressure. The dissociation of NH_3 on iron metal was believed to provide extremely high nitrogen activity for the formation of metal nitride, that established a partial equilibrium between the metastable NH_3 gas phase and a solid nitride phase [Shohoji *et al.*, 1990].

Therefore, because the observed contents of nitrogen were much lower than those in the nitridation in NH_3, the study on the nitridation in the N_2/ H_2/ Ar system was not performed extensively.

4-3-1 Effect of Temperature

Mixtures of nitrogen, hydrogen, and argon were used for the nitridation of 316 stainless steel powder at different temperatures. Figure 4.15 compares the progress of nitridation at three different operating temperatures, using a 90% N_2/ 10% H_2 gas mixture. It is obvious that the nitridation progress of stainless steel in N_2 is slow compared to that in NH_3. Again, the nitridation process may be divided into the same three stages as observed in the nitridation in NH_3. A close-up of the nitridation during the initial stage is shown in Figure 4.16. The induction time decreases with an increase in the operating temperature. The induction time for the nitridation in N_2/ H_2 mixtures is negligibly short compared to the process time needed for reaching the saturation stage.

An increase in the operating temperature significantly enhances the nitridation process. Both dissociation and diffusion of nitrogen are promoted at higher temperatures. However, the nitrogen concentration in the stainless steel shown in Figure 4.15 is much lower than the level obtained by the nitridation in NH_3. A higher operating temperature is required for a higher nitrogen content. On the other hand, stainless steel powder becomes cohesive at temperatures higher than 800 °C and fluidization is no longer possible. Hence, a nitrogen content of about 2% by mass will practically be the maximum in the nitridation in N_2/ H_2 system.

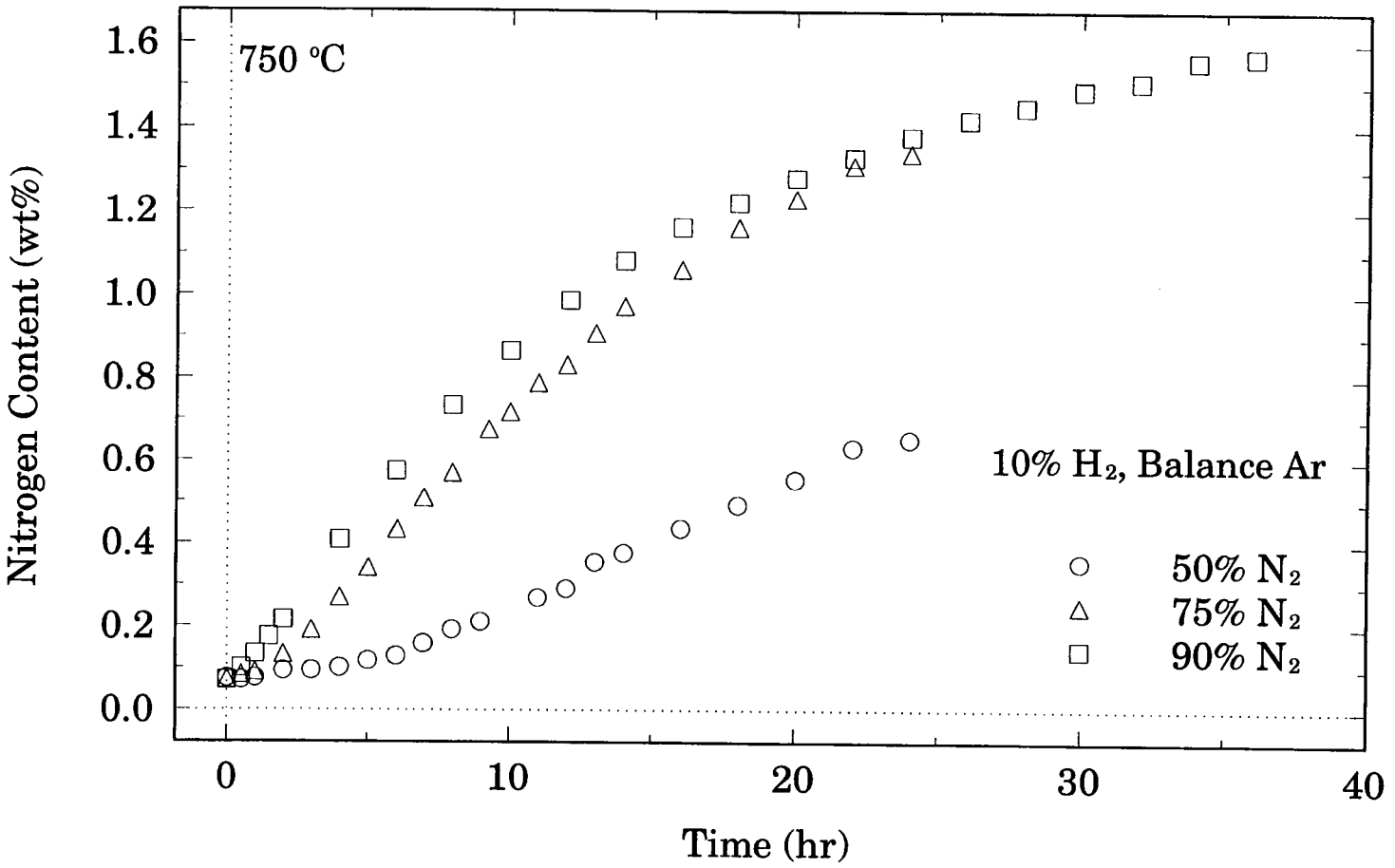

Figure 4.18 Effect of gas composition on 316 stainless steel nitridation in the N_2/ H_2/ Ar system

Figure 4.17 illustrates X-ray diffraction spectra of powder nitrided for 24 hours at 800 °C with the feed gas of 90% N_2 and 10% H_2. X-ray diffraction peaks indicate the co-existence of fcc-Fe and bcc-Fe phases as well as CrN phase in the product. On the other hand, no Fe_4N phase was found in this condition. The calculation of nitrogen required to completely convert Cr in the stainless steel powder into CrN indicates that only part of chromium has reacted with nitrogen to form CrN even when the nitridation process is approaching the steady state. It seems that an equilibrium between Cr and CrN is established under flowing N_2, that can not provide gas-phase nitrogen activity high enough for the complete Cr nitridation.

4-3-2 Effect of Gas Composition

The concentration of N_2 was changed from 50% to 90%, with the content of H_2 kept constant at 10% and Ar used as the balance, and the nitridation was carried out at 750 °C. As shown in Figure 4.18, the progress of nitridation in 90% N_2 is not much different from that in 75% N_2, while it is significantly slow in 50% N_2. When the nitrogen concentration of the gaseous mixture is low, a long induction period is observed.

4-4 Microstructural Change

Sample particles of stainless steel, processed at 550 °C in a 50% NH_3 /50% H_2 gas mixture, were analyzed by XRD, optical microscopy and EMPA. Figure 4.19 shows XRD spectra of selected samples nitrided for different lengths of process time: 0 min., 30 min., 183.5 min., 420 min., and 600 min.. Figure 4.19(a) shows that the stainless steel originally has fcc-Fe structure with a trace of bcc-Fe phase. After 30 minutes of processing, the peaks of fcc-Fe become broad and shift to lower angles, as observed in Figure 4.19(b), because nitrogen initially penetrates into the interstitial fcc-Fe solid solution. The lattice dimension becomes larger with an increase in interstitial

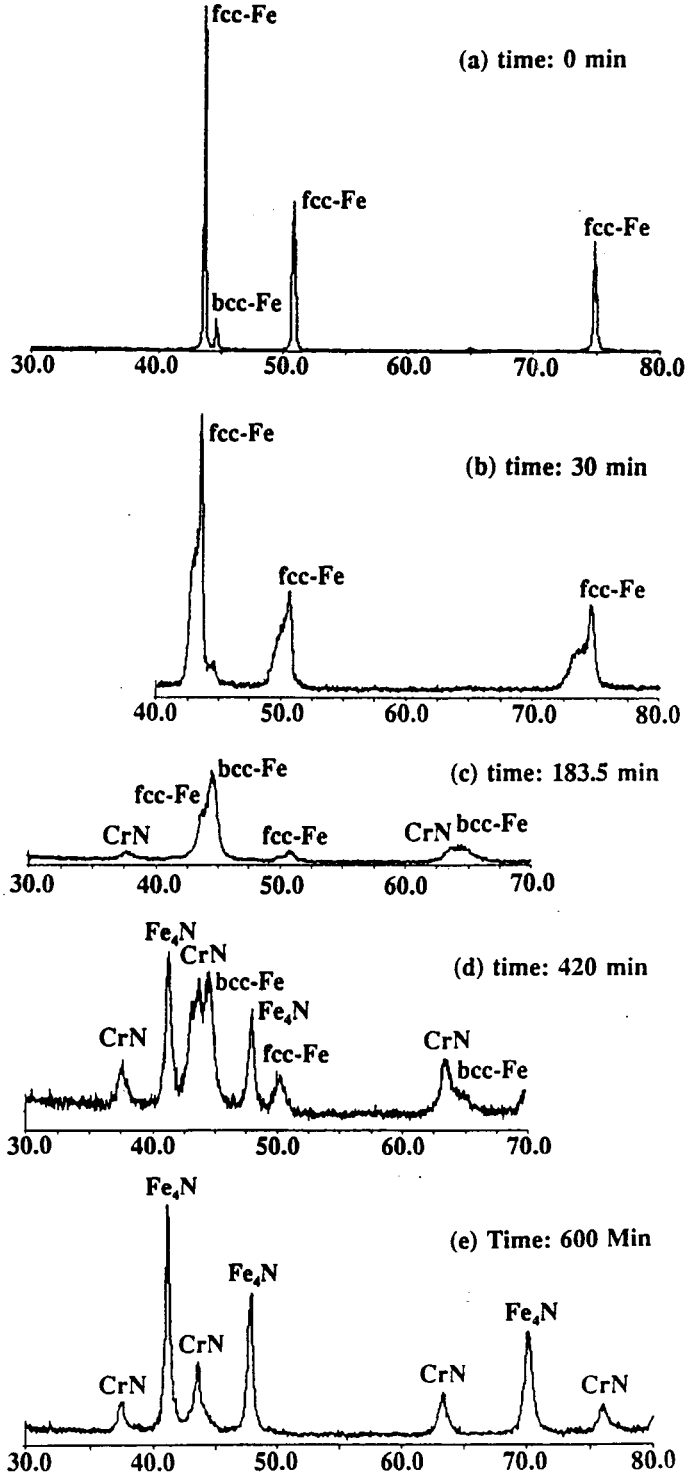

Figure 4.19 XRD charts of 316 stainless steel powder nitrided for different lengths of time in the feed of 50% NH_3 and 50% H_2 gas at 550 °C

nitrogen concentration in the solid solution. As the nitridation progresses, precipitation of CrN phase and formation of bcc-Fe phase develop, as shown in Figure 4.19(c). The development of the bcc-Fe phase results from the chromium element leaving the stainless steel matrix and becoming tied up with nitrogen to form chromium nitride. The removal of chromium from the stainless steel matrix produces an Fe-Ni alloy that has a bcc-Fe microstructure at this temperature, as shown in the Fe-Ni phase diagram by Metals Handbook [1973].

Nitrogen in bcc-Fe has higher diffusivity, but lower solubility than in fcc-Fe [Grieveson *et al.*, 1964]. Hence, once the bcc-Fe becomes supersaturated with nitrogen, it transforms into iron nitride [Rawers *et al.*, 1994]. As the nitrogen concentration increases, a new Fe_4N phase forms around the surface of the particle. The distribution of solid phases in the particle from the surface to the center would be in the order of nitrides (mixtures of iron nitride, Fe_4N, and chromium nitride, CrN), bcc-Fe, and fcc-Fe, all of which are indicated in Figure 4.19(d). As the nitridation progresses, the metal nitrides become predominant while the metal phases diminish. Eventually, only the metal nitrides are found in the saturation stage, as shown in Figure 4.19(e). The possible phase change and nitridation from the surface of a particle may be described as

$$\text{fcc-Fe} \rightarrow \text{fcc-Fe/ fcc-Fe(N)} \rightarrow \text{fcc-Fe(N)/ CrN} \rightarrow \text{fcc(N)/ CrN/ bcc-Fe(N)} \rightarrow \text{CrN/ bcc-Fe(N)} \rightarrow \text{CrN/ bcc-Fe(N)/ } Fe_4N \rightarrow \text{CrN/ } Fe_4N \qquad \textbf{(4.19)}$$

where fcc-Fe(N) and bcc-Fe(N) present nitrogen dissolved in the solid solution of fcc-Fe and bcc-Fe structures, respectively.

Figures 4.20 and 4.21 illustrate optical microscopy images of cross-sectioned samples obtained in the nitridation with NH_3 for 120, 300 and 540 minutes. Figure 4.22 also shows the BSE image of a cross-sectioned sample obtained after 120 minutes. A shell layer has formed around the surface of each particle and progresses from the surface inward. Based on the XRD analysis, the surface layer is considered to be formed when CrN precipitates at the beginning, and iron nitride gradually increases thereafter.

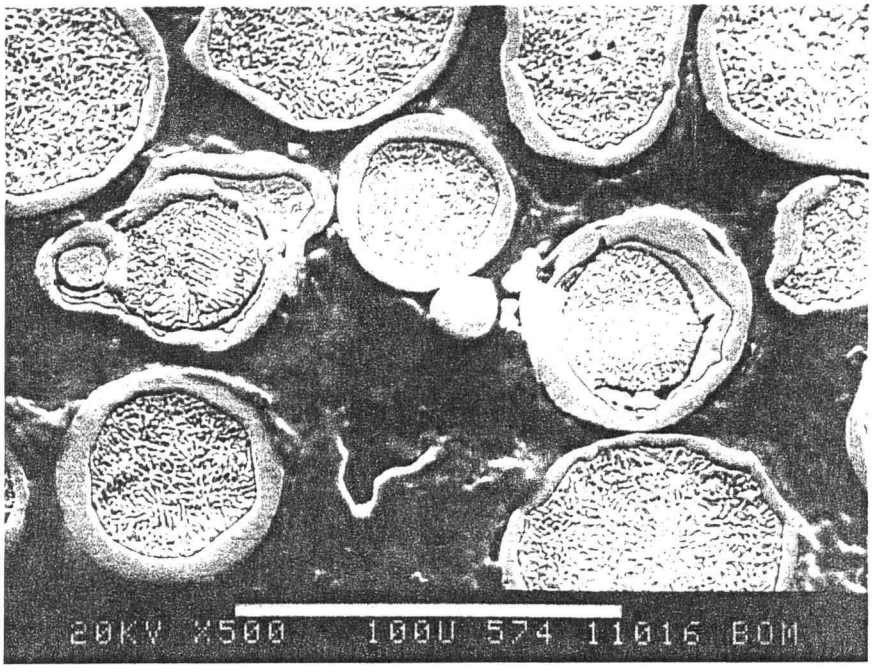

(a)

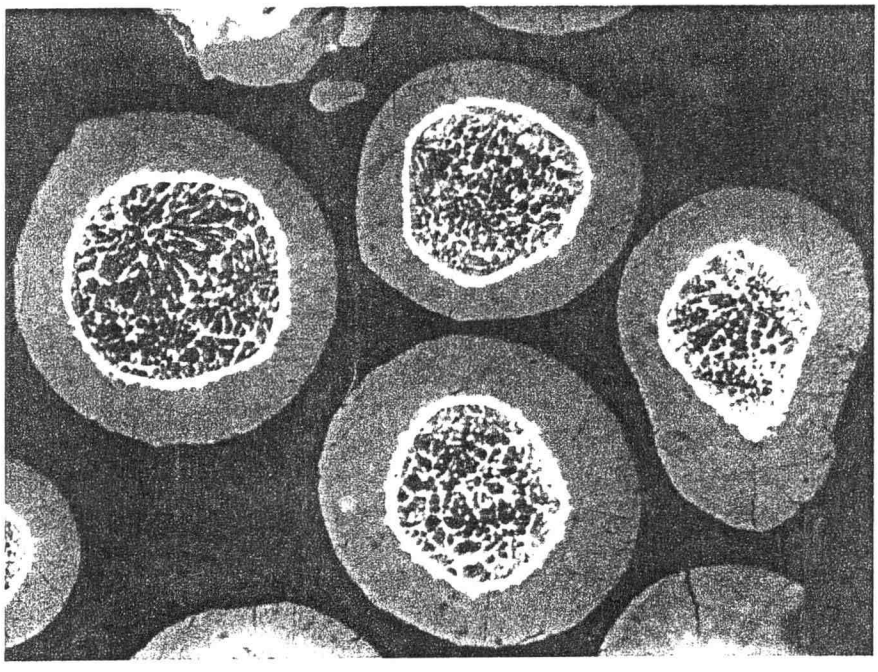

(b)

Figure 4.20 Optical images of cross-sectioned particles, nitrided in the feed of 50% NH_3 and 50% H_2 at 550 °C for (a) 120 min. and (b) 300 min.

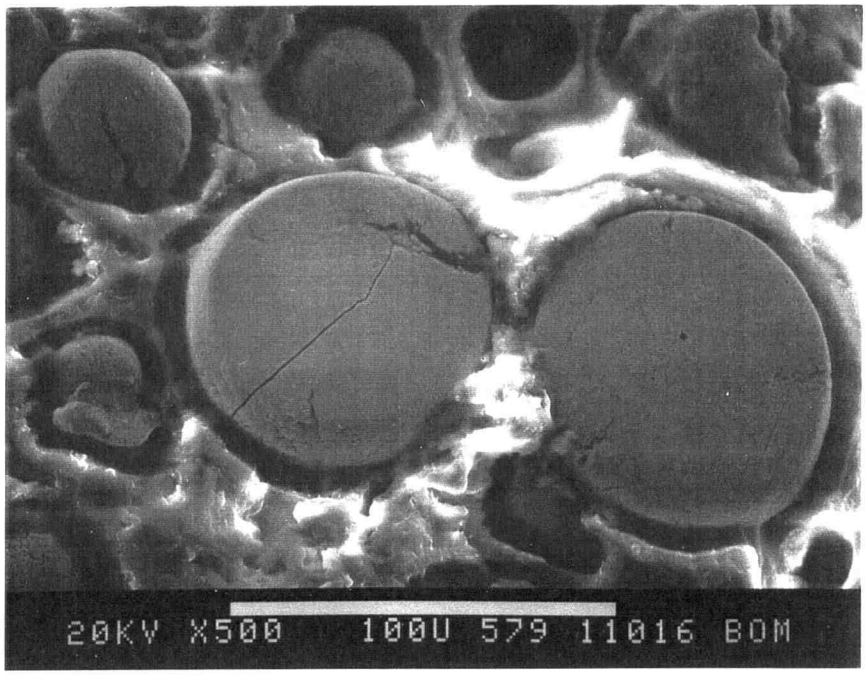

Figure 4.21 Optical image of a cross-sectioned particle, nitrided in the feed of 50% NH_3 and 50% H_2 at 550 °C for 540 min.

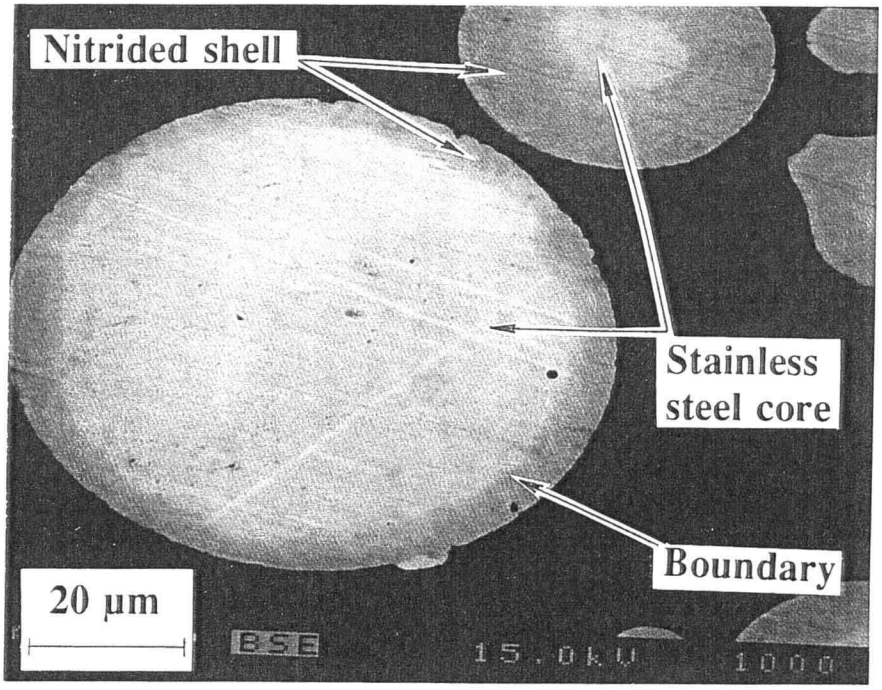

Figure 4.22 BSE image of a cross-sectioned particles, nitrided in the feed of 50% NH_3 and 50% H_2 at 550 °C for 120 min.

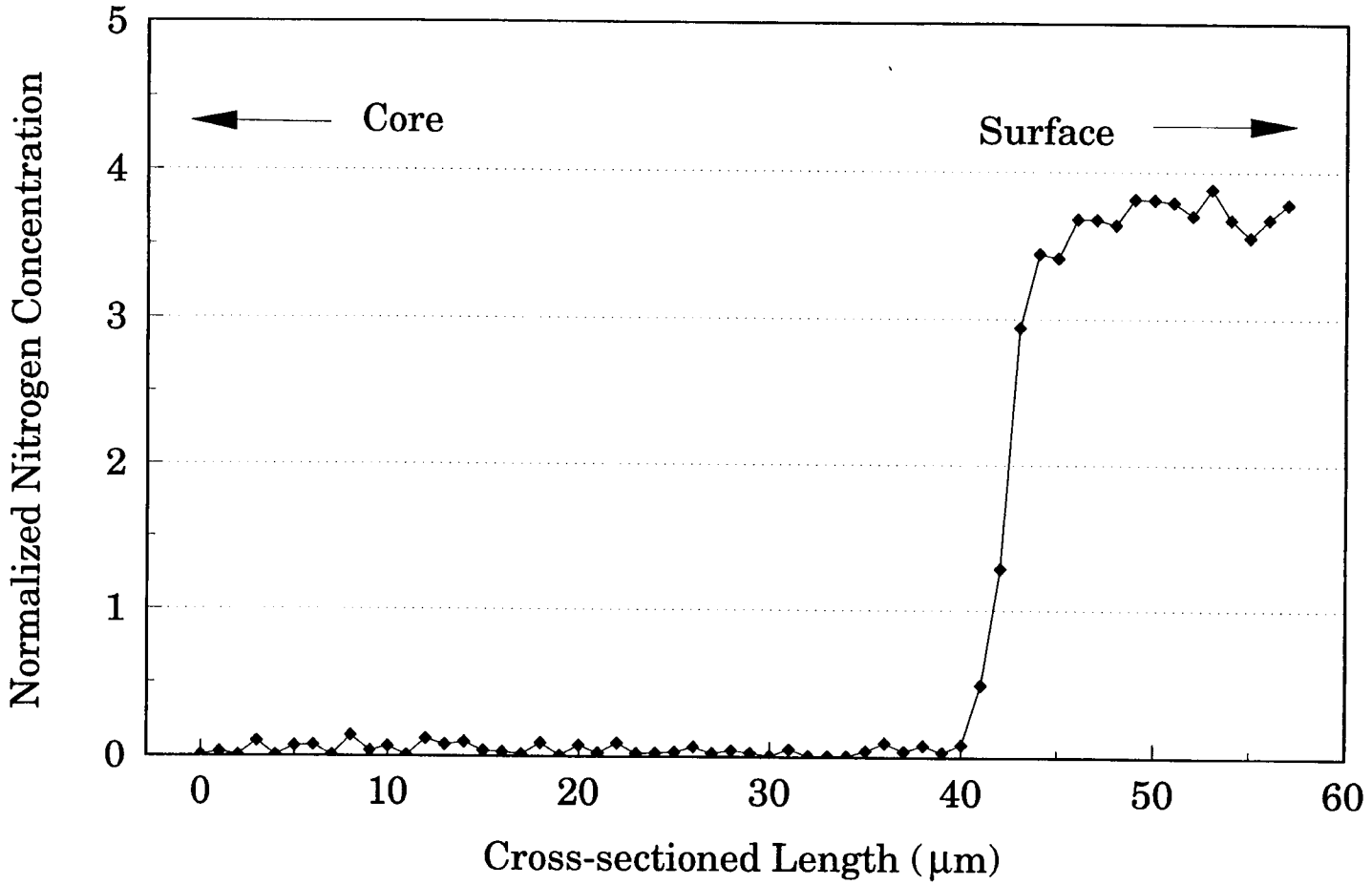

Figure 4.23 The distribution of nitrogen in the cross-sectioned particle shown in Figure 4.20 (b)

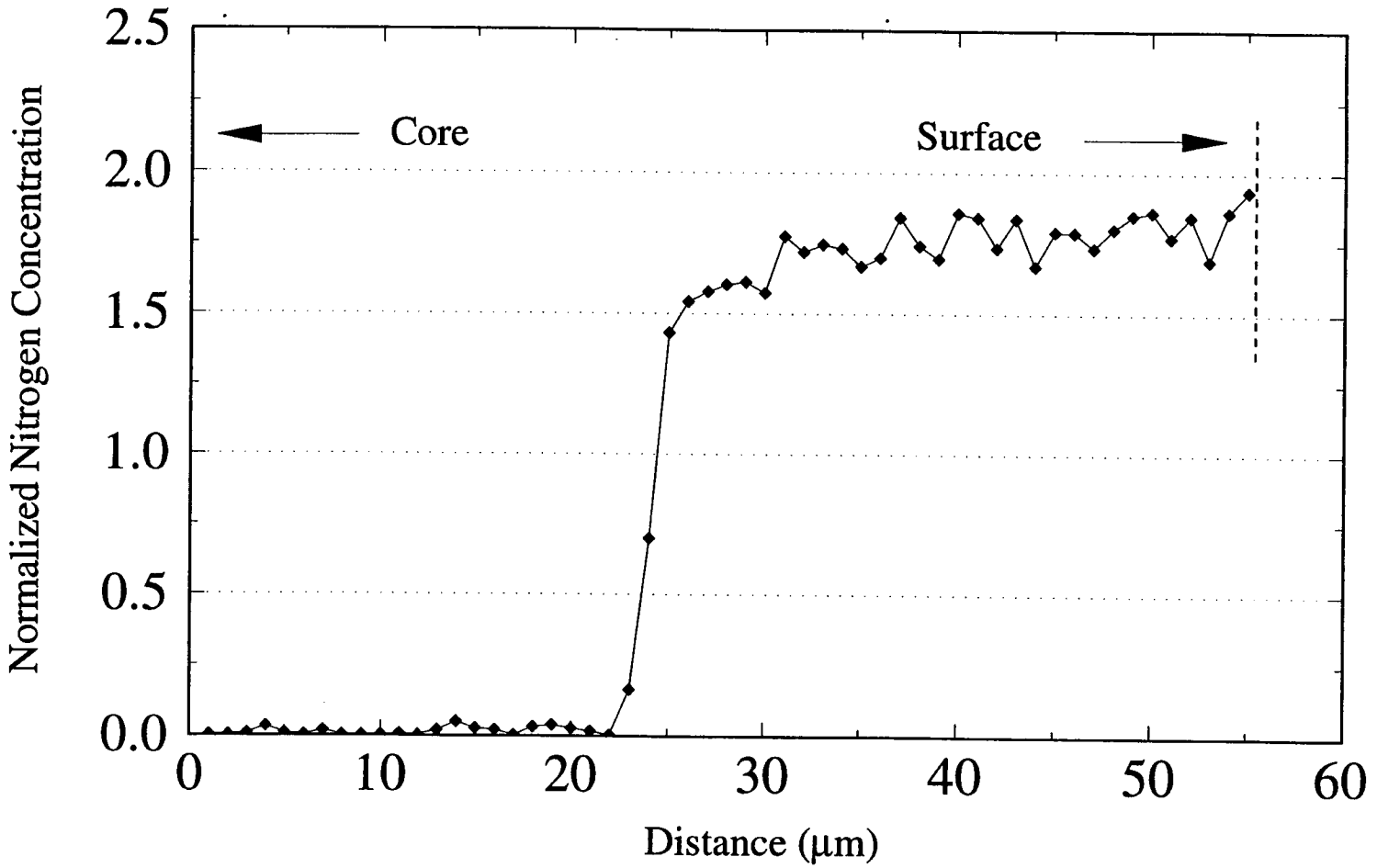

Figure 4.24 The distribution of nitrogen in the cross-sectioned particle nitrided for 9 hours

The distributions of nitrogen in some cross-sectioned particles were also measured by EMPA. During the initial stage of nitridation, the as-received distribution of nitrogen is uniform at a low level. As the nitridation progresses, three different zones may be identified in the nitrogen concentration profile: a surface zone with high, uniform nitrogen concentration, a transitional zone with a sharp decrease in nitrogen concentration, and a core zone with very low nitrogen concentration, as illustrated in Figures 4.23 and 4.24, in which the nitrogen concentration is normalized, being divided by the overall nitrogen content. The surface zone grows inward with time, namely, with the progress of nitridation.

Nitrogen initially diffuses into the interstitial fcc-Fe solid solution. As the nitrogen concentration around the particle surface increases, the surface iron is first transformed into the bcc-Fe phase by the removal of chromium from stainless steel matrix as chromium nitride. A surface bcc-Fe(N)/ CrN layer is then formed, and progresses inward when more nitrogen is added into the particle. At the same time, with increasing nitrogen concentration, the bcc-Fe phase becomes saturation with nitrogen and is gradually transformed into iron nitride. These stages correspond to the period during which the dissociation of NH_3 is unstable, mainly due to the change from fcc-Fe(N) to bcc-Fe(N), and to Fe_4N. Once the surface iron-nitride has become dominant on the particle surface, the NH_3 dissociation is catalyzed mainly by the metal nitrides (chromium nitride and iron nitride) and stabilized. This is considered to be the major reason why it takes a longer time for the NH_3 dissociation to be stabilized than for the enhanced nitridation to begin. Figures 4.25, 4.26, 4.27, and 4.28 compare the nitridation process and the extent of NH_3 dissociation at the outlet of the fluidized bed operated with the feed gas of 100% NH_3 at different temperatures of 550 °C, 600 °C, 650 °C and 750 °C, respectively. A steady state of NH_3 dissociation is reached about the middle of the enhanced nitridation stage, where the formation of Fe_4N seems to start. However, at a high operating temperature of 750 °C, no Fe_4N is found in the nitrided powder, as indicated in Figure 4.12. One possible explanation is that there may be a metastable iron nitride phase developed around the surface of nitrided powder during the high temperature process, that would stabilize the dissociation of ammonia. However, this metastable phase is unstable, and would decompose once

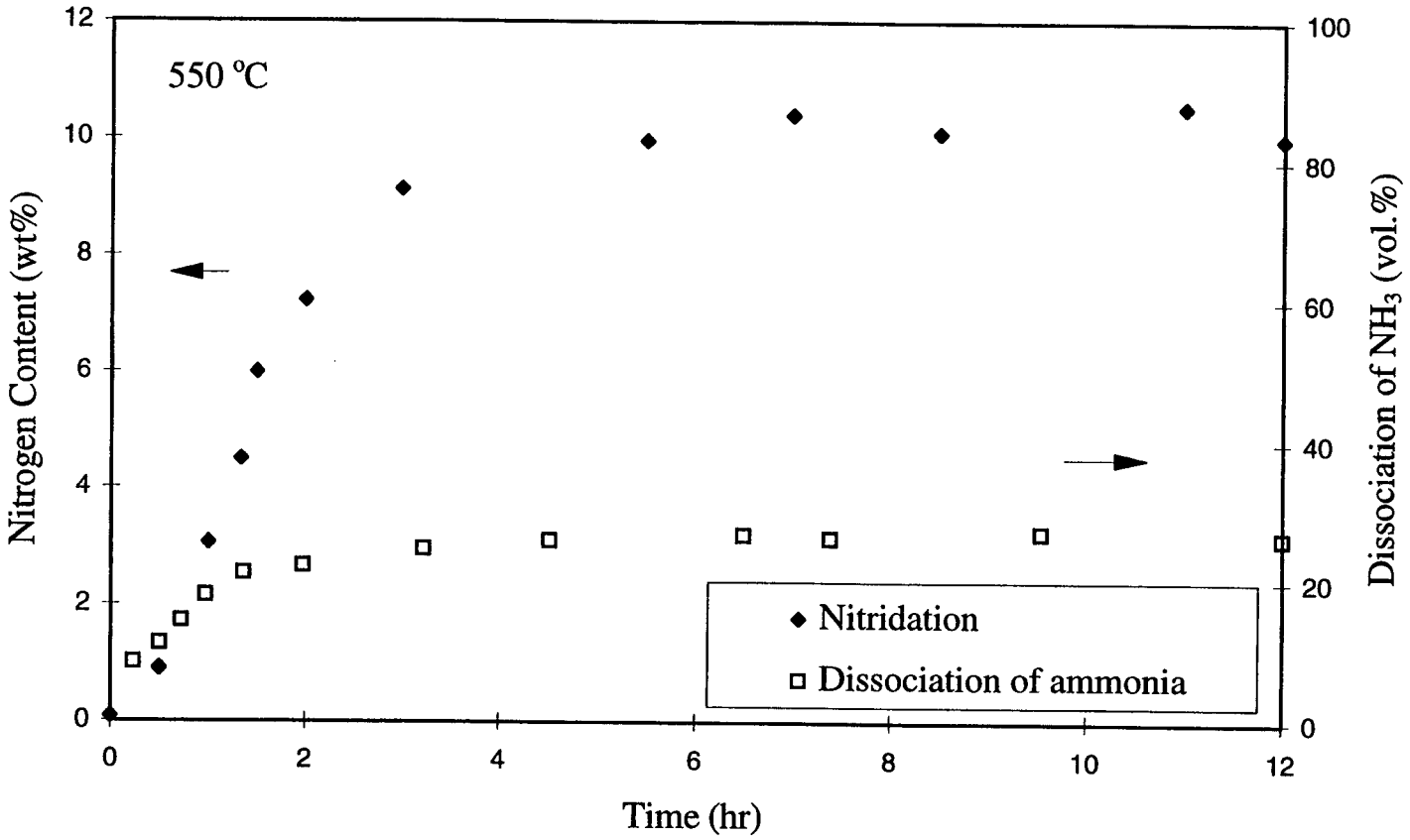

Figure 4.25 Comparison of nitridation process and ammonia dissociation for the feed gas of 100% NH_3 at 550 °C

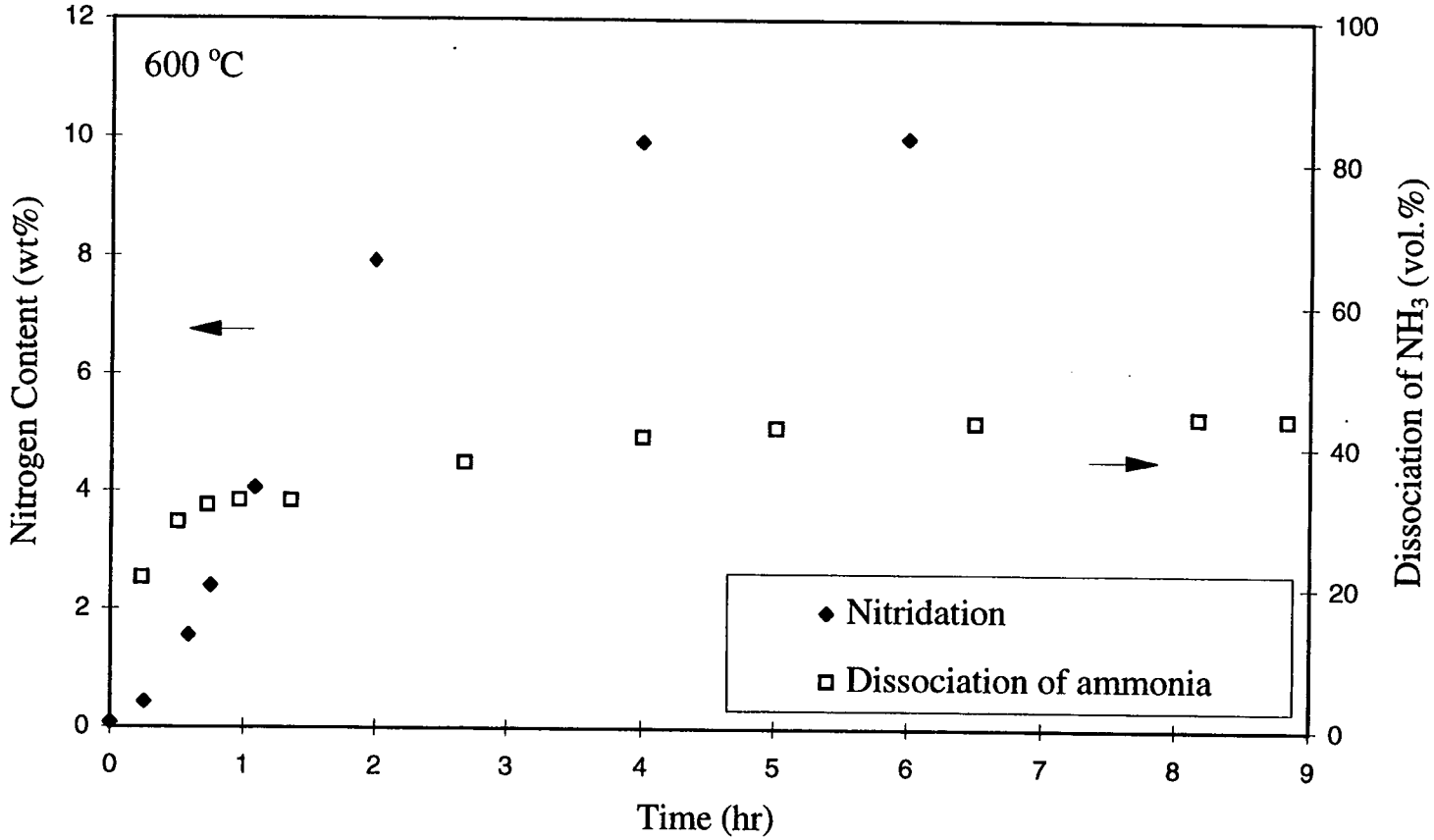

Figure 4.26 Comparison of nitridation process and ammonia dissociation for the feed gas of 100% NH_3 at 600 °C

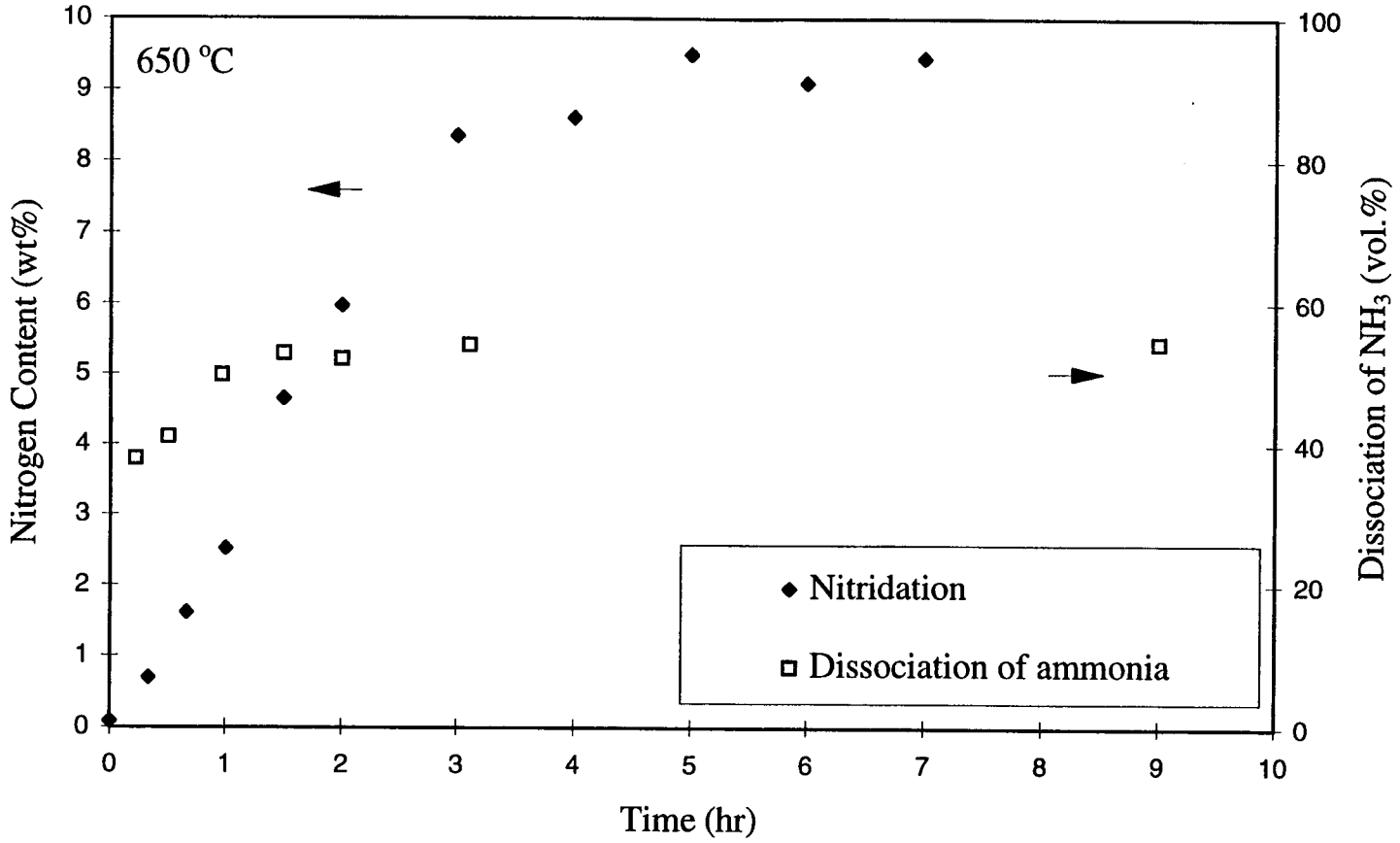

Figure 4.27 Comparison of nitridation process and ammonia dissociation for the feed gas of 100% NH_3 at 650 °C

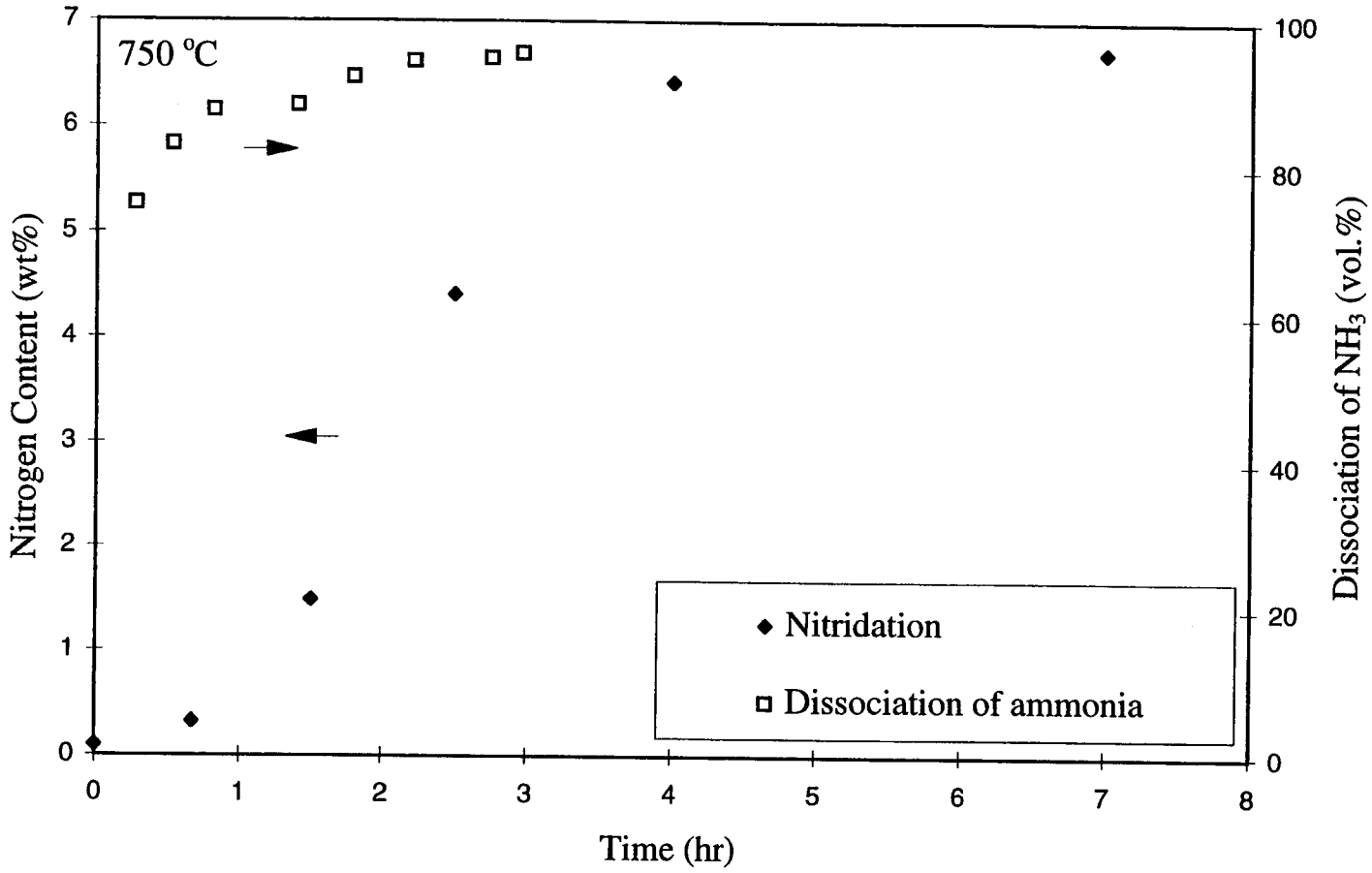

Figure 4.28 Comparison of nitridation process and ammonia dissociation for the feed gas of 100% NH_3 at 750 °C

ammonia environment is removed [Shohoji *et al.*, 1990]. The real mechanism for ammonia dissociation on the surface of nitrided stainless steel powder is not clear.

As indicated in the EMPA profile, shown in Figures 4.23 and 4.24, the surface nitride layer has roughly uniform nitrogen concentration. Nitrogen diffusing through the surface layer is captured in the transitional zone, transforming bcc-Fe into iron nitride and fcc-Fe into bcc-Fe. The transitional zone is thus narrowly confined. Combining EMPA profiles with the overall nitrogen concentration chemically determined allows one to estimate the nitrogen concentration in the shell layer. This rather complex approach needs to be taken, because the magnitude of nitrogen contents from EMPA may be used only as relative values of nitrogen concentration in the particle. Table 4.5 shows that the nitrogen concentration of the shell increases with the process time toward the level corresponding to the combination of Fe_4N and CrN in the solid solution, that is determined from the phase equilibrium of Fe, Cr, and N depending on the operating conditions.

This scenario described above generally explains the progress of nitridation in the enhanced nitridation stage at low operating temperatures. At high temperatures, Fe_4N becomes thermodynamically unstable and may not be formed. Therefore, the mechanism of CrN precipitation may be ascertained from the study of nitridation process at high temperatures. The low temperature nitridation process, which results in CrN and Fe_4N formation, may be better understood from the mechanism of CrN precipitation at high temperatures.

Table 4.5 Estimated nitrogen concentration of surface shell

Process Time, hr	2	7	10
Overall nitrogen content, % in mass	1.67	5.37	9.01
Particle size, μm	89	100	85
Thickness of nitrided shell, μm	6	12	23
Nitrogen concentration of nitrided shell, % in mass	4.73	9.57	9.97

Chapter 5
Nitridation Mechanism

This chapter mainly focuses on the nitridation process in the NH_3 system, in which higher nitridation rates are obtained at lower operating temperatures. A mathematical model is developed for the nitridation process during the enhanced nitridation stage which leads to a high extent of nitrogen addition. The model developed in this chapter may be useful to predict the progress of nitridation in reactors to be designed in the future.

5-1 Induction Stage

The induction stage of nitridation is strongly influenced by the operating temperature, as indicated in Figure 4.9. It seems that the content of nitrogen increases linearly with operating time. On the other hand, X-ray diffraction spectra (see Figure 4.19(b), for instance) suggest that nitrogen diffuses into the interstitial fcc-Fe alloy solution (original 316 stainless steel) to increase the lattice dimension initially (see Figure 4.19(b)). These findings conflict because the process of nitrogen diffusion into the solid solution should not lead to the linear increase in nitrogen content, unless some other transport mechanism controls the process of nitrogen addition.

The diffusivities of nitrogen in fcc-Fe and bcc-Fe solid solutions measured by Grieveson *et al.* [1964] are generally accepted. Their measured results are shown in Table 5.1. According to their work, the rate-controlling step for nitrogen addition into the fcc-Fe solution in the nitrogen and hydrogen gas environment is the diffusion of nitrogen into iron. However, the calculated diffusivity of nitrogen in fcc-Fe from Table 5.1 is extremely small, and hence it will take about 180 hours to complete the nitridation in our study if the process is controlled by diffusion mechanism. Grieveson *et al.* [1964] assumed that the diffusivity was independent of the nitrogen

Table 5.1 Nitrogen diffusivities in fcc and bcc-Fe measured by Grieveson *et al.* [1964].

Nitrogen Diffusion in	Pre-exponential factor k_0 (cm^2/sec)	Activation Energy Q (kJ/mol)
fcc-Fe	0.912	168.6
bcc-Fe	7.8×10^{-3}	79.1

concentration in the solid solution. This assumption would have been appropriate only for their case because the solubility of nitrogen in solid solution was very low, i.e., less than 0.03 wt % in their case. Fast [1971] showed an increase in the diffusivity of carbon in fcc-Fe when carbon concentration increased. This suggests that the diffusion of nitrogen in fcc-Fe solid solution will be enhanced by an increase in nitrogen concentration. However, the increase in diffusion rate is still limited, and there is no explanation for the linear increase in the initial nitrogen addition. Therefore, other mechanisms must be considered, that control the process of nitrogen addition in the induction stage.

One possible explanation may come from the change in the morphology of 316 stainless steel. Figure 5.1 illustrates the BSE image of a cross-sectioned sample particle nitrided for 30 min. in the feed gas mixture of 50% NH_3 and 50% H_2 at 550 °C. The image shows that a new phase forms on the surface of the stainless steel particle and gradually develops to be a surface shell. Moreover, Figure 5.2 compares the surface-topography images of an original stainless steel particle and a particle nitrided for 60 min. in the feed gas of 100% NH_3 at 550 °C. It is clearly observed that a new bump-like phase has developed on the surface of the nitrided particle. The observation in Figure 5.1 corresponds to the formation of lump sites on the surface, shown in Figure 5.2(b), implying that the nitridation process in the induction stage may be intruded by the surface-morphology change, i.e., surface reaction. As discussed in section 4-1-1 for the catalytic dissociation of NH_3, the addition of nitrogen into stainless steel powder may come from two steps: the adsorption of NH_3 onto the surface of metal and the dissociation of adsorbed NH_3 into adsorbed nitrogen. The adsorption of nitrogen is believed to lead to the formation of a chemisorbed phase [Ertl *et al.*, 1976]. Therefore, the development of adsorbed species (adsorbed nitrogen) on the surface of stainless steel may control the induction stage of the nitridation process. The growth of surface shell seems to be the result of the increase in surface chemisorption sites of nitrogen, which may develop linearly around the particle, while the diffusion of nitrogen into the solid solution has minor effect on the initial induction process. After the surface shell is developed, the nitridation is enhanced by the formation of nitride phases from solid matrix, leading to a different

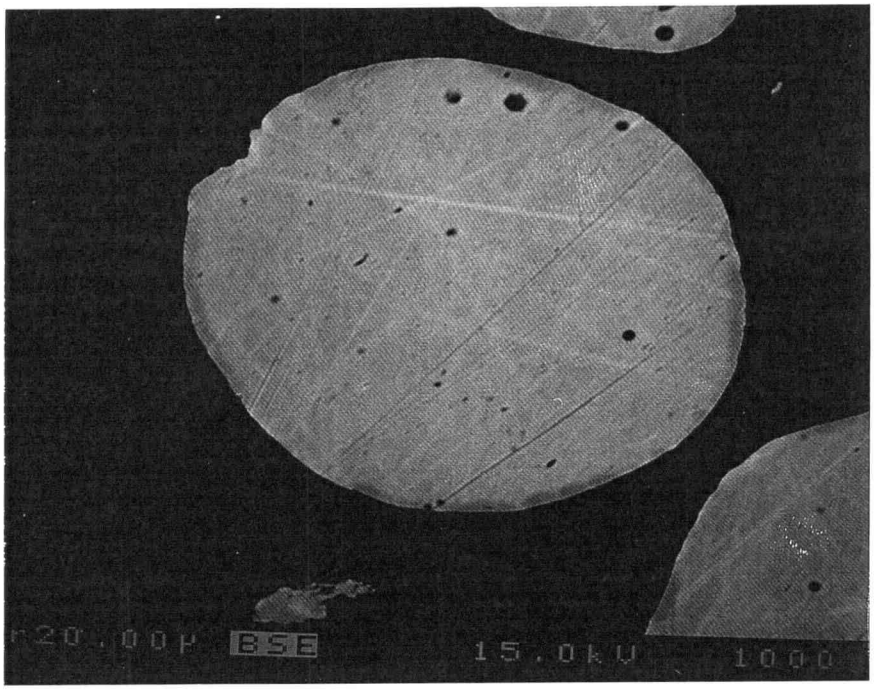

Figure 5.1 BSE image of a cross-sectioned particle, nitrided in the feed of50% NH_3 and 50% H_2 at 550 °C for 30 min.

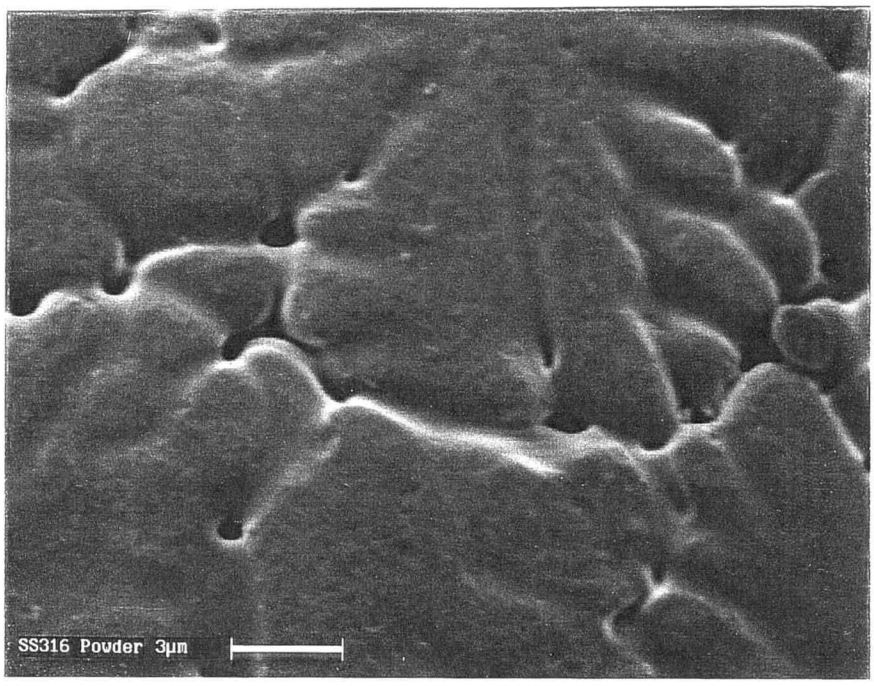

(a)

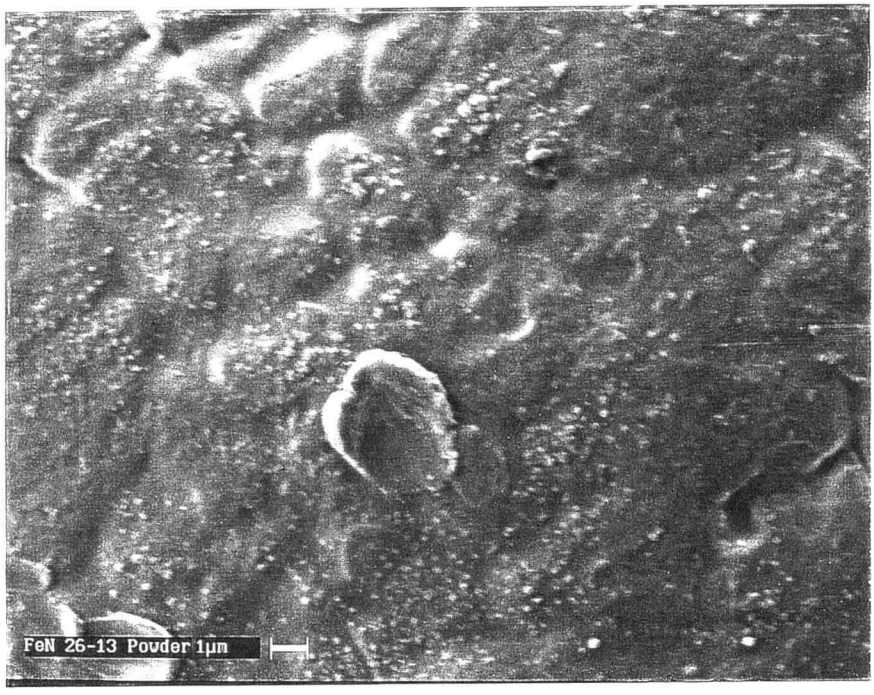

(b)

Figure 5.2 The comparison of the surface morphology images of (a) an original stainless steel particle, and (b) a nitrided particle for 60 min.

mechanism. However, it requires sophisticated analytical equipment to clarify the surface reaction involving the complex process. No further investigation is performed in this study.

5-2 Enhanced Nitridation Stage

After the induction period, the nitridation process is enhanced dramatically, as shown in Figures 4.8 and 4.11. It is believed that the induction stage is completed after a chromium nitride layer is developed entirely on the exterior surface of particles. Hence, nitrogen initially penetrates into the interstitial solid solution. Dependent upon both alloy composition and structure, chromium nitride starts to form as more nitrogen is added to the stainless steel [Rawers *et al.*, 1992]. In this study, the enhanced nitridation stage starts when the nitrogen content in stainless steel powder is approximate 0.5% overall by mass, according to Figure 4.9. Hence, chromium nitride is considered to be formed after the nitrogen content in 316 stainless steel powder reaches approximate 0.5% by mass.

As suggested by the X-ray diffraction of final product particles nitrided at different operating temperatures, shown in Figure 4.12, iron nitride becomes unstable when the operating temperature is high while chromium nitride remains stable in the nitrided solid. In addition, the solid solution of Fe-Ni alloy stays in a form of fcc-Fe structure by the removal of Cr from the matrix at high temperature. At 750 °C, for instance, only the CrN phase is detected. Nitrogen dissolved in solid solution is also found from the peaks of fcc-Fe that become broad and shift to lower angles in Figure 4.12. The amount of nitrogen dissolved in 316 stainless steel solid solution may be determined by comparing the experimental data with the calculated curve from the proposed model, which will be addressed in a later section. This quite complicated method must be used because of the lack of information regarding the nitrogen solubility in 316 stainless steel under NH_3 and H_2 environment in the temperature range of 550 °C to 750 °C.

In this study, therefore, the nitridation is discussed for two different regions: the high operating temperature region where only the CrN phase precipitates and the low operating temperature region in which both the CrN and Fe_4N phases form. The following section will examine the mechanism of CrN formation first and then consider the addition of Fe_4N in the process.

5-2-1 High Temperature Nitridation

Figure 5.3 shows the BSE image of a cross-sectioned particle nitrided at 750 °C in the feed gas of 90% NH_3 and 10% H_2 for 3 hours. A shell on the particle surface is clearly seen. The same particle was also analyzed by EMPA, yielding a uniform nitrogen concentration in the surface layer, as shown in Figure 5.4. The nitrogen in the surface layer consists of nitrogen in CrN and nitrogen dissolved in its solid solution. It is hence recommended to use the shrinking un-reacted core model (SCM) [Yagi and Kunii, 1955 and 1961] to describe the nitridation process during the enhanced nitridation stage at high operating temperatures.

5-2-1-1 Shrinking Un-reacted Core Model (SCM)

The following describes a model known as the shrinking un-reacted core model (SCM). For a heterogeneous reaction between gas and a spherical particle of solid reactant, the reaction may be represented by

$$A\ (g) + b\ B\ (s) \rightarrow Products \qquad (5.1)$$

Generally, the overall reaction process may be simplified by the following steps [Levenspiel, 1993].

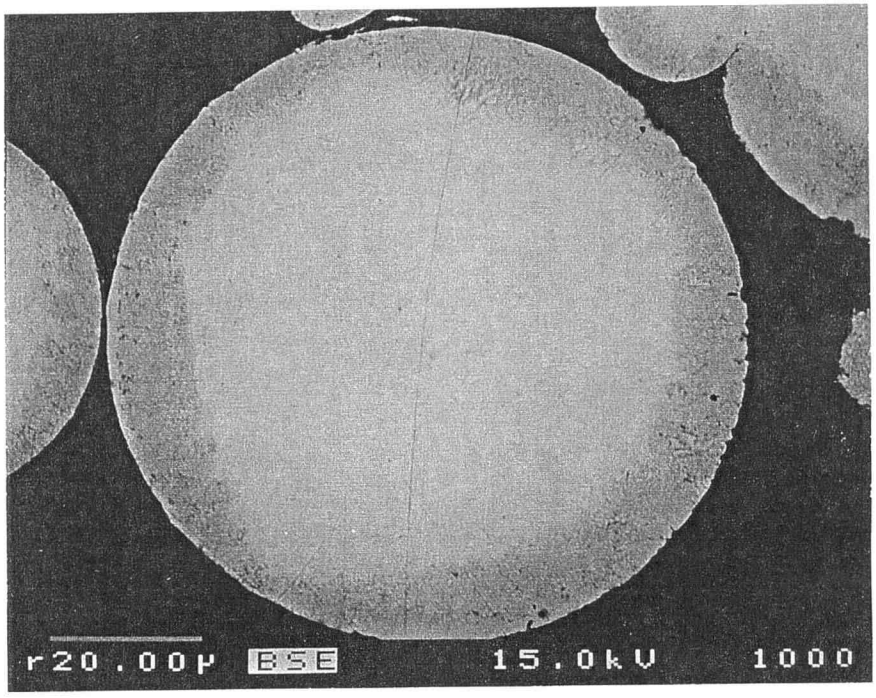

Figure 5.3 BSE image of a cross-sectioned particle, nitrided in the feed of 90% NH_3 and 10% H_2 at 750 °C for 180 min.

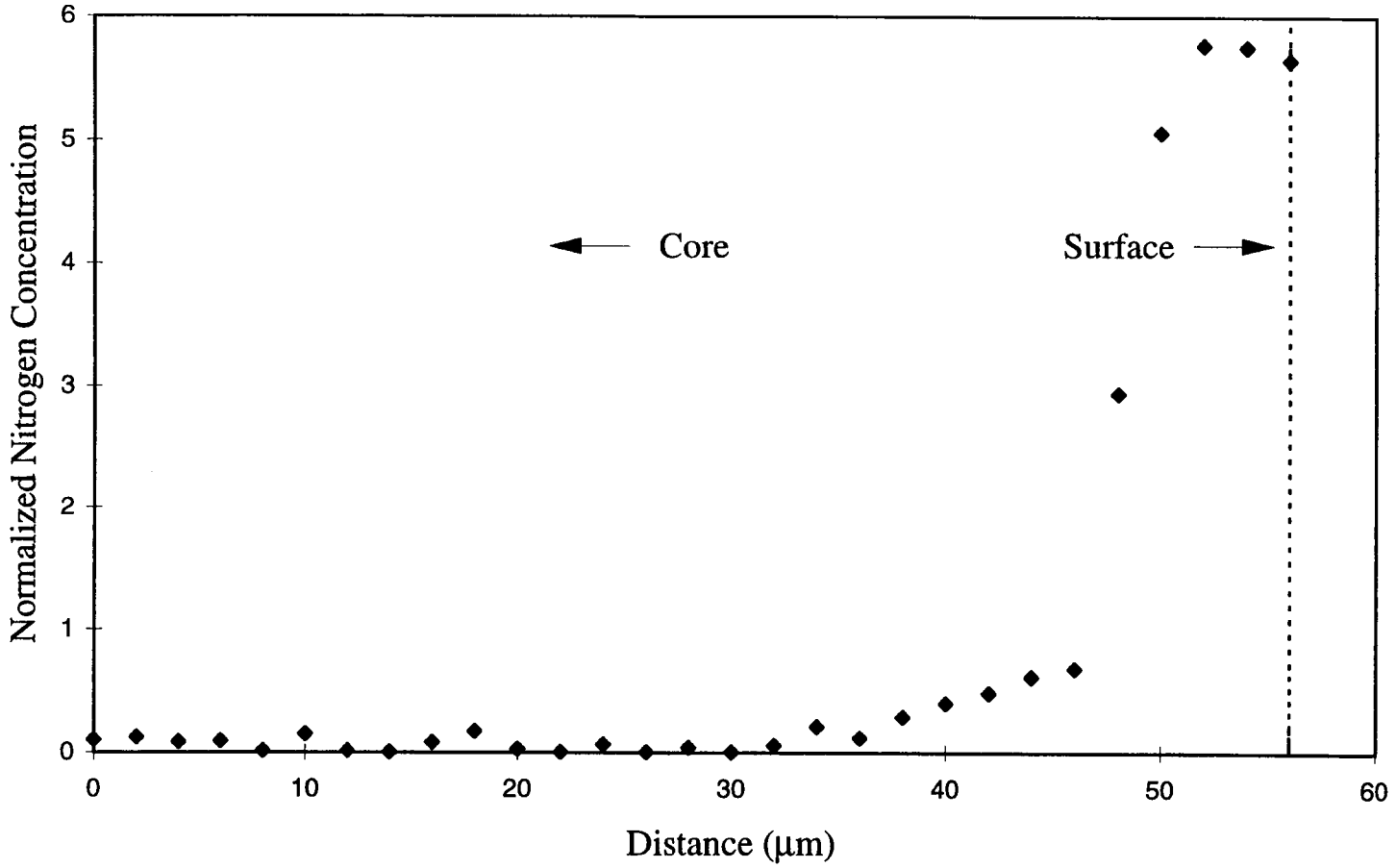

Figure 5.4 The distribution of nitrogen content in the cross-sectioned particle shown in Figure 5.3

i) Diffusion (or mass transport) of gaseous reactant A from the bulk stream through the gas-phase film toward the particle surface.

ii) Modification of A into a form of diffusing species A^*, including atoms, free radicals, and ions, at the particle surface.

iii) Penetration and diffusion of A^* through the product layer to the reactant core surface.

iv) Chemical reaction of the reactant A^* with solid reactant B at the reaction surface, i.e., the boundary between the product layer and the un-reacted reactant core.

Because the gas-phase mass transport is fast in the fluidized bed [Kunii and Levenspiel, 1991], the resistance to the gas film transport is negligible in this case. Assuming first order with respect to A^*, the rate equation for the shrinking un-reacted core model (SCM) with the influences of two resistances is hence given by [Levenspiel, 1993]

$$-\frac{1}{b\,S_{ex}}\frac{dN_B}{dt} = \left[\frac{1}{\frac{R\,(R-r_C)}{r_C\,D_{eff}} + \frac{R^2}{r_C^2\,k''_s}}\right] C_{Ag} \qquad (5.2)$$

$$\text{with } X_B = 1 - \left(\frac{r_C}{R}\right)^3$$

where

N_B: the molar amount of solid reactant B in the particle, which represents Cr in this study.

S_{ex}: the unchanging exterior surface area of the particle.

D_{eff}: the effective diffusivity of A (nitrogen in this study) through the reacted layer.

r_C: the radius of un-reacted core.

C_{Ag}: the concentration of A^* at the particle surface.

k''_s: the first order surface reaction rate constant (with respect to A^*).

Because 316 stainless steel particles are non-porous, and the particle size does not change during the nitridation, the external surface area, S_{ex}, and moles of B, N_B, in Equation (5.2) are given by

$$S_{ex} = 4\pi R^2 \tag{5.3}$$

$$N_B = \frac{4}{3} \pi r_C^3 \rho_B \tag{5.4}$$

where ρ_B represents the molar density of B in a particle.

The reactant A^*, i.e., nitrogen, is supplied by the dissociation of NH_3 gas. However, the form of nitrogen, penetrating into the solid phase, is not clear, which may be nitrogen atoms, free radicals, or ions. Hence, C_{Ag} may need to be replaced by a function of NH_3 and H_2 concentration in the bed, namely, $f(C_A)$. It is noted that the concentration of hydrogen is included in $f(C_A)$ because hydrogen may inhibit the transport of nitrogen in the process. The further discussion will be presented later.

Hence, substituting Equations (5.3) and (5.4) into Equation (5.2), and integrating Equation (5.2) with the boundary conditions:

$t = 0, \quad r_C = R$

$t = t, \quad r_C = r_C$

yields

$$- \int_R^{r_C} \left[\frac{R\,(R - r_C)}{r_C\, D_{eff}} + \frac{R^2}{r_C^2\, k''_s} \right] \frac{r_C^2}{R^2}\, dr_C = \int_0^t f(C_A)\, \frac{b}{\rho_B}\, dt \qquad (5.5)$$

After some manipulation with an assumption of constant D_{eff}, this integration gives the time required for completing the nitridation process. The complete calculation can be seen in Appendix B. It should be mentioned that the effective diffusivity here is related to the transport of nitrogen through the nitride phase, which is different from the nitrogen diffusivities in fcc-Fe or bcc-Fe solid phase. The final equation is shown belows.

$$t = [\, 1 - 3\,(\, 1 - X_B\,)^{\frac{2}{3}} + 2\,(\, 1 - X_B\,)\,]\, \tau_{dff} + [\, 1 - (\, 1 - X_B\,)^{\frac{1}{3}}\,]\, \tau_{rxn} \qquad (5.6)$$

where

$$\tau_{dff} = \frac{R^2\, \rho_B}{6\, b\, D_{eff}\, f(C_A)} \qquad (5.7)$$

$$\tau_{rxn} = \frac{R\, \rho_B}{b\, k''_s\, f(C_A)} \qquad (5.8)$$

Equation (5.6) is a two-parameter model in which τ_{dff} and τ_{rxn} are the two unknowns. From these two, the effective diffusivity D_{eff} and the reaction rate constant k''_s can be evaluated after $f(C_A)$ is determined from gas phase concentration in the bed.

The time for the complete conversion is obtained by setting $X_B = 1$ in Equation (5.6), or

$$t = \tau_{ovl} = \tau_{dff} + \tau_{rxn} \tag{5.9}$$

Dividing Equation (5.6) by τ_{ovl},

$$\frac{t}{\tau_{ovl}} = [\ 1 - 3\ (\ 1-X_B\ )^{\frac{2}{3}} + 2\ (\ 1-X_B\ )\ ]\ \omega + [\ 1 - (\ 1-X_B\ )^{\frac{1}{3}}\ ]\ (1-\omega) \tag{5.10}$$

where

$$\omega = \frac{\tau_{dff}}{\tau_{dff} + \tau_{rxn}} = \frac{\tau_{dff}}{\tau_{ovl}} \tag{5.11}$$

The time for the complete conversion, τ_{ovl}, can be obtained from experimental data. Equation (5.10) then would be solved to find the remaining unknown parameter, ω, from data-fitting. Once the parameter ω is determined, the effects of diffusion and reaction resistances on the process may be evaluated.

5-2-1-2 Model Inspection

The nitrogen content measured by a LECO TC-436 nitrogen analyzer is expressed in terms of the mass of nitrogen per unit mass of nitrided powder, in which the basis, i.e., the mass of nitrided powder, changes with operating time. The basis hence has to be converted into the original mass of stainless steel powder to apply the

model. The extent of conversion is then given, neglecting a small amount of nitrogen contained in the original particle, by

$$W_N = \frac{w_N}{1 - w_N} \tag{5.12}$$

where w_N represents the mass fraction of nitrogen in the nitrided stainless steel powder, and W_N is the mass of nitrogen added per unit mass of original stainless steel powder. If the addition of nitrogen results in the formation of CrN and nitrogen in the solid solution of the surface shell, the concentration of un-reacted Cr per unit mass of stainless steel powder can be expressed using the initial molar concentration, $C_{Cr,\,i}$, of chromium per unit mass of stainless steel powder, as

$$C_{Cr} = C_{Cr,\,i} - \frac{W_N - W_{N,\,sln}}{M_N} \tag{5.13}$$

where $W_{N,\,sln}$ represents the mass of nitrogen dissolved in the solid solution per unit mass of stainless steel powder at any time, M_N is the atomic mass of nitrogen, C_{Cr} expresses the molar concentration of un-reacted Cr per unit mass of stainless steel powder at any time.

Moreover, the initial concentration of chromium, $C_{Cr,\,i}$, can also be written in terms of the nitrogen addition when Cr has reacted completely.

$$C_{Cr,\,i} = \frac{W_{N,\,f} - W_{N,\,sln,\,f}}{M_N} \tag{5.14}$$

where $W_{N,\,f}$ is the final overall mass content of nitrogen added per unit mass of stainless steel powder, which is the sum of nitrogen from CrN and nitrogen from solid solution, and $W_{N,\,sln,\,f}$ is the final mass content of nitrogen dissolved in solid solution

per unit mass of stainless steel. It should be mentioned that $W_{N,\,sln,\,f}$ is dependent on the thermodynamic state of nitrogen solubility in 316 stainless steel powder, which may be determined at the operating temperature.

By combining Equations (5.13) and (5.14), the fraction of Cr that has reacted, X_{Cr}, can be expressed as the nitrogen addition minus nitrogen dissolved in the solid solution.

$$X_{Cr} = 1 - \frac{C_{Cr}}{C_{Cr,\,i}} = \frac{W_N - W_{N,\,sln}}{W_{N,\,f} - W_{N,\,sln,\,f}} \tag{5.15}$$

The result of EMPA analysis indicates that a major amount of nitrogen in the nitrided particle stays in the surface layer, as seen in Figure 5.4. It is then reasonable to assume that the amount of nitrogen which has dissolved in the solid solution of surface layer is proportional to the fraction of CrN formation to simplify the further model-development, or

$$W_{N,\,sln} = W_{N,\,sln,\,f}\, X_{Cr} \tag{5.16}$$

Then, combining Equations (5.15) and (5.16) can simply express the extent of conversion of Cr in terms of the mass of nitrogen addition per unit mass of stainless steel powder as

$$X_{Cr} = \frac{W_N}{W_{N,\,f}} \tag{5.17}$$

Figure 5.5 illustrates the Cr conversion versus operating time, evaluated from the experimental data obtained at 750 °C with the feed of 50% NH_3 and 50% H_2. The estimated average ammonia and hydrogen contents in the bed are 13.7% and 74.2% by

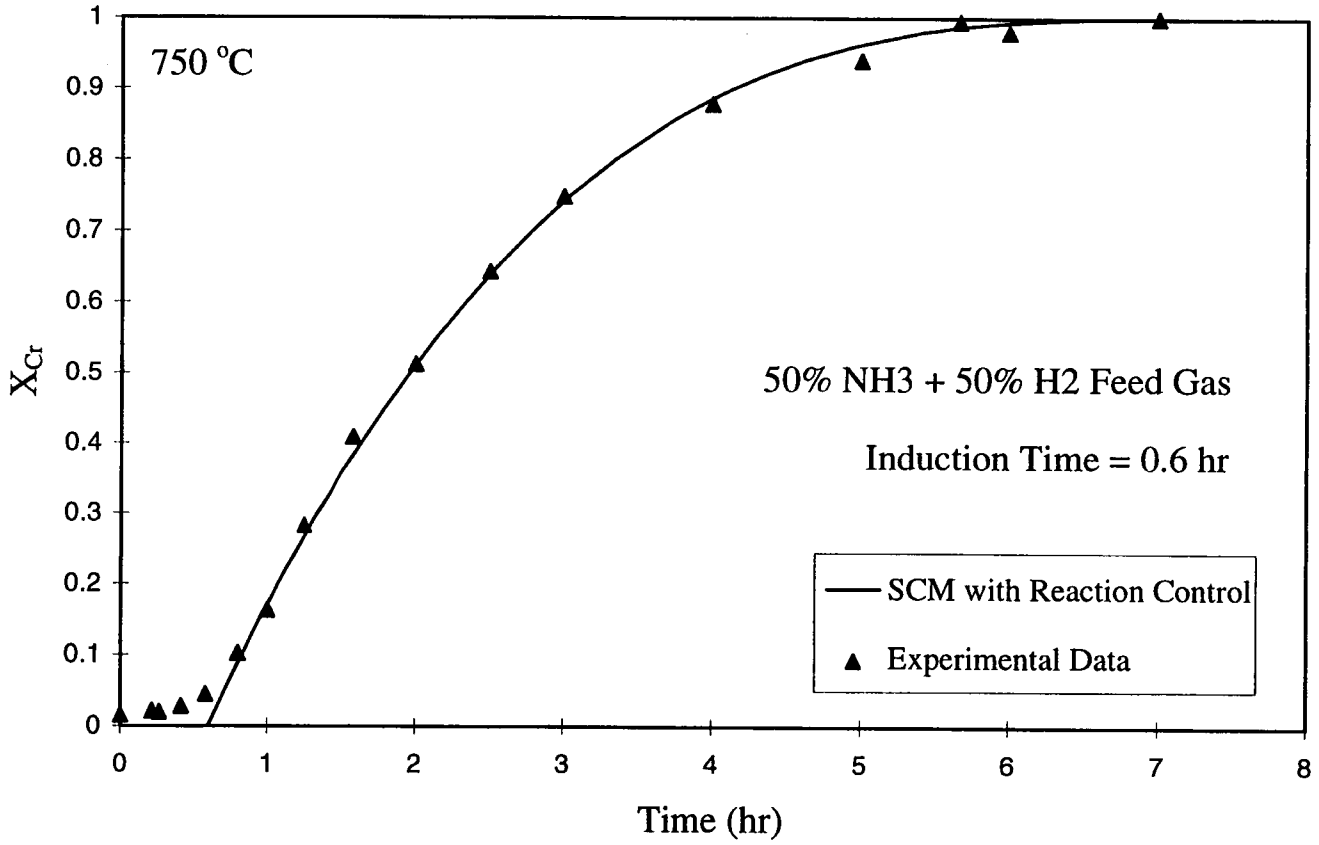

Figure 5.5 Shrinking core model prediction compared with experimental data for Cr conversion v.s. time obtained at 750 °C in the feed of 50% NH_3 and 50% H_2

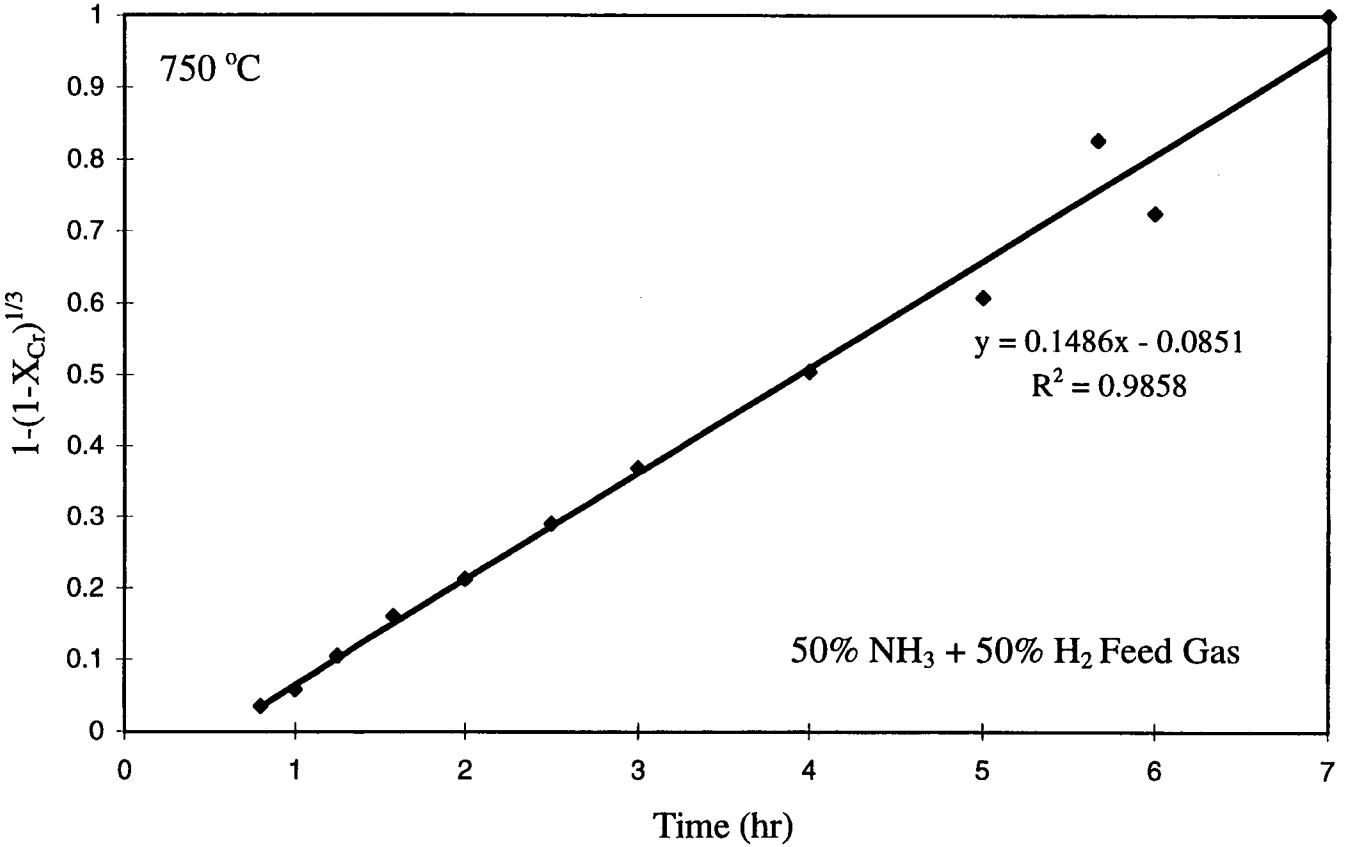

Figure 5.6 The linearity test of the SCM prediction using data obtained at 750 °C in the feed of 50% NH_3 and 50% H_2

volume, respectively. The calculated results by Equation (5.10) with $\omega = 0$, i.e., the reaction resistance domination, are also shown by a solid line with the induction time of 0.6 hour in Figure 5.5, that fits the data well. The linearity test of the SCM with reaction control is shown in Figure 5.6, in which the time for the complete conversion is found to be about 6.7 hours.

In addition, the SCM with chemical reaction control was applied to test data obtained at different nitridation conditions using the feed gas of 70% NH_3, 10% H_2 and 20% Ar at 750 °C. The comparison of the calculated curve with experimental results is plotted in Figure 5.7. The estimated average ammonia and hydrogen contents in the bed are 25.2 and 13.2% by volume, respectively. Figure 5.8 estimates the complete conversion time as about 5.7 hours from the inverse of the slope of the regression line. The initial and final data points are eliminated to avoid the variation influenced by the induction period and the final saturation stage. Hence, the calculated curve, with a complete conversion time of 5.7 hours and an induction time of 0.2 hour, shows a nice fit with experimental data in Figure 5.7.

Therefore, the results suggest that the nitridation process for the formation of CrN in the stainless steel powder can be described by the reaction-controlled shrinking un-reacted core model at 750 °C.

5-2-2 Low Temperature Nitridation

As discussed in section 4-4, the nitridation of 316 stainless steel powder in the fluidized bed using the NH_3 system results in the precipitation of CrN and Fe_4N, as well as nitrogen in solid solution. Table 5.2 shows the comparison of nitrogen measurements by two different methods: the LECO TC-436 nitrogen analysis and Kjeldahl methods. Samples were obtained at 550 °C with the feed gas of 50% NH_3 and 50% H_2. The estimated average ammonia and hydrogen contents in the bed are 42.2% and 55.3% by volume, respectively. The Kjeldahl method detects all nitrogen but nitrogen in CrN. Besides, the insoluble residual remaining in the Kjeldahl flask is identified to be CrN only by the X-ray diffraction. Moreover, the sum of nitrogen

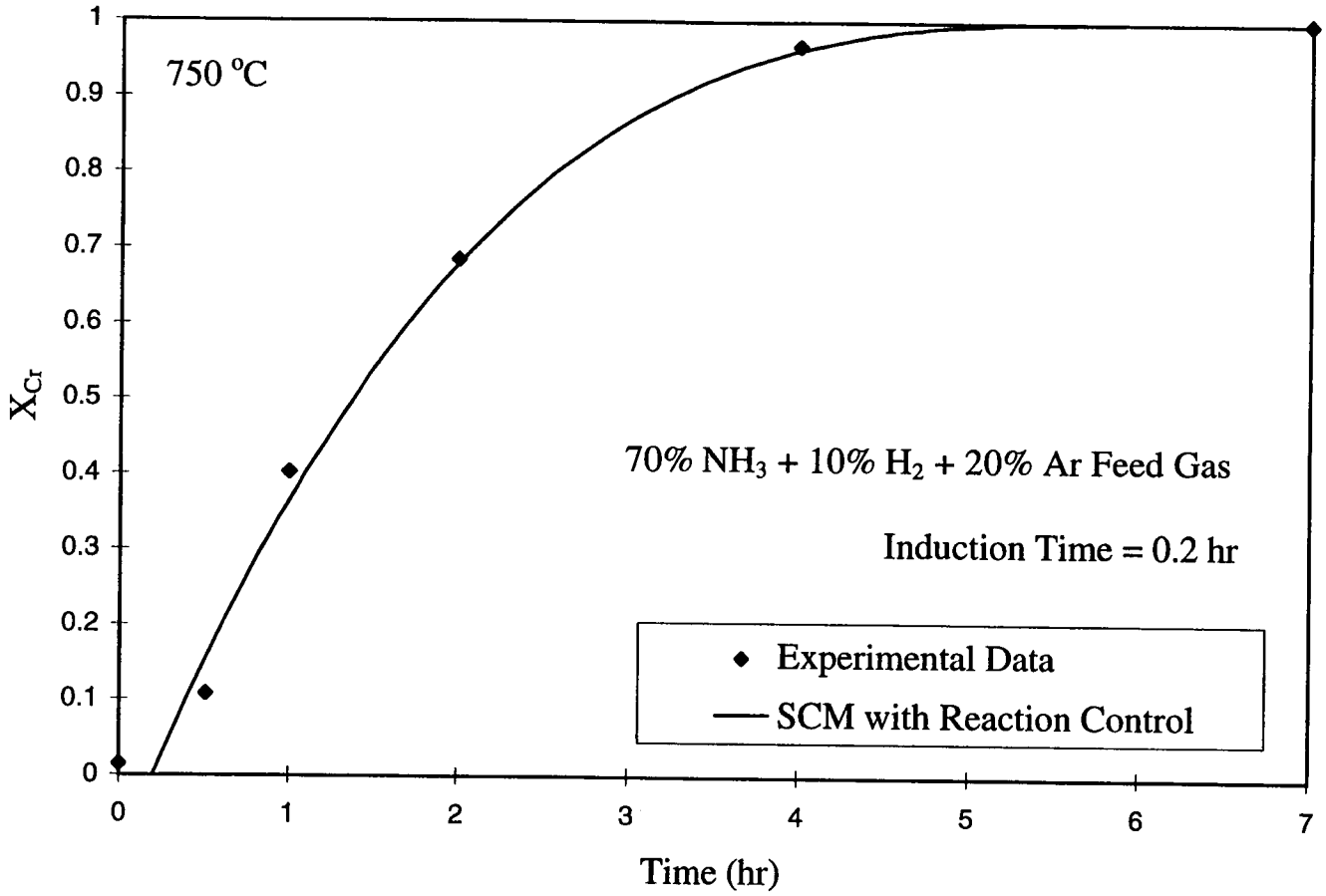

Figure 5.7 Shrinking core model prediction compared with experimental data for Cr conversion v.s. time obtained at 750 °C in the feed of 70% NH_3, 10% H_2, and 20% Ar

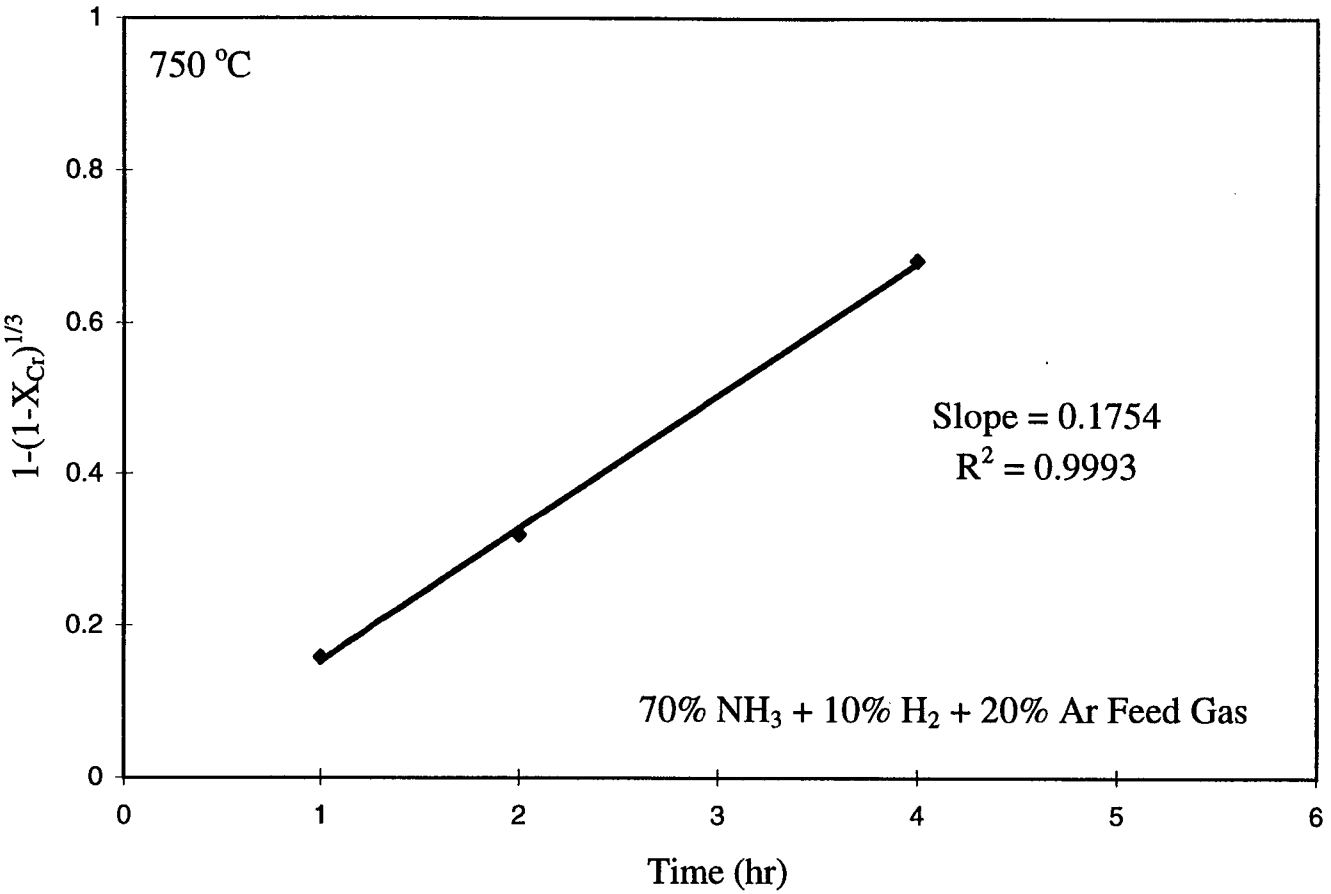

Figure 5.8 The linearity test of the SCM prediction using data obtained at 750 °C in the feed of 70% NH_3, 10% H_2, and 20% Ar

Table 5.2 The comparison of nitrogen contents by the LECO analysis and Kjeldahl's methods of samples obtained at 550 °C with the feed of 50% NH_3 and 50% H_2

Time (hr)	Nitrogen content from LECO Analysis (wt %)	Kjeldahl's Method		
		Nitrogen content# (wt %)	Nitrogen from CrN (wt %)	Overall Nitrogen Content (wt %)
1	0.597	0.434	0.198	0.632
3.06	2.65	0.684	2.294	2.978
4	3.68	0.966	3.086	4.052
6	6.52	2.176	4.570	6.746
7	7.40	3.274	4.833	8.107
8	8.59	4.460	4.668	9.128
10	9.47	4.976	4.976	9.952
10.83	10.2	5.474	5.075	10.54

: Nitrogen from stainless steel solution and/or Fe_4N.

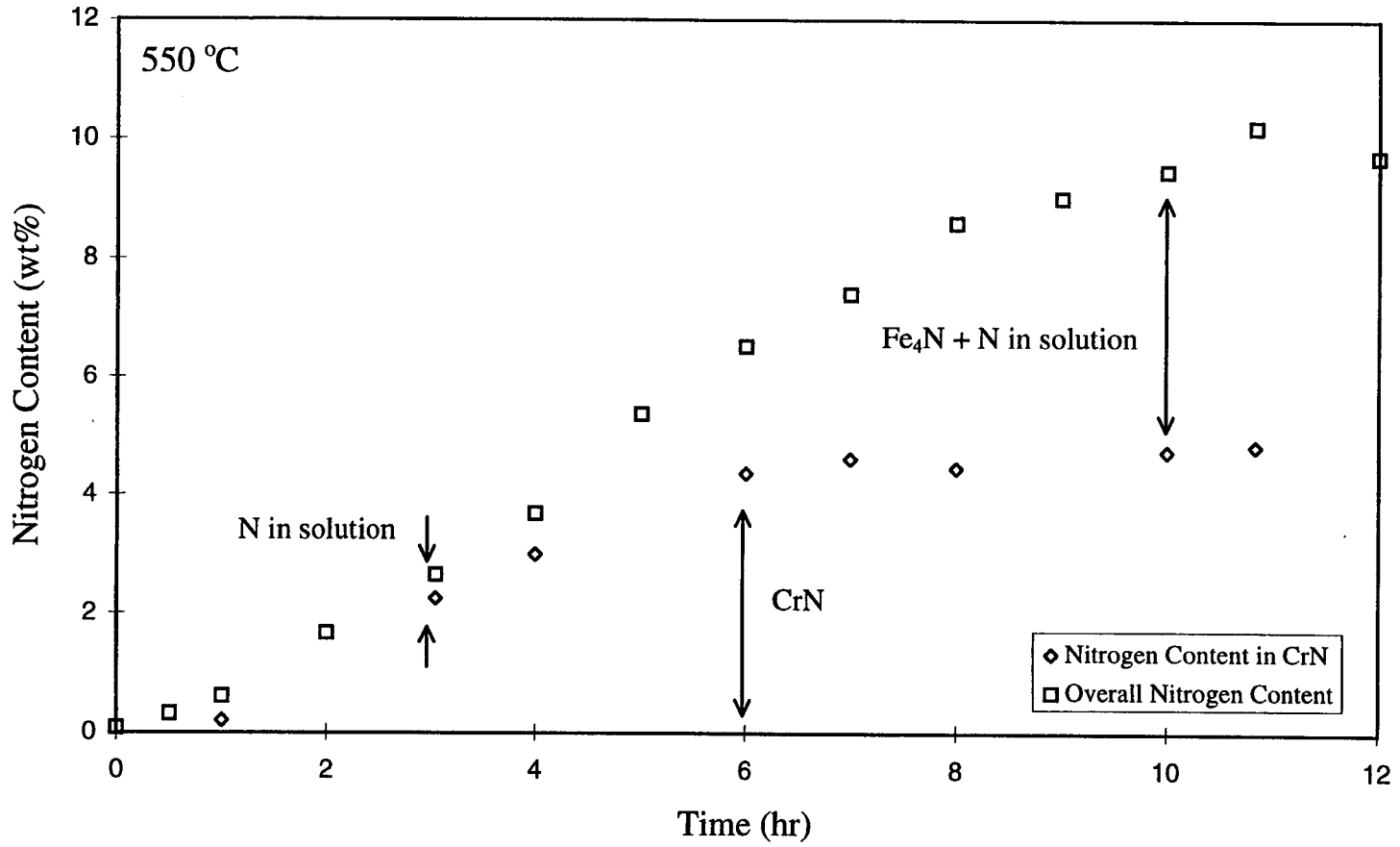

Figure 5.9 Overall nitrogen contents and the amount of nitrogen used to form CrN in products obtained in the feed gas of 50% NH_3 and 50% H_2 at 550 °C

from the Kjeldahl method and that from the insoluble residual shows a good agreement with the overall nitrogen content from LECO's method for the sample obtained at any operating time.

Figure 5.9 shows increases in the overall nitrogen content and the amount of nitrogen used to form CrN with time. The difference of nitrogen contents between these two curves represents the sum of nitrogen dissolved in the alloy solution and nitrogen used to form Fe_4N. However, the difference of nitrogen contents between the two curves is small during the initial stage, and XRD analysis (Figure 4.19) indicates that there is no Fe_4N phase formed during the early enhanced nitridation stage. Moreover, Table 4.5 illustrates an increase in the nitrogen content in the surface layer throughout the nitridation process. Because the nitridation process is controlled by the formation of CrN in the narrowly confined region of the surface, the diffusion of nitrogen in the surface layer is considered fast. Hence, the nitrogen concentration in the surface layer is expected to be continuously and uniformly distributed, as more nitrogen is added. With an increase in operating time, nitrogen tends to stay in the solid solution as the surface shell progresses inward. Nitrogen saturated in the interstitial iron solution may have a higher chance to be trapped in the unit of iron lattice to form a thermodynamically stable phase, i.e., Fe_4N in this study. Practically, however, the process of iron nitride formation may be considered that nitrogen reacts with iron uniformly through the surface layer. In other words, a pseudo-homogeneous reaction may be assumed for the Fe_4N formation after a certain amount of nitrogen is added into the solution. The conversion of Cr at which Fe_4N starts to form in the nitrided stainless steel powder is called a critical point ($X_{Cr,c}$).

Therefore, it is considered that the nitrogen addition in the enhanced nitridation stage is controlled by two mechanisms: the formation of CrN and the precipitation of Fe_4N. Nitrogen dissolved in solid solution may be included in the process of CrN formation, similar to the calculation in the case of high temperature nitridation. Nitrogen is mainly used for the formation of CrN first, which leads to the development of a surface layer. As the surface layer grows inward, Fe_4N gradually precipitates in the surface layer. Nitrogen added is eventually used for the formation of Fe_4N after most of Cr is consumed. A mathematical model for the process in the enhanced

nitridation stage at low temperature may be developed as a combination of two reaction schemes: the formation of CrN surface layer leading to a shrinking un-reacted core, followed by the pseudo-homogeneous iron nitride formation in the surface layer.

The following sections evaluate the proposed model for the formation of CrN first, then develop a model for Fe_4N precipitation at low temperature. The combination of both the models is used to examine experimental data. The gaseous dependencies of reaction rate in the formation of CrN and Fe_4N in the model are also evaluated to propose empirical power-law rate equations in term of NH_3 and H_2 concentrations.

5-2-2-1 Assumptions in Mathematical Model

The understanding of possible microstructural change in nitridation allows one to mathematically model the process at low temperatures. However, some assumptions have to be made before the calculation.

(1) Cr in the stainless steel powder is completely removed from the metal matrix by the reaction with nitrogen.
(2) The fraction of nitrogen dissolved in the solid solution is proportional to the fraction of CrN formation, calculated by Equation (5.16).
(3) After a critical amount of CrN has precipitated, iron nitride starts to precipitate. This critical extent of nitrogen addition is dependent on operating temperature, but independent of the gaseous composition.
(4) The formation of Fe_4N in the surface layer is uniformly distributed.

Above assumptions, based on observing the characteristics of nitridation process, are suggested to simplify the model calculation. The following will derive the equation for the overall nitrogen addition versus processing time.

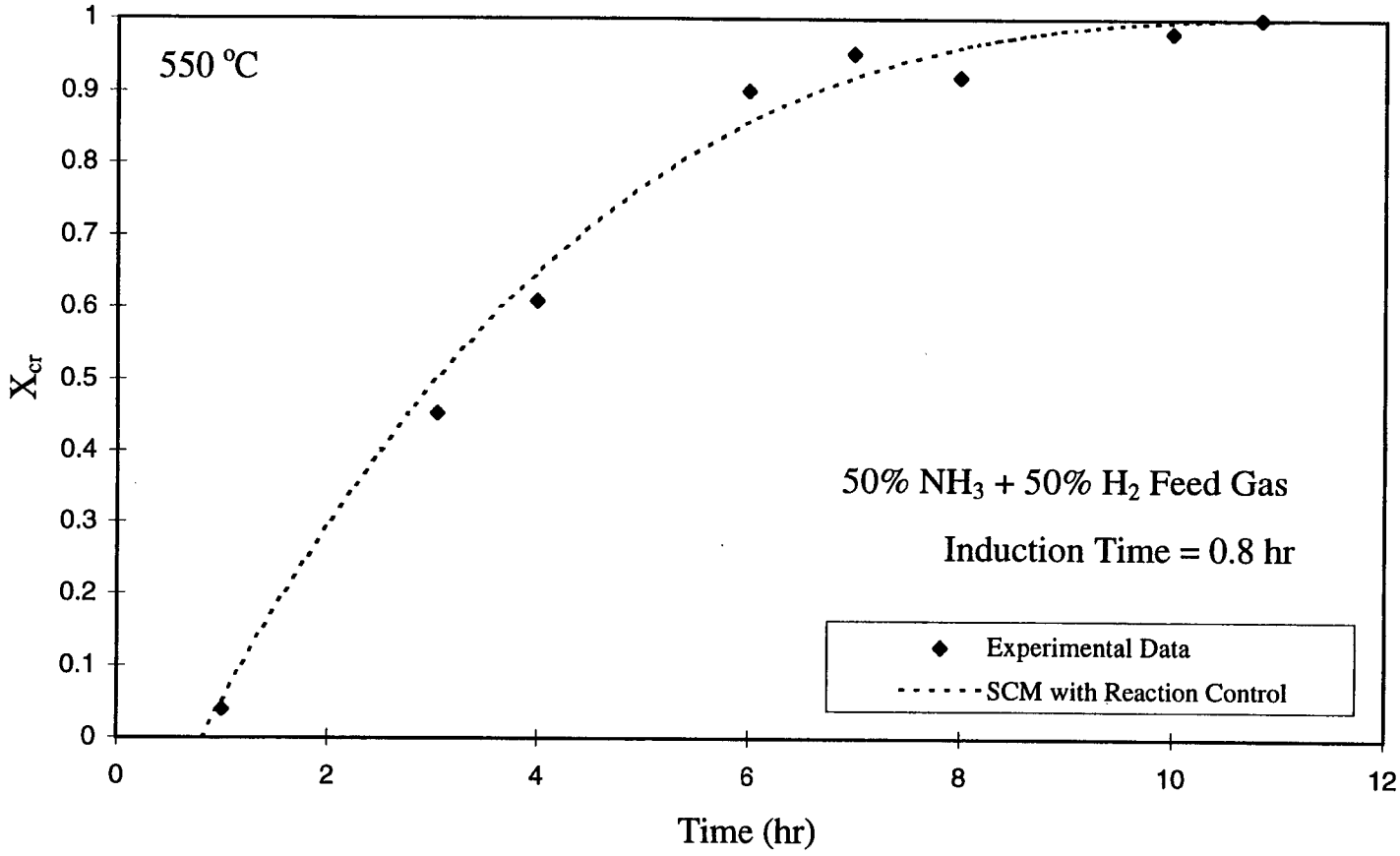

Figure 5.10 SCM prediction compared with Cr nitridation data obtained at 550 °C in the feed of 50% NH_3 and 50% H_2

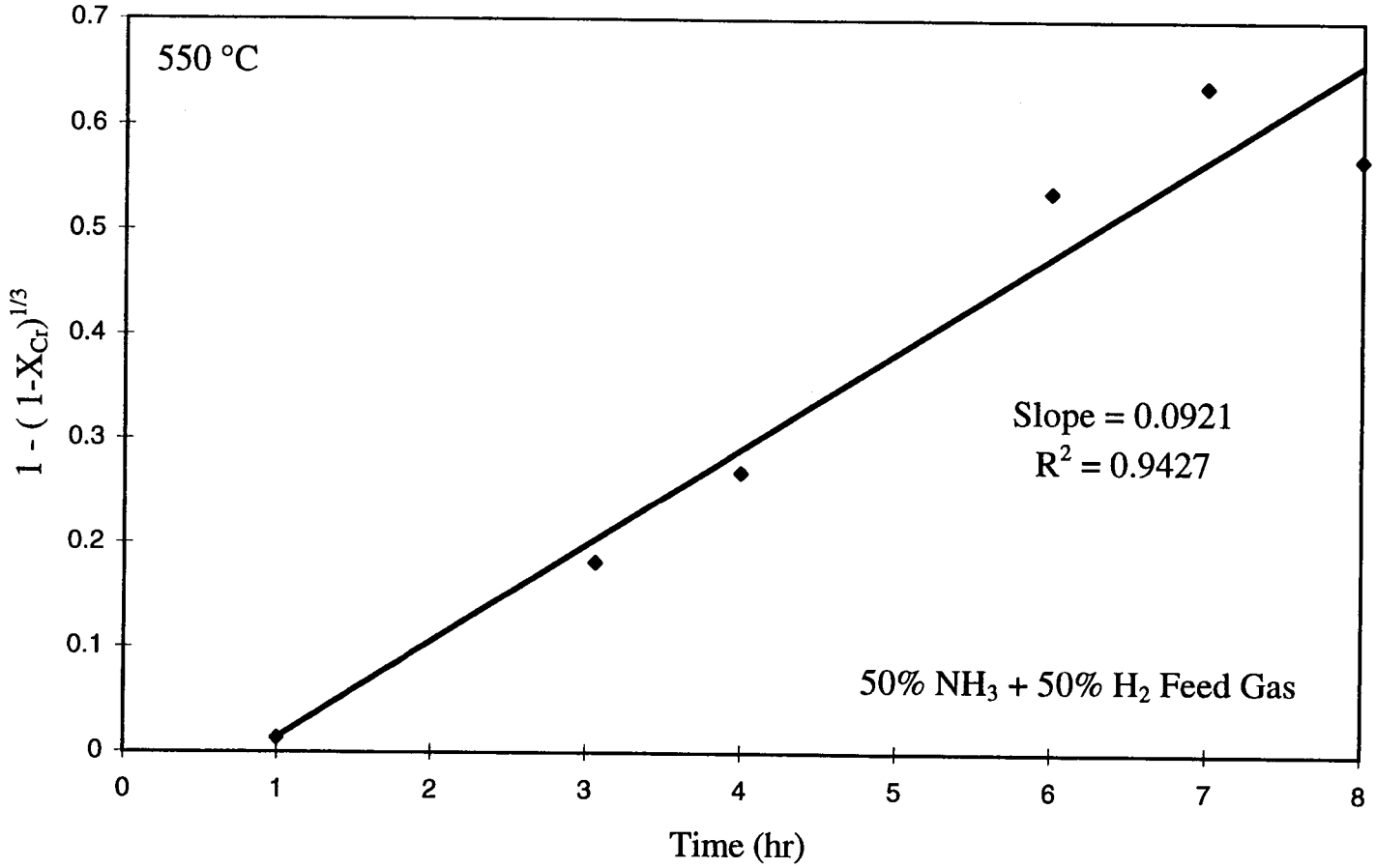

Figure 5.11 The linearity test of the SCM prediction using data obtained at 550 °C in the feed of 50% NH_3 and 50% H_2

5-2-2-2 CrN Formation

Using the data given in Table 5.2, the formation of CrN at 550 °C with the feed of 50% NH_3 and 50% H_2 is simulated by the shrinking un-reacted core model. As illustrated in Figure 5.10, the SCM with reaction control, indicated by the dashed line with an induction time of 0.8 hour, shows a good agreement with the experimental data. The time for the complete conversion of Cr was found to be 10.9 hours, as calculated from the inverse of slope of the regression line in Figure 5.11.

It has been shown that the low temperature CrN formation can also be described by the same kinetic process as that of high temperature case discussed in section 5-2-1-2. Therefore, it is suggested that the formation of CrN in the nitridation of 316 stainless steel powder at temperatures ranging from 550 to 750 °C follows the reaction-controlled shrinking un-reacted core model.

Therefore, for a reaction between chromium and nitrogen in the stainless steel powder,

$$N + Cr \rightarrow CrN \tag{5.18}$$

The expression for the relationship between conversion and processing time is given by

$$X_{Cr} = 1 - \left(1 - \frac{t}{\tau_{rxn,\,Cr}} \right)^3 \tag{5.19}$$

where

$$\tau_{rxn,\,Cr} = \frac{R\,\rho_{Cr}}{k''_{CrN}\,f(C_A)} \tag{5.20}$$

5-2-2-3 Fe_4N Formation

Before considering the precipitation of Fe_4N in the process, the relationship between the nitrogen addition and the amount of Cr and Fe consumed in the stainless steel powder has to be calculated, because the amount of nitrogen that has reacted with Fe is influenced by the amount of CrN formation. The fraction of Cr conversion, X_{Cr}, can be expressed by Equation (5.17) when no Fe_4N phase is formed. However, with the formation of Fe_4N in the process, the calculation has to be adjusted. At the critical point, the addition of nitrogen is the sum of nitrogen in CrN and nitrogen dissolved in the solid solution. Iron nitride starts to form after a certain amount of nitrogen is added into the particle at the critical point, represented as $W_{N,c}$. Thus, the relation between the overall nitrogen addition and the fraction of Cr actually consumed, represented as $X_{Cr,c}$, can be expressed according to Equations (5.15), (5.16) and (5.17).

$$W_{N,c} = X_{Cr,c} \left(W_{N,Cr,f} + W_{N,sln,f} \right) \tag{5.21}$$

where $W_{N,Cr,f}$ represents the amount of nitrogen required to convert Cr into CrN completely. Noting that $W_{N,c}$ consists of nitrogen from CrN and nitrogen from solid solution before Fe_4N is formed. When Fe_4N starts to form, the molar fraction of reacted iron, X_{Fe}, can be calculated by subtracting the amount of nitrogen having reacted with Cr and the amount of nitrogen dissolved in the alloy solution of surface layer from the overall amount of nitrogen addition.

$$X_{Fe} = \frac{W_N - X_{Cr} \left(W_{N,Cr,f} + W_{N,sln,f} \right)}{W_{N,f} - \left(W_{N,Cr,f} + W_{N,sln,f} \right)} \tag{5.22}$$

The fraction of Fe that has reacted, X_{Fe}, hence can be estimated by the fraction of Cr conversion, X_{Cr}, and the addition of nitrogen, W_N, at any time. The conversion

for the Cr reaction, X_{Cr}, may also be estimated by the SCM with chemical reaction control, Equations (5.19) and (5.20), as discussed in the preceding section.

Iron nitride is produced in the surface layer, the process of which may be described by the pseudo-homogeneous model. The reaction of iron nitride formation may be expressed as

$$N + 4\ Fe \rightarrow Fe_4N \tag{5.23}$$

Since it is approximated that the process of iron nitridation takes place in the surface shell uniformly, the rate of reaction based on the volume of surface shell may be expressed by the following equation.

$$-r_s = -\frac{1}{4\ V_s}\frac{dN_{Fe,\,s}}{dt} = k'''_{Fe_4N}\ f'(C_A)\ C_{Fe,\,s} \tag{5.24}$$

Notice that k'''_{Fe_4N} is the rate constant of reaction (5.23) based on unit volume of stainless steel; $f'(C_A)$ represents the dependency of the reaction rate on the gaseous reactant concentration in the process of iron nitride formation; $N_{Fe,\,s}$ is the molar amount of Fe in the surface layer; V_s is the volume of the surface layer in a stainless steel particle; and $C_{Fe,\,s}$ represents the apparent Fe concentration in the surface layer, i.e., moles of un-reacted Fe per unit volume of the surface layer. It should be noted that the gaseous concentration dependency of reaction rate, $f'(C_A)$, may be different from $f(C_A)$ in the process of CrN formation because different mechanisms may be involved in the process.

$C_{Fe,\,s}$ can be related to the conversion of Fe into Fe_4N in the surface shell.

$$C_{Fe,\,s} = \frac{N_{Fe,\,s}}{V_s} = C_{Fe,\,0}\,(\,1 - X_{Fe,\,s}\,) \qquad (5.25)$$

where $C_{Fe,\,0}$ is the initial Fe concentration in a particle, and $X_{Fe,\,s}$ is the conversion of Fe in the surface layer.

Plugging Equation (5.25) into Equation (5.24) gives

$$\frac{dX_{Fe,\,s}}{dt} = 4\,k'''_{Fe_4N}\,f'(C_A)\,(\,1 - X_{Fe,\,s}\,) \qquad (5.26)$$

However, Equation (5.26) is based on the surface layer of a particle, which grows with the processing time due to the formation of CrN. The conversion of Fe on the basis of stainless steel particle, X_{Fe}, has to be derived. The overall amount of un-reacted Fe in the entire particle can be expressed with the sum of un-reacted Fe in the surface shell and in the inner core.

$$C_{Fe} = C_{Fe,\,0}\,(1 - X_{Fe}) = C_{Fe,\,s}\,\phi + C_{Fe,\,0}\,(1 - \phi) \qquad (5.27)$$

where ϕ represents the volumetric fraction of surface layer in a particle.

From Equations (5.25) and (5.27), the conversions of Fe based on the surface layer is related to that on the particle as

$$X_{Fe,\,s} = \frac{X_{Fe}}{\phi} \qquad (5.28)$$

Hence, applying this relation to Equation (5.26) and rearranging, on may find the rate equation

$$\frac{dX_{Fe}}{dt} + \left(K(C_A) - \frac{d(\ln\phi)}{dt} \right) X_{Fe} = K(C_A)\,\phi \qquad (5.29)$$

where

$$K(C_A) = 4\, k'''_{Fe_4N} f'(C_A) \qquad (5.30)$$

ϕ, the volumetric fraction of the surface layer in a particle, is determined from the process of Cr formation, and is expressed by the conversion of Cr in the process as

$$\phi = X_{Cr} \qquad (5.31)$$

X_{Cr} has been calculated by Equation (5.19). Hence, substituting Equations (5.19) and (5.31) into Equation (5.29) and integrating with the initial condition, $t_{ini} = t_{Fe,\,i}$ and $X_{Fe} = 0$, the rate equation becomes

$$X_{Fe} = \left[1 - \left(1 - \frac{t}{\tau_{rxn,\,Cr}} \right)^3 \right] \left(1 - e^{-K(C_A)\,(t - t_{Fe,\,i})} \right) \qquad (5.32)$$

and $t_{Fe,\,i}$ represents the critical time when Fe_4N starts to precipitate, i.e., at $X_{Cr} = X_{Cr,\,c}$. Equation (5.32) is the form to be used for the Fe_4N formation in the nitridation of stainless steel powder. The detailed calculation of integration can also be seen in Appendix C.

It should be mentioned that the first term on the right hand side of Equation (5.32) represents the fraction of surface layer in the particle at any time of the process, which will not exceed one. Hence, after the surface layer extends to the entire particle, i.e., $t \geq \tau_{rxn,\,Cr}$, Equation (5.32) is reduced to the uniform conversion model (UCM).

$$X_{Fe} = 1 - e^{-K(C_A)\,(\,t\,-\,t_{Fe,\,i}\,)} \tag{5.33}$$

5-2-3 Model Evaluation

The nitrogen in the nitrided stainless steel powder is present in three different forms: nitrogen in solid solution, nitrogen in CrN, and nitrogen in Fe_4N. The combination of nitrogen dissolved in solid solution and reacted with chromium follows the shrinking core model. The following nitrogen addition in Fe_4N is calculated from the pseudo-homogeneous model applied in the surface layer. From the combination of CrN formation and Fe_4N precipitation, a general equation is hence shown here to represent the fraction extent of overall nitrogen-addition in the stainless steel powder.

$$X_N = \frac{W_N}{W_{N,\,f}} = \frac{X_{Cr}\,(\,W_{N,\,Cr,\,f} + W_{N,\,sln,\,f}\,) + (\,X_{Fe}\,W_{N,\,Fe,\,f}\,)\,\Psi}{W_{N,\,f}} \tag{5.34}$$

where

$$\Psi = \begin{matrix} 0 & at\ X_{Cr} \leq X_{Cr,\,c} \\ 1 & at\ X_{Cr} > X_{Cr,\,c} \end{matrix} \tag{5.35}$$

The possible total amount of reacted Fe, $W_{N, Fe, f}$, is dependent on the reaction temperature. Ψ is defined as unity while the formation of Fe_4N takes place after X_{Cr} has reached $X_{Cr, c}$. $W_{N, f}$ may be measured from the experimental data obtained in the final saturation stage while $W_{N, Cr, f}$ is evaluated by knowing the composition of Cr in the stainless steel powder. On the other hand, $W_{N, sln, f}$ needs to be adjusted to fit experimental data before the formation of Fe_4N because of the lack of information of nitrogen solubility in 316 stainless steel powder at temperatures in the range of this study. Thus, $W_{N, Fe, f}$ can be determined.

The following section describes an example of calculations using the proposed model, and compares the calculated results with the experimental data obtained at 550 °C with the feed of 50% NH_3 and 50% H_2. The estimated average NH_3 and H_2 contents in the bed are 42.2% and 55.3%, respectively. The procedure of calculations is presented below.

(1) Calculate X_N in Equation (5.34) from experimental data.
(2) Evaluate $W_{N, Cr, f}$ and $W_{N, sln, f}$ from Figure 5.9.
(3) Determine the induction time and $\tau_{rxn, Cr,}$ from Figure 5.10, and then X_{Cr}.
(4) Choose $t_{Fe, i}$, and hence $X_{Cr, c}$ at the critical point.
(5) Give a value of $K(C_A)$ in Equation (5.32) to find X_{Fe}, and then X_N as a function of processing time.
(6) Repeat step (5) by changing $K(C_A)$ till the curve fits the experimental data in step (1) best.

It should be mentioned that the above calculation is based on the assumption that the final amount of nitrogen dissolved in the solid solution, $W_{N, sln, f}$, and nitrogen in CrN, $W_{N, Cr, f}$, are known. $X_{Cr, c}$ can be determined by the difference of nitrogen contents obtained from LECO's and Kjeldahl methods. The parameter, $K(C_A)$, is the only adjustable parameter that needs to be chosen to fit experimental data. The detailed calculation, operated by the Excel spreadsheet, is shown in Appendix D.

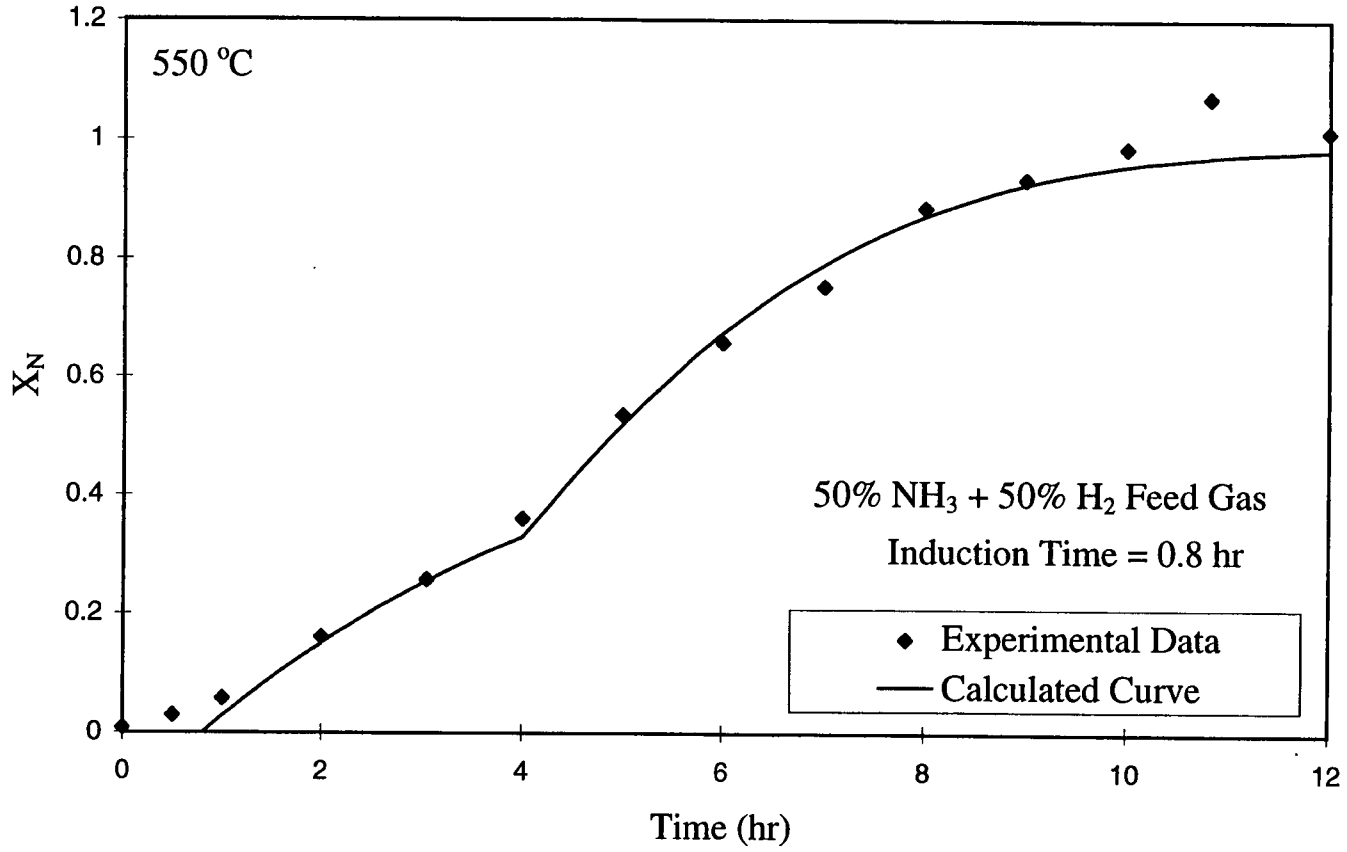

Figure 5.12 Comparison of calculated results with the experimental data obtained at 550 °C in the feed of 50% NH_3 and 50% H_2

A comparison of experimental data with the calculated curve is shown in Figure 5.12. The model calculation is based on the uniform particle size, 70 μm, which is the mean particle size of sample powder used in this study. The figure shows that the model described above agrees well with experimental data with an estimate of $X_{Cr,c} = 0.647$, i.e., $t_{Fe,i} = 4$ hours, and an induction time of 0.8 hour. In a later section, the calculated curves will be tested for different composition of gas mixtures at 550 °C, with the same value of $X_{Cr,c}$ applied. However, before the proposed model is inspected at different composition of gas mixtures in the bed, it is necessary to calculate the gaseous concentration dependencies of reaction rate in the formation of CrN and Fe_4N during the nitridation process.

5-2-3-1 Effects of NH_3 and H_2 on CrN Formation

Ammonia and hydrogen contents in the bed influence the nitridation process, as illustrated in Figures 4.13 and 4.14. The dependency of reaction rate on the gas concentration in the formation of CrN, $f(C_A)$, may be expressed as a function of NH_3 and H_2 molar concentrations.

$$f(C_A) = \frac{C_{NH_3}{}^m}{C_{H_2}{}^n} \qquad (5.36)$$

As developed from Equation (5.19), the nitridation rate of CrN formation in the enhanced nitridation stage is represented in term of the gaseous concentration dependency, rate constant, and the un-reacted solid reactant (Cr) which is related to the amount of nitrogen addition. In order to evaluate $f(C_A)$, the slopes of nitrogen-addition versus time curves at a fixed operating temperature and at a fixed extent of nitrogen-addition but for different gas mixtures need to be used. A series of runs were made at 550 °C with different NH_3 and H_2 contents in the bed, as shown in Table 5.3. The nitridation rates at a nitrogen-addition of 3 wt%, at which the process is

Table 5.3 Nitridation rates measured at 3 wt % nitrogen-addition from data obtained with different NH_3 and H_2 mixtures at 550 °C

Nitridation Rate at 3 wt % of Nitrogen Addition	Average NH_3 content in the bed (vol. %)@	Average H_2 content in the bed (vol. %)@
1.39	42.2	55.3
1.73	42.2	36.3
2.34	42.2	17.3
5.22	80.6	14.6
4.38	73.2	22.4
3.17	58.0	19.9
1.11	25.8	14.6

@ : Adopted from Table 4-2-2.1.

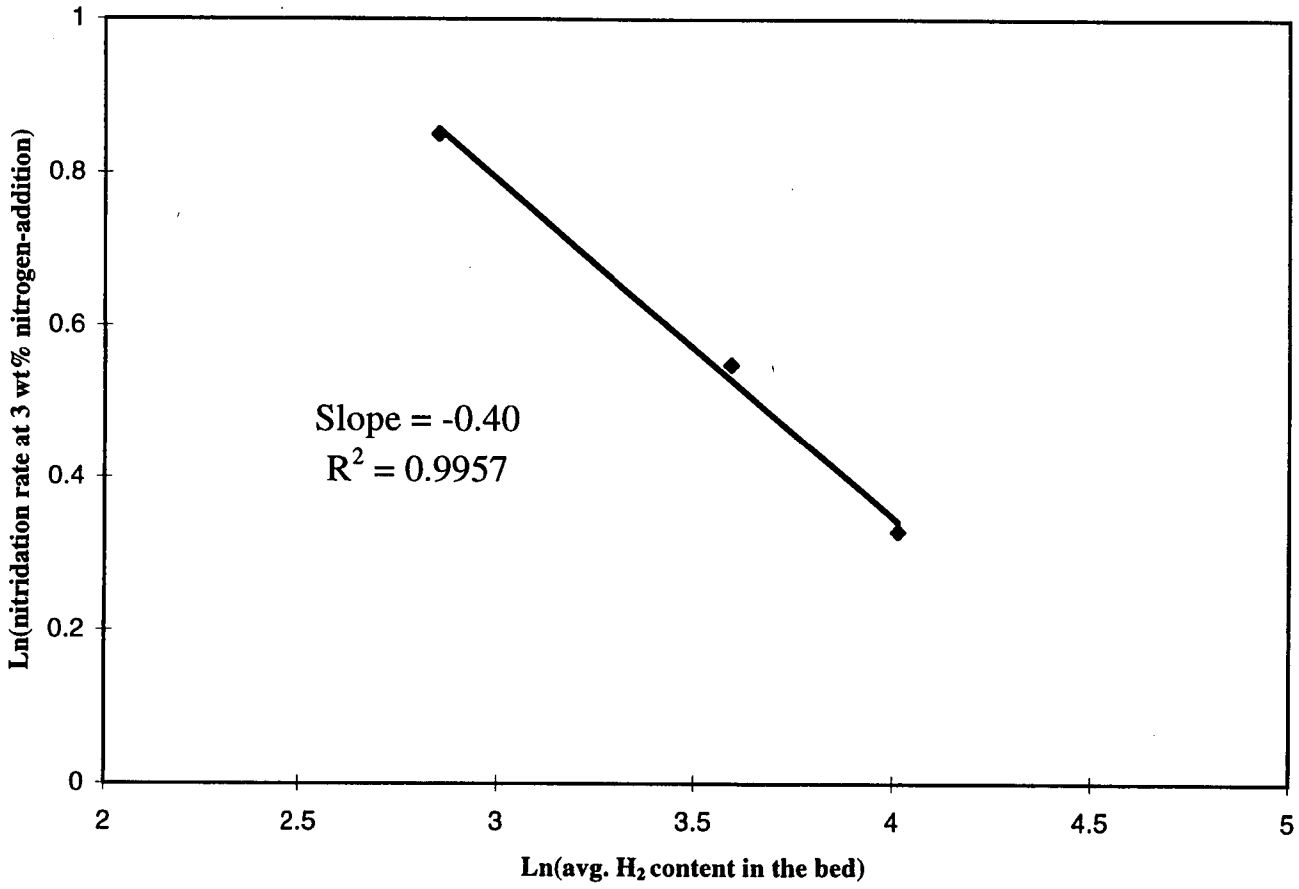

Figure 5.13 Effect of H_2 concentration on the rate of CrN precipitation

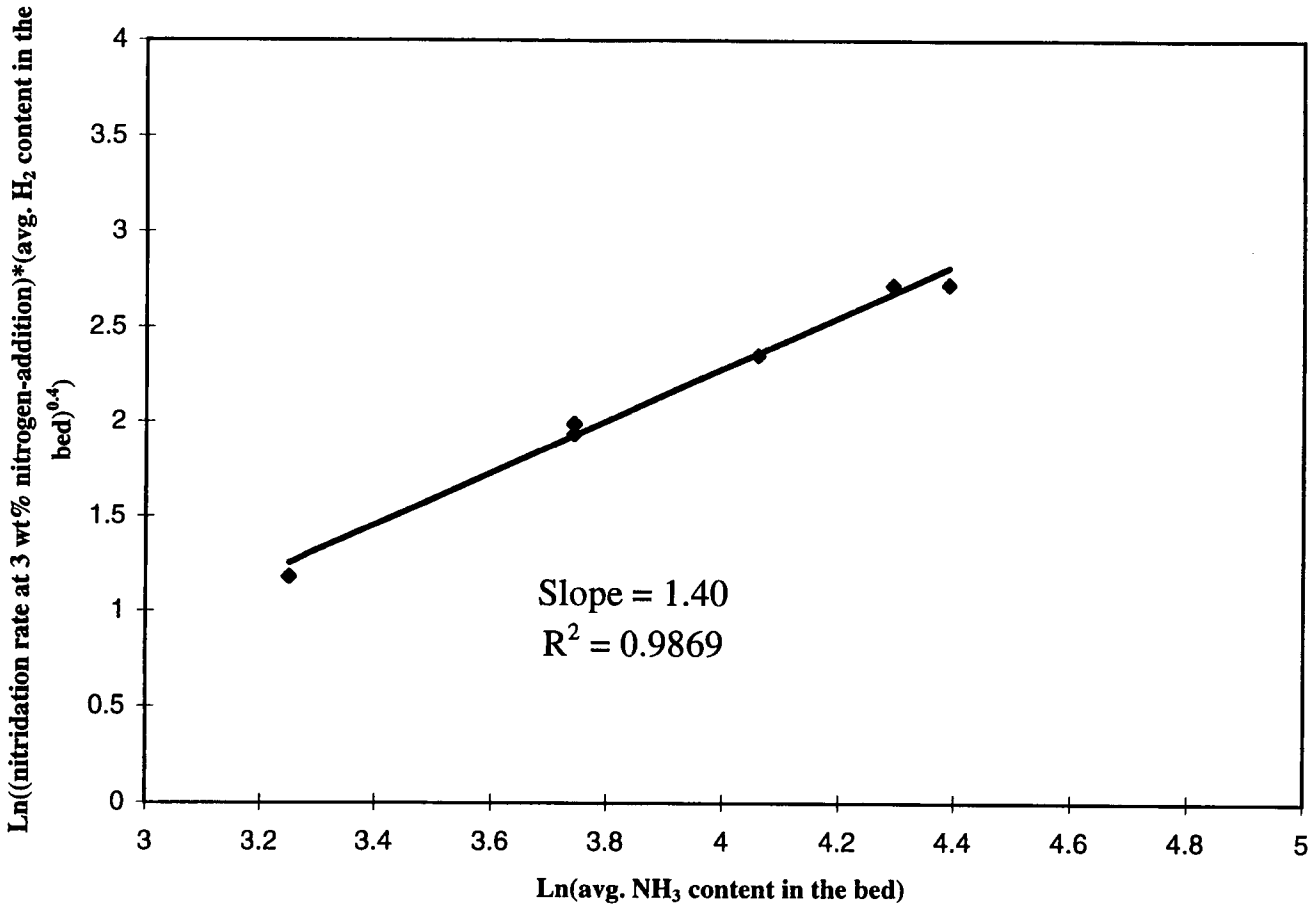

Figure 5.14 Effect of NH_3 concentration on the rate of CrN precipitation

controlled by the formation of CrN, are evaluated to find the effects of ammonia and hydrogen on the process. Figure 5.13 shows the plot of nitridation rates at 3 wt% nitrogen-addition versus hydrogen concentration (from Figure 4.13), in which ammonia concentration is fixed. The log-log plot suggests that the effect of hydrogen is represented by a power law with an exponent of -0.40. Thus, by applying the obtained hydrogen dependency, nitridation rates at different ammonia and hydrogen contents are evaluated to determine the effect of ammonia. Figure 5.14 suggests that the effect of ammonia concentration may be represented by a power of 1.40. Therefore, the dependency of the nitridation process on the gaseous concentration may be expressed as

$$f(C_A) = \frac{C_{NH_3}^{1.40}}{C_{H_2}^{0.40}} \tag{5.37}$$

The result suggests that ammonia gas has a dominant effect on the nitridation process in the bed while hydrogen gas shows a minor, but inhibiting effect on the process.

5-2-3-2 Effects of NH_3 and H_2 on Fe_4N formation

A power law equation similar to Equation (5.36) may also be used to represent the gaseous concentration dependency of reaction rate in the formation of Fe_4N, $f'(C_A)$. It is noticed that the dependency of Fe_4N formation can not be explicitly obtained from the overall nitrogen-addition data, because both gaseous dependencies of reaction will be presented in the process.

Hence, an attempt is made to exclude the effect of CrN formation from the overall gaseous dependency of reaction. For the formation of Fe_4N, the gaseous dependency of reaction rate, $f'(C_A)$, needs to be evaluated using Equations (5.30) and

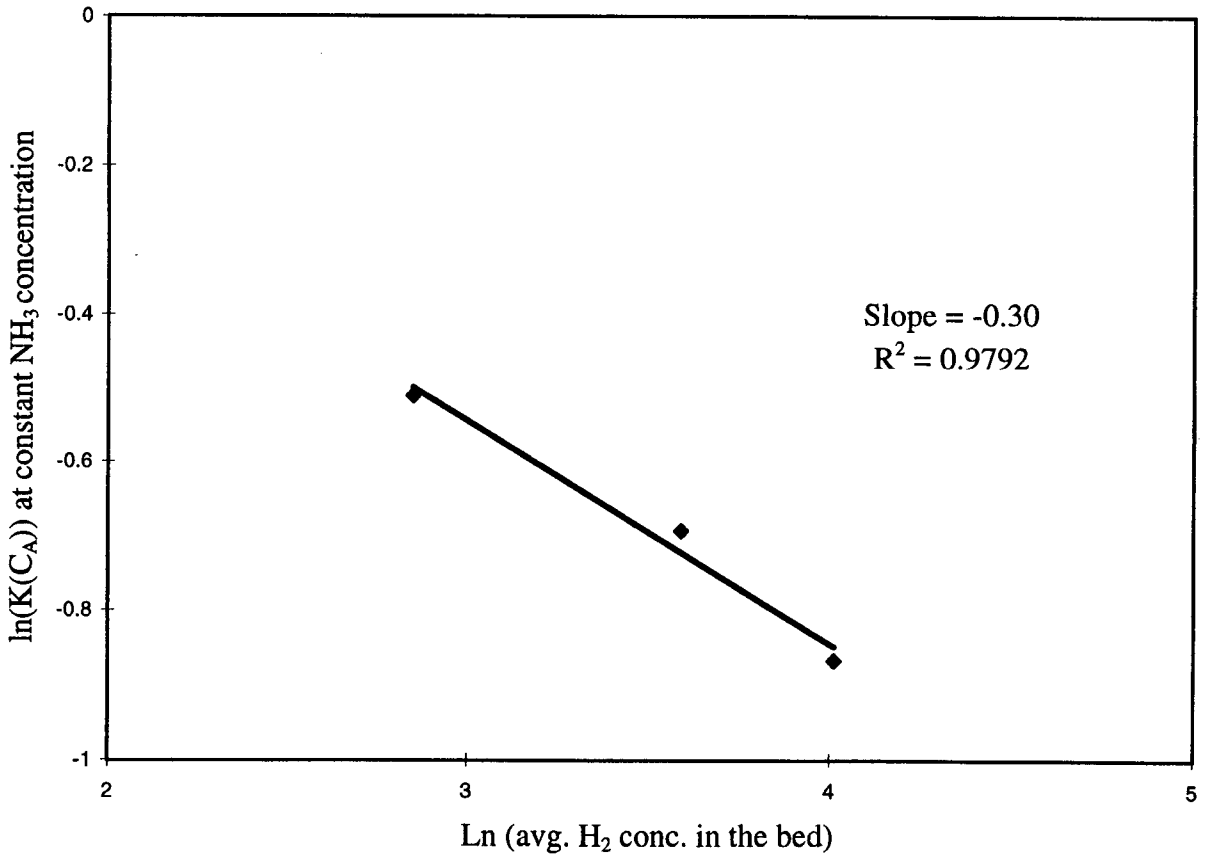

Figure 5.15 Effect of H_2 concentration on the rate of Fe_4N formation

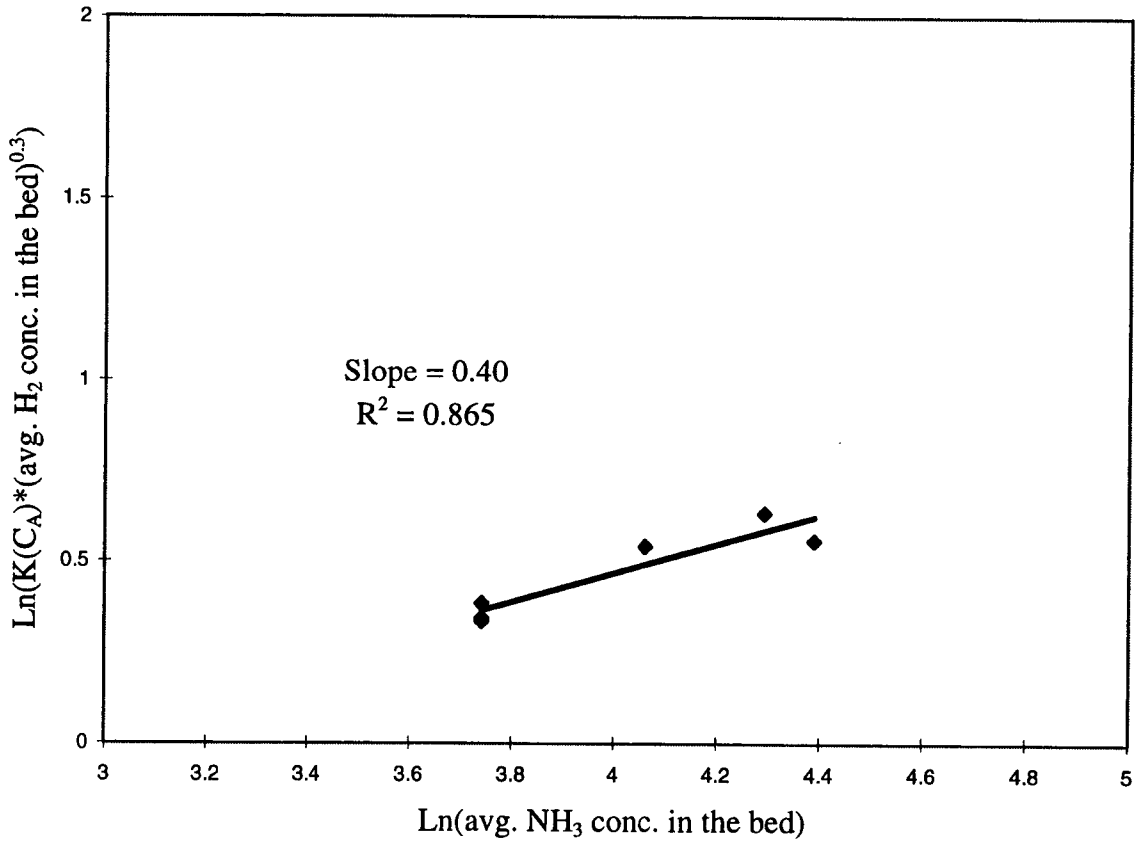

Figure 5.16 Effect of NH_3 concentration on the rate of Fe_4N formation

(5.32). For different gas mixtures at 550 °C, $K(C_A)$ may be estimated to fit experimental data. According to Equation (5.30), $K(C_A)$ can be used to determine $f'(C_A)$ when k'''_{Fe_4N} is constant at constant operating temperature. Thus, the relation between $K(C_A)$ and gas compositions, NH_3 and H_2, will lead to a power-law rate expression.

Figure 5.15 shows the plot of estimated $K(C_A)$ versus average H_2 concentration in the bed when NH_3 concentration is fixed. The effect of H_2 concentration on the formation of Fe_4N is found to be approximately -0.30. Following the same procedure gives an exponent of about 0.40 for NH_3 concentration, as indicated in Figure 5.16. The procedure of evaluation is also presented in Appendix D. The gaseous concentration dependency of Fe_4N formation rate is expressed as

$$f'(C_A) = \frac{C_{NH_3}^{0.40}}{C_{H_2}^{0.30}} \qquad \textbf{(5.38)}$$

During the nitridation process, the gaseous concentration dependency of reaction rate is first determined by the formation of CrN, i.e., as given by Equation (5.37). After Fe_4N starts to precipitate, an additional gaseous concentration dependency for Fe_4N formation, represented by Equation (5.38), has to be included.

Moreover, it is found that the effect of H_2 concentration on the reaction rate of CrN formation is minor and very similar to that of Fe_4N precipitation. On the other hand, the effect of NH_3 concentration on CrN formation is more significant than that on Fe_4N formation.

5-2-3-3 Fitting with Experimental Data

After finding the gaseous concentration dependency of reaction rate on the nitridation process, a proposed model can be examined to compare with experimental

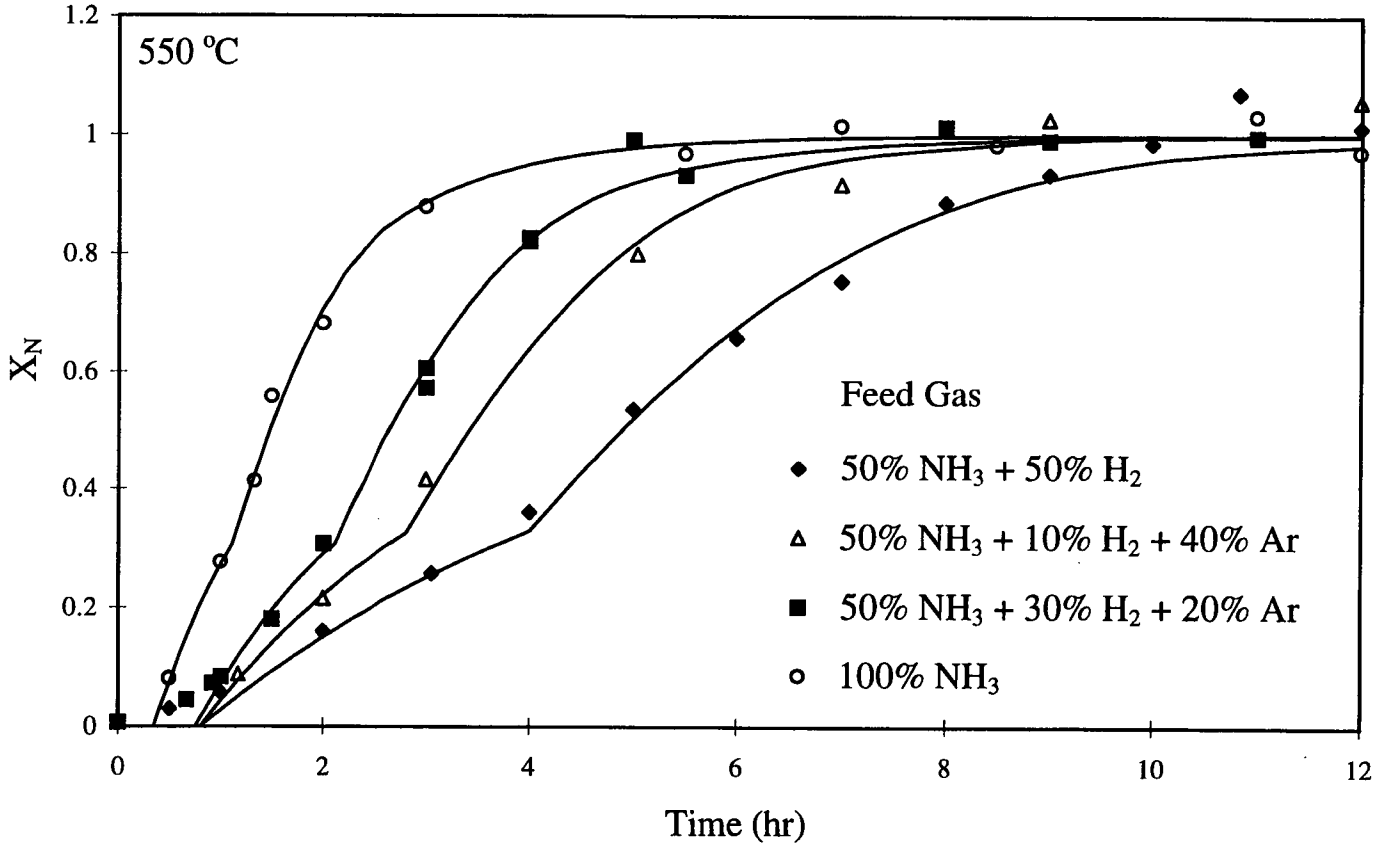

Figure 5.17 Comparison of calculated results with the experimental data obtained at 550 °C at different gas compositions

data for different gas mixtures at 550 °C. Figure 5.17 illustrates the comparison of the experimental data with the calculated curves for different feed gas mixtures. The actual gas composition may be found from Table 4.4. The critical point, $X_{Cr,c}$, may represent a characteristic difference of reaction rate between the formation of CrN and that of Fe_4N, which may vary as a function of the processing temperature. On the other hand, one may expect that $X_{Cr,c}$ is independent of gaseous composition in the process. Hence, $X_{Cr,c}$ is fixed at 0.647 in Figure 5.17. The detailed process of calculation may also be seen in Appendix D. The proposed model shows a nice fit with each set of experimental data.

5-2-3-4 Effect of Particle Size

As discussed in section 5-2-2-2 for CrN formation, the conversion of Cr follows the shrinking core model (SCM) with chemical reaction control. Equations (5.19) and (5.20) represent the rate expression of this model. Equation (5.20) indicates that the time for the complete conversion of Cr is proportional to the radius of particles. Hence, collecting experimental data with different particle sizes is an important process to further confirm the proposed model for CrN formation.

In the present study, major part of 316 stainless steel powder has a narrow size distribution, approximately from 45 μm to 120 μm, as shown in Figure 3.2. The particle size of nitrided powder may be assumed to be uniform at 70 μm, as shown in Table 3.1. Selected powder of particle size ranging from 88 μm to 104 μm with an average particle size of 96 μm was prepared from the original powder through screen separation. Two experimental runs, one using the original powder and the other using the selected powder, were made at 550 °C with the feed gas of 70% NH_3, 10% H_2 and 20% Ar to test the effect of particle size on the nitriding process. A comparison of experimental data for these two different ranges of particle size is plotted in Figure 5.18. The calculated values from the proposed model are also shown for the comparison with the data of these two cases, as plotted by the dotted and solid lines. It is found that the complete conversion time of the SCM for the selected larger

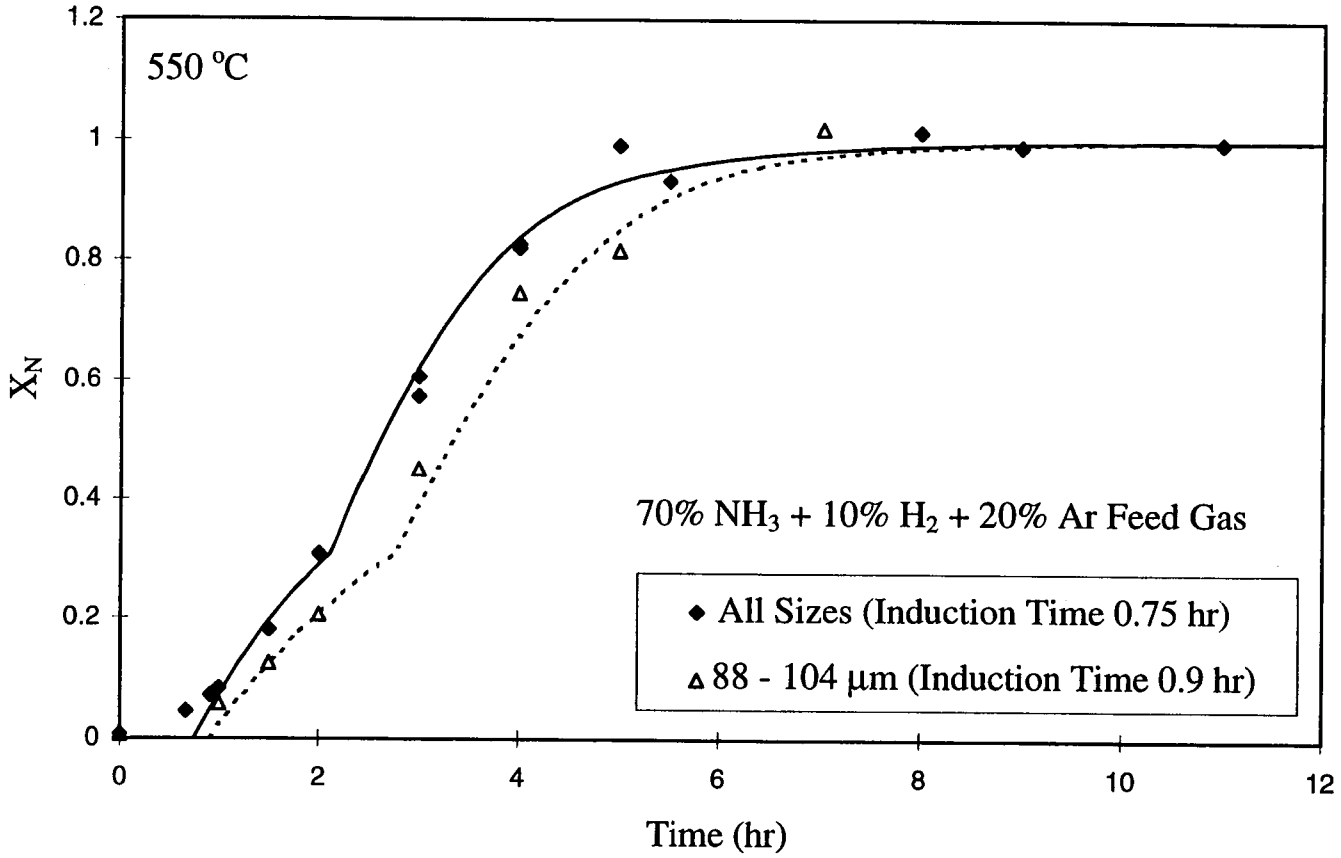

Figure 5.18 Effect of particle size on the nitridation process

particles is longer than that for the original powder by a factor approximately equal to the ratio of their average particle sizes. Hence, the result suggests that the proposed model can represent the kinetic process of nitriding 316 stainless steel powder in NH_3/ H_2 system at temperatures ranging from 550 °C to 750 °C.

5-2-3-5 Apparent Activation Energy

As predicted from Figures 5.5 and 5.10, the apparent complete conversion times for the CrN formation are estimated to be 6.73 hours when operated at 750 °C with the feed of 50% NH_3 and 50% H_2 (the estimated average concentrations, NH_3 = 9.7% and H_2 = 76.9%), and 10.9 hours at 550 °C with the feed of 50% NH_3 and 50% H_2 (the estimated average concentrations, NH_3 = 42.2% and H_2 = 55.3%). The apparent complete conversion for the CrN formation represented by the SCM with chemical reaction control should be inversely proportional to the rate constant and the gaseous concentration dependency of reaction rate (Equation (5.37)), according to Equation (5.20). Hence, one may be able to estimate the apparent activation energy for the reaction of CrN formation in the range from 550 to 750 °C. The estimated apparent activation energy for the precipitation of CrN in the NH_3 system is found to be about 111.1 kJ/mol.

From a microscopic point of view, forming a new phase of CrN requires the movement of nitrogen and chromium atoms in the solid phase, because chromium atoms are uniformly distributed and surrounded by iron atoms in alloy solution. The activation energies of nitrogen diffusion in fcc-Fe and bcc-Fe, listed in Table 5.1, are 168.6 and 79.1 kJ/mol, respectively. The movement of nitrogen in the stainless steel solid solution may be enhanced by an increase in the nitrogen content, reducing the activation energy of diffusion. On the other hand, Cr atoms in the stainless steel alloy can only move via the substitutional diffusion, which has very high activation energy. The activation energies of Cr movement in fcc-Fe and bcc-Fe are 291.8 and 250.8 KJ/mol, respectively [Smithells Metals Reference Book, 1992]. It seems that the formation of CrN would be restrained by the movement of Cr atoms, which has high

activation energy. However, the estimated apparent activation energy for the formation of CrN is small, suggesting that the reaction would be easy to progress. Therefore, some other mechanisms that enhance the process may be involved. The actual mechanism of CrN formation is not clear.

5-2-3-6 Effect of Gas on Induction Period

As calculated from the proposed model, the lengths of induction period are evaluated for different average ammonia and hydrogen concentrations at 550 °C and shown in Table 5.4. As concluded in section 4-2-2, the induction period seems to become shorter as ammonia concentration increases, i.e., the nitridation is enhanced. On the other hand, hydrogen concentration shows no effect (or minor effect) on the induction stage.

5-3 Final Saturation Stage

Table 5.5 illustrates the nitrogen contents of 316 stainless steel powder in the final saturation stage, evaluated at different processing temperatures using different gas mixtures. The measured saturated nitrogen content shows minor influence from gas composition, but decreases significantly with processing temperature. The saturated nitrogen content is determined by alloy composition, the formation of metal nitrides, and the solubility of nitrogen in 316 stainless steel. Among them, the stability of Fe_4N, which is varied by the processing temperature as shown in section 4-2-1, strongly influences the level of the saturated nitrogen content.

During the nitridation process, flow of NH_3 and/or H_2 may establish a metastable state that is in equilibrium with iron nitride [Shohoji *et al.*, 1990; Katsura, 1992]. Hence, the condensation of iron nitride in solid solution is influenced by the partial equilibrium, which may be determined by the processing temperature and gas composition in the bed. However, experimental results suggest that the difference in

Table 5.4 The estimated induction periods for different gas mixtures at 550 °C

Initial Induction Time (hr)	Average NH_3 concentration (vol.%)	Average H_2 concentration (vol.%)
1.2	25.8	14.6
0.8	42.2	55.3
0.8	42.2	36.3
0.8	42.2	17.3
0.75	58	19.9
0.7	73.2	22.4
0.35	80.6	14.6

the extent of condensed iron nitride for different gas composition is small at the same temperature. Therefore, further sophisticated measurements and thermodynamic analysis may be needed to find the level of nitrogen content in the final saturation stage at different operating conditions, i.e., operating temperature and gas composition.

Table 5.5 Estimated saturated nitrogen content of nitrided products obtained with different temperatures and gas composition

Temperature (°C)	Average NH_3 Composition (vol.%)	Average H_2 Composition (vol.%)	Estimated Saturated Nitrogen Content (wt%)
550	80.6	14.6	10.20
	73.2	22.4	10.40
	58	19.9	10.20
	42.2	7.8	10.30
	42.2	17.3	10.20
	42.2	36.3	10.00
600	36.7	58.9	10.02
	68.4	23.7	10.00
650	28.1	64.6	8.59
	47.2	41.5	9.00
	51.6	36.3	9.35
750	13.7	74.2	6.11
	18.8	52.2	6.14
	26.2	52.2	6.57

Chapter 6
Summary of Results

316 stainless steel power was nitrided in a fluidized-bed reactor. Two gas systems were used in this study, covering different temperature ranges: NH_3/ H_2/ Ar in the range of 450 - 750 °C and N_2/ H_2/ Ar from 650°C to 800 °C. The study on the nitridation of stainless steel under the NH_3 system was more emphasized. The effects of operating temperature, hydrogen and ammonia on the nitridation process and the precipitation of CrN and Fe_4N phases, as well as the dissociation of NH_3 were studied. Figure 6.1 illustrates the detailed view of studies. The results are summarized in the following two sections.

Part One: NH_3 Dissociation

(1) The rate of the thermal dissociation of NH_3 in the empty bed was stable, and found to be of 0.5 order with respect to NH_3 concentration, yielding an apparent activation energy of 109.9 kJ/mol.

(2) The NH_3 dissociation in the fluidized bed was enhanced by 316L stainless steel powder. The dissociation rate was not stable initially and gradually reached steady state. The variation is related to the formation of nitride phase on the surface of the powder.

(3) The rate of catalytic NH_3 dissociation was assumed to be of first order with respect to NH_3 concentration, which was applied to rate data in both the initial and final stages. Apparent activation energies of 110.7 and 83.4 KJ/mol were obtained, respectively. The apparent activation energy for the initial NH_3 catalytic dissociation is similar to that of the NH_3 thermal dissociation (109.9 KJ/mol), implying that the thermal dissociation dominates initially and then catalytic reaction enhances the process of dissociation later.

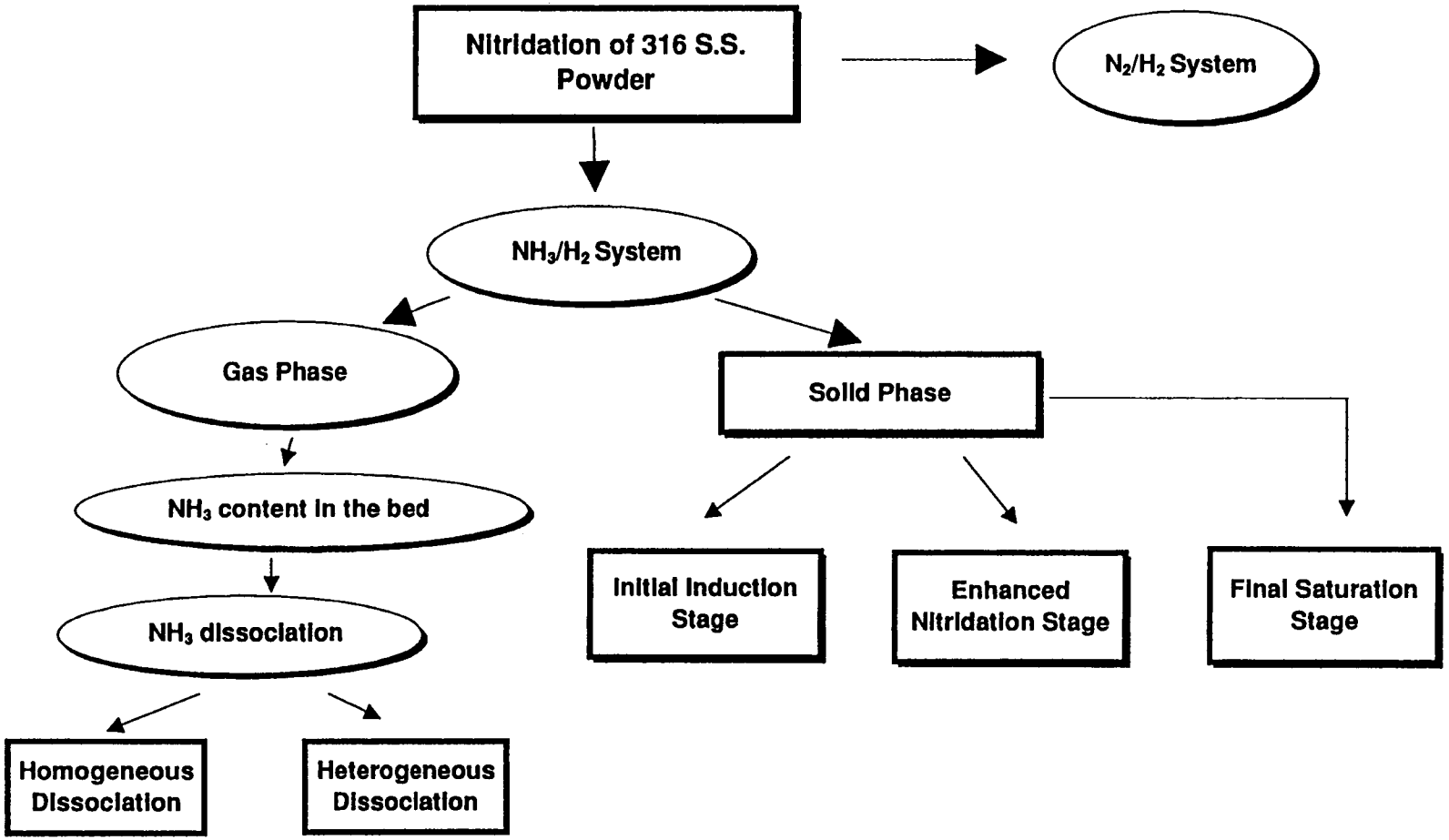

Figure 6.1 An overall view of studies

Part Two: Nitridation of 316L Stainless Steel Powder

(1) Nitridation of 316 stainless steel powder in the fluidized bed system yields product powder of an extremely high nitrogen content, which may be controlled by selecting the operating temperature and nitriding gas mixtures.

(2) The progress of nitridation may be divided into three stages: an induction stage, an enhanced nitridation stage, and a final saturation stage.

(3) The nitrogen content in the final saturation stage is strongly temperature-dependent, because of the stability of Fe_4N in the stainless steel solid solution.

(4) The induction stage is influenced by the operating temperature and NH_3 concentration. The higher the operating temperature and/or NH_3 concentration, the shorter the induction period. On the other hand, hydrogen concentration shows no effect on the induction stage. The process in this stage seems to be controlled by the surface morphological change, related to the surface reaction. However, the actual mechanism is not clear.

(5) Nitrogen, generated from the dissociation of NH_3, initially penetrates into the interstitial alloy solution, i.e., fcc-Fe, and reaches its saturation. A further increase in the nitrogen-concentration results in the development of a surface layer on the particle, that progresses inward. The precipitate of CrN is believed to have caused the development of the surface layer, in which Fe_4N forms after a critical level of nitrogen addition is reached at low operating temperatures.

(6) The surface shell development can also be observed at high operating temperatures. However, only the CrN phase is found in the stainless steel solid solution.

(7) The gaseous concentration dependency of the reaction rate of CrN formation may be represented by a power-law rate expression of 1.40 with respect to NH_3 and -0.40 with respect to H_2.

(8) The gaseous concentration dependency of the reaction rate of Fe_4N precipitation may be represented by a power law of 0.40 with respect to NH_3 and -0.30 with respect to H_2.

(9) The calculated curve for the nitridation of stainless steel powder can approximately describe the effect of average particle size of powder, that is predicted by the proposed reaction-controlled shrinking core model.

(10) A mathematical model based on the shrinking un-reacted core model with reaction control was tested for the formation of CrN and a good agreement with experimental results was obtained at temperatures in the range of 550 - 750 °C. For the two-phase precipitates at low operating temperatures, a pseudo-homogeneous model may be used to represent the formation of Fe_4N in the shell of CrN growing from the surface inward.

Chapter 7
Recommendations for Future Work

A wide range of nitrogen contents covering from 0.1% to 10% by mass can be obtained in the fluidized-bed nitridation of 316 stainless steel, dependent upon the processing temperature, processing time and gas mixtures used. This process has a potential to be commercialized. However, some suggestions are listed here to be studied in the future.

(1) The consolidation of nitrided stainless steel powder of different levels of nitrogen content needs to be investigated for mechanical properties.

(2) This study shows that the induction period seems to be reduced with an increase in ammonia concentration and processing temperature. However, the real mechanism, which may involve the surface reaction, is not clear. A further investigation is suggested to complete the kinetic of nitridation process.

(3) The processing temperature strongly influences the saturated nitrogen content, which mainly is determined by the stability of Fe_4N in the solid solution. Therefore, thermodynamic study on nitrogen content in 316 stainless steel powder may be helpful to provide a reliable data for final the possible nitrogen content in powder.

(4) Although the solubility of nitrogen in 316 stainless steel solid solution is small, it is necessary to obtain data for applying the proposed model. The thermodynamic study is needed.

(5) The microscopic study of CrN formation is needed to clarify the reaction mechanism of chromium and nitrogen.

Bibliography

Al-Shammeri, K.K. and J.M. Saleh: "Absorption and Decomposition of Ammonia on Metal Films of Nickel, Palladium, Tungsten, and Aluminum," *Journal of Physical Chemistry*, **90**, 2906(1986).

Anthamatten, B.A., P.J. Uggowitzer, M.L. Cue, M.O. Spiegel, and G. Stein: "New high nitrogen ferric steels," *High Nitrogen Steel*-88, 18-20 May, 1988, Lille, France, J. Foct and A. Hendry, ed., The Institute of Metals, London, U.K., 58(1989).

Beraha, E. and B. Shpigler: *Color Metallography*, AMS, Metal Park, Ohio, U.S.A., 1977.

Bozso, F., G. Ertl, M. Grunze, and M. Weiss: "Interaction of Nitrogen with Iron Surface I. Fe(100) and Fe(111)," *Journal of Catalysis*, **49**, 18(1977).

Degallaix, S., J. Foct, and A. Hendry: "Mechanical behaviour of high-nitrogen stainless steels," *Materials Science and Technology: MST*, **2**, 946(1986).

Dressler, S.: "Plasma Treatments," *Surface Modification Technologies*, T.S. Sudarshan, ed., Marcel Dekker, New York, New York, U.S.A., 1983.

Ertl, G. and M. Huber: "Mechanism and Kinetics of Ammonia Decomposition on Iron," *Journal of Catalysis*, **61**, 537(1980).

Ertl, G., M. Grunze, and M. Weiss: "Chemisorption of N_2 on an Fe(100) surface," *Journal of Vacuum Science and Technology*, **13**(1), 314(1976).

Fast J.D.: *Interaction of Metals and Gases: Kinetics and Mechanisms*, Barnes & Noble, New York, U.S.A., 1971.

Fast, J.D.: *Interaction of Metals and Gases: Vol.1 Thermodynamics and Phase Relations*, Academic Press, New York, U.S.A., 1965.

Goldstein, J.I., D.E. Newbury, P. Echlin, D.C. Joy, C. Fiori, and E. Lifshin: *Scanning Electron Microscopy and X-ray Microanalysis*, Plenum, New York, 1981.

Grieveson, P. and E.T. Turkdogan: "Kinetics of Reaction of Gaseous Nitrogen with Iron Part II: Kinetics of Nitrogen Solution in Gamma Iron," *Transactions of the Metallurgical Society of AIME*, **230**, 1604(1964).

Grieveson, P. and E.T. Turkdogan: "Kinetics of Reaction of Gaseous Nitrogen with Iron Part I: Kinetics of Nitrogen Solution in Gamma Iron," *Transactions of the Metallurgical Society of AIME*, **230**, 407(1964).

Hargis, L.H.: *Analytical Chemistry*, Englewood Cliffs, New Jersey, U.S.A., 1988.

Hendry, A.: "Developments in high-nitrogen stainless steels," *WAT-CET European Technical Conference*, Wire Assoc. Int., Guildford, CE., U.S.A., 50(1993).

HNS-88, High Nitrogen Steels - 88, Conference Proceedings, Lille, France, May 18-20, 1988, J. Foct and A. Hendry, eds., The Institute of Metals, London, 1989.

HNS-90, High Nitrogen Steels - 90, Conference Proceedings, Oct. 10-12, 1990, Aachen, Germany, G. Stein and H. Witulski, eds., Verlag Stahleisen MbH, Dusseldorf, Germany.

Imai, Y., T. Masumoto, and M. Sakamoto: "The Effect of Nickel on the Solubility and Diffusion of Nitrogen in α-Iron," *Journal of the Japan Institute Metals*, **31**(9), 1095(1967).

Irvine, K.J., D.T. Llewellyn, and F.B. Pickering: *The Metallurgical Evolution of Stainless Steel*, American Society for Metals, Metals Park, Ohio, U.S.A., 1979.

Jaraiz, E., S. Kimura, and O. Levenspiel: "Vibrating beds of fine particles: estimation of particle forces from expansion and pressure drop experiments," *Powder Technology*, **72**, 23(1992).

Jovanovic, Z.: "Kinetic Study on the Production of Silicon Nitride by Direct Nitridation of Silicon in a Fluidized-bed: Experiment and Modeling," Ph.D. Dissertation, Department of Chemical Engineering, Oregon State University, 1994.

Jovanovic. Z., S. Kimura, and O. Levenspiel: "Effect of Hydrogen and Temperature on the Kinetics of the Fluidized-bed Nitridation of Silicon," *Journal of American Ceramic Society*, **77**[1], 186(1994).

Katsura, M.: "Thermodynamics of nitride and hydride formation by the reaction of metals with flowing NH_3," *Journal of Alloys and Compounds*, **182**, 91(1992).

Kikuchi, M., M. Kajihara, and K. Frisk: "Solubility of nitrogen in austenitic stainless steels," *High Nitrogen Steel-88*, 18-20 May, 1988, Lille, France, J. Foct and A., Hendry, ed., 63(1989).

Kossowsky, R.: *Surface Modification Engineering Vol. II*, CRC press, Boca Raton, Florida, U.S.A., 1989.

Kossowsky, R. and S.C. Singhal, ed.,: *Surface Engineering*, Martinus Nijhoff Publishers, Dordrecht, The Netherlands, 1984.

Kunii, D. and O. Levenspiel: *Fluidization Engineering*, Butterworth-Heinemann, Stoneham, Massachusetts, U.S.A., 1991.

Lankreijer, R.M., M.A.J. Somers, and E.J. Mittemeijer: "Kinetics of nitride precipitation in Fe-Al and Fe-Si alloys on nitriding," *High Nitrogen Steel-88*, 18-20 May, 1988, Lille, France, J. Foct and A. Hendry, ed., 108(1989).

Lee, S.L. and A. Hendry: "High-Nitrogen Stainless Steels by Powder Processing," *High Nitrogen Steels*, Proc. of 3rd Int. Conf., 1993, V. Gavriljuk and V.M. Nadutov, ed., Inst. of Metal Physics, Kiev, Ukraine, 675(1993).

Levenspiel, O.: *Chemical Reaction Engineering*, John Wiley & Sons, New York, U.S.A., 1972.

Levenspiel, O.: Chapter 21, "Solid Catalyzed Reactions, Introduction", *The Chemical Reactor Omnibook*, OSU Book Stores Inc., Corvallis, OR, U.S.A., 1993.

Lin, D.C.: *Kinetic Study on the Synthesis of Si_3N_4 via the Ammonization of SiO Vapor*, Ph.D. Dissertation, Department of Chemical Engineering, Oregon State University, U.S.A., 1995.

Liu, Y.D. and S. Kimura: "Fluidization and entrainment of difficult-to-fluidized fine powder mixed with easy-to-fluidize large particles," *Powder Technology*, **75**, 189(1993).

Löffler, D.G. and L.D. Schmidt: "Kinetics of NH_3 Decomposition on Iron at High Temperatures," *Journal of Catalysis*, **44**, 244(1976).

Löffler, D.G. and L.D. Schmidt: "Kinetics of NH_3 Decomposition on Polycrystalline Pt," *Journal of Catalysis*, **41**, 440(1976).

Logan, S.R., R.L. Moss and C. Kemball: "The Catalytic Decomposition of Ammonia on Evaporated Iron Films," *Trans. Faraday Soc.*, **54**, 922(1958).

Lotz, C.R. and F. Sebba: "Energies of Activation for Decomposition of Ammonia Catalyzed by the Nitrides of the 4th Series Transition Elements," *Transactions of Faraday Society*, **53**, 1246(1957).

Lula, R.A.: *Stainless Steel*, 1st edition, American Society for Metals, Metals PArk, Ohio, U.S.A., 1986.

Marshall, P.: *Austenitic Stainless Steels, Microstructure and Mechanical Properties*, 1st edition, Elsevier Applied Science Publishers, New York, U.S.A., 1984.

Metals Handbook, vol. 1, 10th edition, American Society for Metals, Metals Park, Ohio, U.S.A., 1990.

Metals handbook, vol. 8, 8th edition, American Society for Metals, Metals Park, Ohio, U.S.A., 304, 1973.

Nandy S. and T. Lenz: "Observations on Catalytic Dissociation of Ammonia at High Temperatures and Pressures," *American Institute of Chemical Engineers Journal*, **30**(3), 504(1984).

Norström, L.A.: "The influence of nitrogen and grain size on yield strength in Type AISI 316L austenitic stainless steel," *Metal Science*, **11**, 208(1977).

Peckner, D. and I.M. Bernstein: *Handbook of Stainless Steels*, McGraw-Hill Book Company, New York, U.S.A., 3-7(1977).

Rawers, J.C., N.A. Gokcen, and R.D. Pehlke: "High Nitrogen Concentration in Fe-Cr-Ni Alloys," *Metallurgical Transactions A*, **24A**, 73(1993).

Rawers, J. and A. Petty: "High pressure nitrogen gas alloying of Fe-Cr-Ni alloys," *Journal of Materials Science*, **28**(13), 3489(1993).

Rawers, J., J. Dunning, and R. Reed: "Nitride Formation in HIP-Melted Metals," *High Nitrogen Steel-90*, 10-12 Oct., 1990, Dusseldorf, Germany, G. Stein and H. Witulski, ed., 63(1990).

Rawers, J., G. Asai, R. Doan, and J. Dunning: "Mechanical and microstructural properties of nitrogen high pressure melted Fe-Cr-Ni alloys," *Journal of Materials Research*, **7**(5), 1083(1992).

Rawers, J., T. Wang, R. Krabbe, and S. Kimura: "Nitriding stainless steel in a fluidized bed," *Journal of Materials Synthesis and Processing*, 1995, in review.

Rawers, J., K. Frisk, and D. Govier: "Nitrogen in pressure-diffused powder iron alloys," *Materials Science and Engineering*, **A177**, 243(1994).

Rayaprolu, D.B., and A. Hendry: "High Nitrogen Stainless Steel Wire," *Materials Science and Technology: MST*, **4**, 136(1988).

Reimer, L.: *Scanning Electron Microscopy*, Springer Series Optical Sciences Vol. 36, Springer Berlin, Hcidelberg, 1985.

Shahapurkar, D.S. and W.M. Small: "Nitrogen Solubility in Complex Liquid Fe-Cr-Ni Alloys," *Metallurgical Transactions B*, **18B**, 225(1987).

Shohoji, N., T. Marcelo, and M. Katsura: "Influence of metastable species (non-graphitic carbon and ammonia gas) in the reactants on the composition of the reaction product (carbide, carbonitride and nitride)," *Solid State Ionics*, 38, 187(1990).

Small, W.M.: "Analysis of nitrogen solubility in austenitic Fe-Cr and Fe-Ni alloys," *Scripta Metallurgica et Materialia*, **24**, 107(1990).

Smithells Metals Reference Book, 7th edition, E.A. Brandes and G.B. Brook, ed., Butterworth-Heinermann Ltd., Linacre House, Oxford, U.K., 1992.

Source Book on Stainless Steels, 2nd edition, American Society for Metals, Metals Park, Ohio, U.S.A., 1976.

Stein, G. and H. Witulski, ed.: *High Nitrogen Steels: Proc. of HNS 90*, Verlag Stahleisen MbH, Dusseldorf, Germany, 1990.

Stein, G., J. Menzel, and H. Dorr: "Industrial manufacture of massively nitrogenated alloyed steels," *High Nitrogen Steel-88*, 18-20 May, 1988, Lille, France, J. Foct and A. Hendry, ed., 32(1989).

Steel A Handbook for Materials Research and Engineering: Vol. 1 Fundamentals, V.D. Eisenhüttenleute ed., Springer-Verlag Verlag Stahleisen, Düsseldorf, 1992.

Sudarshan, T.S. ed.,: *Surface Modification Technologies*, Marcel Dekker, New York, New York, U.S.A., 1983.

Temkin, M. and V. Pyzhev: "Kinetics of Ammonia Synthesis on Promoted Iron Catalysts," *Acta Physicochimica U.R.S.S.*, **12**(3), 327(1940).

Uggowitzer, P.J. and M.O. Speidel: "Ultrahigh-Strength Austenitic Steels," High Nitrogen Steels-90, 10-12 Oct., 1990, Dusseldorf, Germany, G. Stein and H. Witulski, ed., 156(1990).

Vajo, J.J., W. Tsai, and W.H. Weinberg: "Steady-State Decomposition of Ammonia on the Pt (110)-(1X2) Surface," *Journal of Physical Chemistry*, **90**, 6531(1986).

Yagi, S., and Kunii, D., *5th Symposium (International) on Combustion*. Reinhold, New York, 1955, p.231; *Chemical Engineering Science (Japan)*, **19**, 500(1955).

Yagi, S., and Kunii, D.: "Fluidized-solids reactors with continuous solids feed-I Residence time of particles in fluidized beds," *Chemical Engineering Science*, **16**, 364(1961).

Yagi, S., and Kunii, D.: "Fluidized-solids reactors with continuous solids feed-II Conversion for overflow and carryover particles," *Chemical Engineering Science*, **16**, 372(1961).

Yagi, S., and Kunii, D.: "Fluidized-solids reactors with continuous solids feed-III Conversion in experimental fluidized-solids reactors," *Chemical Engineering Science*, **16**, 380(1961).

Appendices

Appendix A
Calculating Concentration of NH_3 and H_2

The following shows the procedure for calculating average NH_3 and H_2 concentration in the fluidized bed of 316 stainless steel powder, according to the developed in section 4-1.

1. The calculations are basically divided into two sections: final steady state and beginning state.
2. Each state includes two stages of calculation:
   A. finding the ammonia dissociation fraction before entering the bed.
   B. applying the proposed rate equation for NH_3 dissociation in the bed.
3. For stage A, the extent of ammonia dissociation is applied by using Equation (4.11).
4. After step 3 is completed, the outlet gas composition from the bed can be calculated from Equations (4.17) and (4.18). The calculation is completed by trial and error using the Excel spreadsheet.
5. In each state, the average gas composition, mainly NH_3 and H_2, is estimated by taking log-mean of inlet and outlet concentrations.
6. Finally, an arithmetic average of calculated log-mean values of composition from both states is used to represent the estimated average gas composition in the fluidized bed of stainless steel powder.
7. In the spreadsheet, the equations and parameters are set up to be ready for both steady and beginning states at different temperatures.
8. The only variable is the conversion of ammonia dissociation after the bed. So, input the composition of feed gas. Find the conversion $X_{a,\,out}$, and the outlet gas composition will be calculated by spreadsheet and shown.
9. Average NH_3 and H_2 concentrations, measured from the steady and beginning states.

Test to find the outlet (leaving the bed) NH3 concentration, when the inlet condition is known.

Input your information: **Final Steady State**

1. Inlet Gases (vol.%): Total Flowrate = 4270 cm^3/min

NH3 = 50 % H2 = 0 % Ar = 50 %

Epsilon = 0.5

2. Operation Temperature = 550 C Reactor Volume = 225.7 cm^3

3. System Pressure= 806.6 mmHg Void Volume in bed = 168.4480916 cm^3

4. Powder Weight in the bed = 450 grams

Calculation Results: **Guess Xa,out (leaving bed) =>** 0.313

Inlet Gases			Before Bed
NH3	H2	Ar	Xa
50	0	50	0.0205061

Average gas fraction (%) Final Steady State			
NH3	N2	H2	Ar
38.32619015	3.891269949	11.67380985	46.10873005
X,avg =	0.168786689	Error(%) =	-0.07809198

(1) Pre-calculate the inlet conditions :

Initial NH3 concentration (Cao) : 7.857E-06 mol/cm^3

Initial NH3 molar flowrate (Fao) : 0.0926252 mol/min

(2) Find gas condition before entering the bed :

Homogeneous NH3 dissociation with reaction order n=0.5

Because the amount of NH3 dissociation is small, we may assume the constant dissociation rate.

The performance equation :

$$V/Fao = (X,out-X,in)/(-r,a) \qquad \text{V and k are constant}$$
$$= X,out/(k*Ca^{0.5})$$

So, X,out is proportional to Ca,o^0.5/Fao, that is proportional to 1/(P,a^0.5) at same total flowrate.

That means at same total flowrate and temperature : **X,out is proportional to 1/[(NH3 inlet %)^0.5]**

References :

Temp. C	NH3 Flow-rat cm^3/min	P mm-Hg	Xa,in	Xa.out,ref
550	4216	806.1	0	0.029
600	3916	806.6	0	0.046
650	3665	806.6	0	0.104
700	3435	809	0	0.133
750	3250	813.4	0	0.15

Calculation results :

The equation to calculate is = Xa, out = Xa,out,ref (at same temp.)*(Input NH3 %/100%)^0.5

NH3 dissociation in the outlet (X,out) = 0.0205061 **<== Check if temp. right.**

(3) Find outlet gas condition from the bed

Dissociation Rate Constant :

Homogeneous : 1/2 order			Heterogeneous : first order		
	n =	0.5	n =	1	
	E =	26.3 kcal/mol	E,i =	26.5	kcal/mol
	k,0 =	3.60E+04	k,0,i =	1.43E+07	
			E,f =	20.9	kcal/mol
Therefore,			K,0,f =	3.38E+06	
k,homog=	0.00374078	k,cat,ini =	1.314893		
		k,cat,finl =	9.5371383		

Operation Temperature = 550 C

Find dissociation of NH3 in the bed (with s.s. powder) **<== Final Steady State**

W/Fao	Integration (1)	Integration (2)	error (%) : W/Fao to Integration (2)
4858.2897	8392.7528	4854.4958	-0.07809198

Therefore, NH3 dissociation in inlet (Xa,in) = 0.020506097 Ca,in = 7.61778E-06 mol/cm^3

NH3 dissociation in outlet (Xa,out) = 0.313 Ca,out = 4.66733E-06 mol/cm^3

We may use log-mean to calaulate the average NH3 concentration in the bed

Ca,avg = 6.0226E-06 Ca,avg/Ca,o = 0.766523803

Final Solution : **At final steady State**		Xa,avg =	0.168786689		
So, the volumetric flowrate fraction					
NH3,avg =	38.3261902 %	N2,avg =	3.8912699 %	Ar,avg =	46.10873005 %
		H2,avg =	11.67381 %	Ar,avg =	46.10873005

(1) Neglect homogeneous term

k,cat,finl = 9.53713828

Step = 70

Guess Final X = 0.44

Delta X = 0.00599277

Xa	Xa,avg	Integration
0.0205061		
0.02649887	0.02350248	82.861936
0.03249164	0.02949525	83.620518
0.03848441	0.03548802	84.388526
0.04447718	0.04148079	85.166138
0.05046995	0.04747356	85.953535
0.05646272	0.05346633	86.750901
0.06245549	0.0594591	87.558429
0.06844826	0.06545187	88.376314
0.07444103	0.07144464	89.204756
0.0804338	0.07743741	90.04396
0.08642657	0.08343018	90.894138
0.09241934	0.08942295	91.755507
0.09841211	0.09541572	92.628288
0.10440488	0.10140849	93.512711
0.11039765	0.10740126	94.40901
0.11639042	0.11339403	95.317425
0.12238319	0.1193868	96.238205
0.12837596	0.12537957	97.171602
0.13436873	0.13137234	98.117878
0.1403615	0.13736511	99.077303
0.14635427	0.14335788	100.05015

(2) Consider homogeneous and catalysis terms

k,cat,finl = 9.537138283 k,homog = 0.00374078

Step = 70

Guess Final X = 0.313

Delta X = 0.004178484

Xa	Xa,avg	Integration
0.0205061		
0.0246846	0.022595339	54.77773062
0.0288631	0.026773823	55.1177029
0.0330415	0.030952307	55.46052486
0.03722	0.035130792	55.80623276
0.0413985	0.039309276	56.15486348
0.045577	0.04348776	56.50645451
0.0497555	0.047666245	56.86104401
0.053934	0.051844729	57.21867078
0.0581125	0.056023213	57.57937432
0.0622909	0.060201698	57.9431948
0.0664694	0.064380182	58.31017309
0.0706479	0.068558666	58.68035081
0.0748264	0.072737151	59.05377029
0.0790049	0.076915635	59.43047461
0.0831834	0.081094119	59.81050765
0.0873618	0.085272604	60.19391404
0.0915403	0.089451088	60.58073924
0.0957188	0.093629572	60.97102952
0.0998973	0.097808057	61.36483201
0.1040758	0.101986541	61.76219467
0.1082543	0.106165025	62.16316636

0.15234704	0.14935065	101.03671
0.15833981	0.15534342	102.03726
0.16433258	0.16133619	103.05211
0.17032535	0.16732896	104.08157
0.17631812	0.17332173	105.12596
0.18231089	0.1793145	106.1856
0.18830366	0.18530727	107.26083
0.19429643	0.19130004	108.35199
0.2002892	0.19729281	109.45945
0.20628197	0.20328558	110.58357
0.21227474	0.20927835	111.72472
0.21826751	0.21527112	112.88331
0.22426028	0.22126389	114.05973
0.23025305	0.22725666	115.25439
0.23624582	0.23324943	116.46773
0.24223859	0.2392422	117.70018
0.24823136	0.24523497	118.95221
0.25422413	0.25122774	120.22427
0.2602169	0.25722051	121.51687
0.26620967	0.26321328	122.83049
0.27220244	0.26920605	124.16565
0.27819521	0.27519882	125.52289
0.28418798	0.28119159	126.90277
0.29018075	0.28718436	128.30584
0.29617352	0.29317713	129.73271
0.30216629	0.2991699	131.18398
0.30815906	0.30516267	132.66028
0.31415183	0.31115544	134.16227
0.3201446	0.31714821	135.69062
0.32613737	0.32314098	137.24604
0.33213014	0.32913375	138.82925
0.33812291	0.33512652	140.44099
0.34411568	0.34111929	142.08206
0.35010845	0.34711206	143.75325
0.35610122	0.35310483	145.4554
0.36209399	0.3590976	147.18939
0.36808676	0.36509037	148.9561
0.37407953	0.37108314	150.75649
0.3800723	0.37707591	152.59152
0.38606507	0.38306868	154.4622
0.39205784	0.38906145	156.36958
0.39805061	0.39505422	158.31475
0.40404338	0.40104699	160.29884
0.41003615	0.40703976	162.32304
0.41602892	0.41303253	164.38857
0.42202169	0.4190253	166.49672
0.42801446	0.42501807	168.6488
0.43400723	0.43101084	170.84622
0.44	0.43700361	173.09042
	sum =	8392.7528

0.1124328	0.11034351	62.56779685
0.1166112	0.114521994	62.97613682
0.1207897	0.118700478	63.38823789
0.1249682	0.122878963	63.80415266
0.1291467	0.127057447	64.2239347
0.1333252	0.131235931	64.6476386
0.1375037	0.135414416	65.07531999
0.1416821	0.1395929	65.50703557
0.1458606	0.143771384	65.9428431
0.1500391	0.147949869	66.38280147
0.1542176	0.152128353	66.82697071
0.1583961	0.156306837	67.27541201
0.1625746	0.160485322	67.72818775
0.166753	0.164663806	68.18536156
0.1709315	0.16884229	68.6469983
0.17511	0.173020775	69.11316412
0.1792885	0.177199259	69.5839265
0.183467	0.181377743	70.05935427
0.1876455	0.185556228	70.53951763
0.191824	0.189734712	71.02448823
0.1960024	0.193913196	71.51433914
0.2001809	0.198091681	72.00914495
0.2043594	0.202270165	72.50898178
0.2085379	0.206448649	73.01392732
0.2127164	0.210627134	73.52406088
0.2168949	0.214805618	74.0394634
0.2210733	0.218984102	74.56021756
0.2252518	0.223162587	75.08640774
0.2294303	0.227341071	75.61812015
0.2336088	0.231519555	76.15544283
0.2377873	0.23569804	76.69846567
0.2419658	0.239876524	77.24728056
0.2461443	0.244055008	77.80198133
0.2503227	0.248233493	78.36266388
0.2545012	0.252411977	78.92942622
0.2586797	0.256590461	79.50236849
0.2628582	0.260768946	80.08159308
0.2670367	0.26494743	80.66720466
0.2712152	0.269125914	81.25931021
0.2753936	0.273304399	81.85801918
0.2795721	0.277482883	82.46344346
0.2837506	0.281661367	83.0756975
0.2879291	0.285839852	83.69489837
0.2921076	0.290018336	84.32116587
0.2962861	0.29419682	84.95462256
0.3004645	0.298375305	85.59539384
0.304643	0.302553789	86.24360809
0.3088215	0.306732273	86.89939672
0.313	0.310910758	87.56289423
	sum =	4854.495764

Test to find the outlet (leaving the bed) NH3 concentration, when the inlet condition is known.

Input your information: Initial **Steady State**

1. Inlet Gases (vol.%):		Total Flowrate =	4270	cm^3/min	
NH3 =	50 %	H2 =	0 %	Ar =	50 %
Epsilon =	0.5				
2. Operation Temperature =	550 C		Reactor Volume =	225.7	cm^3
3. System Pressure=	806.6 mmHg		Void Volume in bed =	162.0867684	cm^3
4. Powder Weight in the bed =	500 grams				

Calculation Results: **Guess Xa,out (leaving bed) =>** 0.089

Inlet Gases			Before Bed
NH3	H2	Ar	Xa
50	0	50	0.0205061

Average gas fraction (%) Final Steady State			
NH3	N2	H2	Ar
46.00059068	1.333136442	3.999409325	48.66686356
X,avg =	0.054786207	Error(%) =	-0.55637534

(1) Pre-calculate the inlet conditions :

Initial NH3 concentration (Cao) : 7.857E-06 mol/cm^3

Initial NH3 molar flowrate (Fao) : 0.0926252 mol/min

(2) Find gas condition before entering the bed :

Homogeneous NH3 dissociation with reaction order n=0.5

Because the amount of NH3 dissociation is small, we may assume the constant dissociation rate.

The performance equation :

$$V/Fao = (X,out-X,in)/(-r,a) = X,out/(k*Ca^{0.5})$$ V and k are constant

So, X,out is proportional to Ca,o^0.5/Fao, that is proportional to 1/(P,a^0.5) at same total flowrate.

That means at same total flowrate and temperature : **X,out is proportional to 1/[(NH3 inlet %)^0.5]**

References :

Temp. C	NH3 Flow-r: cm^3/min	P mm-Hg	Xa,in	Xa.out,ref
550	4216	806.1	0	0.029
600	3916	806.6	0	0.046
650	3665	806.6	0	0.104
700	3435	809	0	0.133
750	3250	813.4	0	0.15

Calculation results :

The equation to calculate is = Xa, out = Xa,out,ref (at same temp.)*(Input NH3 %/100%)^0.5

NH3 dissociation in the outlet (X,out) = 0.0205061 **<== Check if temp. right.**

(3) Find outlet gas condition from the bed

Dissociation Rate Constant :

Homogeneous : 1/2 order			Heterogeneous : first order		
	n =	0.5	n =	1	
	E =	26.3 kcal/mol	E,i =	26.5	kcal/mol
	k,0 =	3.60E+04	k,0,i =	1.43E+07	
			E,f =	20.9	kcal/mol
Therefore, at temp.=	550 C		K,0,f =	3.38E+06	
k,homog= 0.0037408	k,cat,ini =	1.31489301			
	k,cat,finl =	9.53713828			

Operation Temperature = 550 C

Find dissociation of NH3 in the bed (with s.s. powder) **<== Initial Steady State**

W/Fao	Integration (1)	Integration (2)	error (%) : W/Fao to Integration (2)
5398.09966	22181.263	5368.06597	-0.55637534

Therefore, NH3 dissociation in inlet (Xa,in) = 0.020506097 Ca,in = 7.61778E-06 mol/cm^3

NH3 dissociation in outlet (Xa,out) = 0.089 Ca,out = 6.85278E-06 mol/cm^3

We may use log-mean to calaulate the average NH3 concentration in the bed

Ca,avg = 7.229E-06 Ca,avg/Ca,o = 0.920011814

Final Solution : **At Initial steady State**		Xa,avg =	0.054786207		
So, the volumetric flowrate fraction					
NH3,avg =	46.000591 %	N2,avg =	1.33313644 %	Ar,avg =	48.66686356 %
		H2,avg =	3.99940932 %	Ar,avg =	48.66686356

(1) Neglect homogeneous term

k,cat,ini = 1.314893

Step = 70

Guess Final X = 0.211

Delta X = 0.0027213

Xa	Xa,avg	Integration
0.0205061		
0.02322744	0.0218668	272.24511
0.02594878	0.0245881	273.37211
0.02867012	0.0273095	274.50541
0.03139146	0.0300308	275.64508
0.0341128	0.0327521	276.79116
0.03683415	0.0354735	277.9437
0.03955549	0.0381948	279.10277
0.04227683	0.0409162	280.26841
0.04499817	0.0436375	281.44069
0.04771951	0.0463588	282.61966
0.05044085	0.0490802	283.80538
0.05316219	0.0518015	284.9979
0.05588354	0.0545229	286.19729
0.05860488	0.0572442	287.4036
0.06132622	0.0599655	288.6169
0.06404756	0.0626869	289.83724
0.0667689	0.0654082	291.06469
0.06949024	0.0681296	292.2993
0.07221158	0.0708509	293.54115
0.07493293	0.0735723	294.7903
0.07765427	0.0762936	296.0468

(2) Consider homogeneous and catalysis terms

k,cat,ini = 1.314893014 k,homog = 0.00374078

Step = 70

Guess Final X = 0.089

Delta X = 0.000978484

Xa	Xa,avg	Integration
0.0205061		
0.02148458	0.020995339	73.267872
0.02246307	0.021973823	73.36304039
0.02344155	0.022952307	73.45837407
0.02442003	0.023930792	73.55387348
0.02539852	0.024909276	73.64953908
0.026377	0.02588776	73.74537131
0.02735549	0.026866245	73.84137064
0.02833397	0.027844729	73.93753753
0.02931246	0.028823213	74.03387244
0.03029094	0.029801698	74.13037582
0.03126942	0.030780182	74.22704815
0.03224791	0.031758666	74.32388989
0.03322639	0.032737151	74.4209015
0.03420488	0.033715635	74.51808346
0.03518336	0.034694119	74.61543624
0.03616185	0.035672604	74.7129603
0.03714033	0.036651088	74.81065612
0.03811881	0.037629572	74.90852419
0.0390973	0.038608057	75.00656497
0.04007578	0.039586541	75.10477895
0.04105427	0.040565025	75.20316661

0.08037561	0.0790149	297.31073
0.08309695	0.0817363	298.58216
0.08581829	0.0844576	299.86114
0.08853963	0.087179	301.14774
0.09126098	0.0899003	302.44204
0.09398232	0.0926216	303.74411
0.09670366	0.095343	305.05401
0.099425	0.0980643	306.37181
0.10214634	0.1007857	307.69759
0.10486768	0.103507	309.03142
0.10758902	0.1062284	310.37337
0.11031037	0.1089497	311.72351
0.11303171	0.111671	313.08193
0.11575305	0.1143924	314.4487
0.11847439	0.1171137	315.82389
0.12119573	0.1198351	317.20759
0.12391707	0.1225564	318.59987
0.12663841	0.1252777	320.00081
0.12935976	0.1279991	321.4105
0.1320811	0.1307204	322.82901
0.13480244	0.1334418	324.25644
0.13752378	0.1361631	325.69285
0.14024512	0.1388845	327.13835
0.14296646	0.1416058	328.59301
0.1456878	0.1443271	330.05692
0.14840915	0.1470485	331.53018
0.15113049	0.1497698	333.01286
0.15385183	0.1524912	334.50507
0.15657317	0.1552125	336.00689
0.15929451	0.1579338	337.51842
0.16201585	0.1606552	339.03975
0.16473719	0.1633765	340.57097
0.16745854	0.1660979	342.11219
0.17017988	0.1688192	343.66351
0.17290122	0.1715405	345.22501
0.17562256	0.1742619	346.79681
0.1783439	0.1769832	348.379
0.18106524	0.1797046	349.97169
0.18378659	0.1824259	351.57498
0.18650793	0.1851473	353.18898
0.18922927	0.1878686	354.81379
0.19195061	0.1905899	356.44954
0.19467195	0.1933113	358.09632
0.19739329	0.1960326	359.75424
0.20011463	0.198754	361.42343
0.20283598	0.2014753	363.104
0.20555732	0.2041966	364.79606
0.20827866	0.206918	366.49973
0.211	0.2096393	368.21513
	sum =	22181.263

0.04203275	0.04154351	75.30172843
0.04301124	0.042521994	75.4004649
0.04398972	0.043500478	75.4993765
0.0449682	0.044478963	75.59846373
0.04594669	0.045457447	75.69772707
0.04692517	0.046435931	75.79716702
0.04790366	0.047414416	75.89678407
0.04888214	0.0483929	75.99657872
0.04986063	0.049371384	76.09655147
0.05083911	0.050349869	76.19670281
0.0518176	0.051328353	76.29703325
0.05279608	0.052306837	76.39754329
0.05377456	0.053285322	76.49823345
0.05475305	0.054263806	76.59910422
0.05573153	0.05524229	76.70015611
0.05671002	0.056220775	76.80138965
0.0576885	0.057199259	76.90280534
0.05866699	0.058177743	77.00440369
0.05964547	0.059156228	77.10618524
0.06062395	0.060134712	77.20815048
0.06160244	0.061113196	77.31029996
0.06258092	0.062091681	77.41263419
0.06355941	0.063070165	77.51515369
0.06453789	0.064048649	77.617859
0.06551638	0.065027134	77.72075065
0.06649486	0.066005618	77.82382916
0.06747334	0.066984102	77.92709507
0.06845183	0.067962587	78.03054892
0.06943031	0.068941071	78.13419125
0.0704088	0.069919555	78.23802259
0.07138728	0.07089804	78.34204349
0.07236577	0.071876524	78.44625449
0.07334425	0.072855008	78.55065614
0.07432273	0.073833493	78.65524899
0.07530122	0.074811977	78.76003358
0.0762797	0.075790461	78.86501048
0.07725819	0.076768946	78.97018024
0.07823667	0.07774743	79.07554341
0.07921516	0.078725914	79.18110055
0.08019364	0.079704399	79.28685223
0.08117213	0.080682883	79.39279901
0.08215061	0.081661367	79.49894145
0.08312909	0.082639852	79.60528013
0.08410758	0.083618336	79.71181562
0.08508606	0.08459682	79.81854848
0.08606455	0.085575305	79.9254793
0.08704303	0.086553789	80.03260865
0.08802152	0.087532273	80.13993711
0.089	0.088510758	80.24746526
	sum =	5368.06597

Appendix B
Integration of Equations (5.11) from Eqaution (5.5)

The following illustrates the integration from Equation (5.5) to Equation (5.11).

$$- \int_R^{r_C} \left[\frac{R\,(R - r_C)}{r_C\, D_{eff}} + \frac{R^2}{r_C^2\, k''_s}\right] \frac{r_C^2}{R^2}\, dr_C = \int_0^t f(C_A)\, \frac{b}{\rho_B}\, dt \qquad (5.5)$$

with the boundary conditions:

$t = 0,\ r_C = R$

$t = t,\ r_C = r_C$

Rearranging the left hand side of Equation (5.5) and integrating the right hand side of Equation (5.5).

$$- \int_R^{r_C} \left[\frac{1}{D_{eff}} \left(r_C - \frac{r_C^2}{R}\right) + \frac{1}{k''_s}\right] dr_C = f(C_A)\, \frac{b}{\rho_B}\, t \qquad (B.1)$$

Now, integrating the left hand side of Equation (5.5).

$$- \frac{1}{D_{eff}}\left[\frac{1}{2}(r_C^2 - R^2) - \frac{1}{3R}(r_C^3 - R^3)\right] - \frac{1}{k''_s}(r_C - R) = f(C_A)\frac{b}{\rho_B}t \qquad (B.2)$$

Rearranging,

$$\frac{-1}{D_{eff}}\left[\frac{R^2}{2}\left(\left(\frac{r_C}{R}\right)^2 - 1\right) - \frac{R^2}{3}\left(\left(\frac{r_C}{R}\right)^3 - 1\right)\right] - \frac{R}{k''_s}\left(\frac{r_C}{R} - 1\right) = f(C_A)\frac{b}{\rho_B}t \qquad \textbf{(B.3)}$$

In the shrinking core model, the conversion of reactant B is proportional to the volumetric fraction of surface layer in a spherical particle. Hence, the conversion of reactant B and the radius of un-reacted core, r_C, are correlated as

$$X_B = 1 - \left(\frac{r_C}{B}\right)^3 \qquad \textbf{(B.4)}$$

Rearranging Equation (B.4)

$$\frac{r_C}{R} = \left(1 - X_B\right)^{\frac{1}{3}} \qquad \textbf{(B.5)}$$

Plugging Equation (B.5) into Equation (B.3) yields

$$\frac{-R^2}{6\,D_{eff}}\left\{3\left[\left(1 - X_B\right)^{\frac{2}{3}} - 1\right] - 2\left[\left(1 - X_B\right) - 1\right]\right\} - \frac{R}{k''_s}\left[\left(1 - X_B\right)^{\frac{1}{3}} - 1\right] = f(C_A)\,\frac{b}{\rho_B}t \qquad \textbf{(B.6)}$$

Rearranging Equation (B.6) gives Equation (5.6)

$$t = [1 - 3(1 - X_B)^{\frac{2}{3}} + 2(1 - X_B)]\tau_{diff} + [1 - (1 - X_B)^{\frac{1}{3}}]\tau_{rxn} \quad (5.6)$$

where

$$\tau_{diff} = \frac{R^2 \rho_B}{6\, b\, D_{eff} f(C_A)} \quad (5.7)$$

$$\tau_{rxn} = \frac{R \rho_B}{b\, k''_s f(C_A)} \quad (5.8)$$

Appendix C
Manipulation of Integration from Equations (5.29) to (5.32)

The following shows the manipulation in the integration from Equation (5.29) to Equation (5.32).

Equations (5.29) is a linear differential equation. The general solution can be expressed as

$$X_{Fe} = \frac{1}{P(t)} \int [K(C_A)\ \phi]\ P(t)\ dX_{Fe} + C\ \frac{1}{P(t)} \qquad \textbf{(C.1)}$$

where C is a constant, and

$$P(t) = e^{\int [\ K(C_A) - \frac{d(\ln\phi)}{dt}\ ]\ dt} \qquad \textbf{(C.2)}$$

The integration Equation (C.2) gives

$$P(t) = \frac{1}{\phi}\ e^{K(C_A)t} \qquad \textbf{(C.3)}$$

Hence, plugging Equation (C.3) into Equation (C.2) and integrating, the general solution of X_{Fe} becomes

$$X_{Fe} = [1 - (\ 1 - \frac{t}{\tau_{rxn,\ Cr}}\ )^3]\ (\ 1 + C\ e^{-K(C_A)t}\ ) \qquad \textbf{(C.4)}$$

The initial condition, $X_{Fe} = 0$ at $t = t_{Fe,\,i}$, is applied to Equation (C.4), and the constant C is found to be -1. Therefore, the equation for the conversion of Fe on the basis of the particle becomes

$$X_{Fe} = [1 - (1 - \frac{t}{\tau_{rxn,\,Cr}})^3] \; (1 - e^{-K(C_A)\,(t - t_{Fe,\,i})}) \qquad \textbf{(5.32)}$$

After the fraction of surface layer in a particle reaches one, Equation (5.32) is simplified and resumed to

$$X_{Fe} = 1 - e^{-K(C_A)\,(t - t_{Fe,\,i})} \qquad \textbf{(5.33)}$$

Appendix D
Calculation of Model Prediction

The following illustrates the procedure for calculating $X_{Cr,c}$ (Part A), gaseous dependency of reaction rate in Fe_4N formation (Part B), and evaluating curves (Part C) at 550 °C.

Part (A): Find $X_{Cr,c}$.

1. Determine $W_{N,Cr,f}$ from the Kjeldahl method.
2. Find $W_{N,f}$ from experimental data. This value may vary, depending on the actual alloying composition in original 316 stainless steel powder.
3. Determine $W_{N,sln,f}$ comparing the Kjeldahl and LECO methods.
4. From the data by the Kjeldahl method, find the time required to complete the formation CrN from Cr. Hence, Equation (5.19) may be determined.
5. Guess $X_{Cr,c}$ to fit experimental data obtained by the LECO method.
6. Compare the calculated curve with experimental data, and determine the induction time.

Part (B): Evaluation of $f'(C_A)$.

1. For different feed gas mixtures, $X_{Cr,c}$ may be assumed to be constant at the same temperature.
2. The procedure is similar to Part (A).
3. For step 4 of Part (A), Equation (5.37) is applied to find the time for completed conversion of Cr to CrN.
4. Guess a value of $K(C_A)$ to best-fit experimental data.
5. Compare the findings of $K(C_A)$ and average NH_3 and H_2 concentrations to find an empirical expression of $f'(C_A)$.

Part (C): Calculated curve.

1. From the findings of $X_{Cr,c}$ and $f'(C_A)$, a calculated curve can be obtained and compared with the experimental data.

FeN 20, 50% NH3 + 50% H2

W,N,sln, f =	0.5	wt%	NH3,avg=	42.2	H2,avg= 55.3
W,N, Cr, f =	4.887994442	wt%	W,N,f =	10.60742857	wt%
W,N, Fe, f =	5.219434127	wt%	W,N,Fe=W,N-X,Cr,c(W,N,Cr,f+W,N,sln,f)		
			W,N,Fe,f=W,N,f-(W,N,Cr,f+W,N,sln,f)		
		LECO TC-	KJ mehtod		x(%)

No.	Time (hr)	436 Nitrogen(wt%)	LECO Nitrogen Addition, W,N	LECO Dimensionless Nitrogen Addition	Nitrogen (wt%)	KJ Nitrogen Addition	Nitrogen from CrN
1	0	0.0757	0.075757348	0.007141915			
2	0.5	0.308	0.308951571	0.029125963			
3	1	0.597	0.600585495	0.05661933	0.432	0.433874337	0.198
4	2	1.67	1.698362656	0.160110685			
5	3.0583	2.65	2.72213662	0.256625496	0.679	0.683641929	2.243
6	4	3.68	3.820598007	0.360181356	0.957	0.966246984	2.994
7	5	5.37	5.674733171	0.534977269			
8	6	6.52	6.974753958	0.65753485	2.13	2.176356391	4.37
9	7	7.4	7.991360691	0.753373981	3.17	3.273778788	4.61
10	8	8.59	9.397221311	0.88590946	4.27	4.460461715	4.46
11	9	9.01	9.902187054	0.933514375			
12	10	9.47	10.46062079	0.986159909	4.74	4.975855553	4.74
13	10.833	10.2	11.35857461	1.070813208	5.19	5.474106107	4.83
Final	12	9.71	10.75423635	1.013840091			

See Chart 8

See chart 5 for dimensionless chart

Fe4N forming after 4 hrs

W,N,sln, i = 0 Time to complete CrN reaction 10.9 hrs

Induction Time for initial stage 0.8 hr

===> X,Cr,c= 0.647472759

SCM UCM

Nitrogen Addition (from CrN), W,N,Cr	Time (hr)	calculation SCM model (X,Cr)	W,N,Cr	W,N,sln	calculation T(t)=phi	X,Fe	W,N,Fe
	0.8	0	0	0			
0.198392818	1	0.054042033	0.264157157	0.027021017			
	1.2	0.106101099	0.518621582	0.053050549			
2.294464847	1.4	0.156214262	0.763574446	0.078107131			
3.086407026	1.6	0.204418588	0.999196923	0.102209294			
	1.8	0.250751141	1.225670186	0.125375571			
4.569695702	2	0.295248987	1.443175406	0.147624493			
4.832791697	2.2	0.337949189	1.651893756	0.168974594			
4.6682018	2.4	0.378888813	1.85200641	0.189444406			
	2.6	0.418104923	2.043694539	0.209052461			
4.975855553	2.8	0.455634584	2.227139315	0.227817292			
5.075128717	3	0.491514862	2.402521913	0.245757431			
	3.2	0.52578282	2.570023503	0.26289141			
	3.4	0.558475524	2.72982526	0.279237762			
	3.6	0.589630039	2.882108354	0.29481502			
	3.8	0.619283429	3.02705396	0.309641715			
	4	0.647472759	3.164843249	0.32373638	0.647472759	2.15652E-16	1.12558E-15
	4.2	0.674235094	3.295657394	0.337117547	0.674235094	0.054322275	0.283531534
	4.4	0.699607499	3.419677567	0.34980375	0.699607499	0.108191617	0.564699018
	4.6	0.723627038	3.537084942	0.361813519	0.723627038	0.16119173	0.841329619
	4.8	0.746330777	3.648060691	0.373165389	0.746330777	0.212985559	1.111664096
	5	0.76775578	3.752785985	0.38387789	0.76775578	0.263304286	1.374299378
	5.2	0.787939112	3.851441999	0.393969556	0.787939112	0.311937701	1.628138283
	5.4	0.806917837	3.944209904	0.403458919	0.806917837	0.358725775	1.872345554
	5.6	0.824729022	4.031270873	0.412364511	0.824729022	0.403551305	2.106309454
	5.8	0.841409729	4.112806079	0.420704865	0.841409729	0.446333499	2.329608296
	6	0.856997025	4.188996694	0.428498512	0.856997025	0.487022391	2.541981286
	6.2	0.871527974	4.26002389	0.435763987	0.871527974	0.525593988	2.7433032
	6.4	0.88503964	4.326068841	0.44251982	0.88503964	0.562046064	2.933562407
	6.6	0.897569089	4.387312719	0.448784545	0.897569089	0.596394509	3.112841854
	6.8	0.909153386	4.443936696	0.454576693	0.909153386	0.628670188	3.281302635
	7	0.919829595	4.496121946	0.459914797	0.919829595	0.658916226	3.439169839
	7.2	0.92963478	4.54404964	0.46481739	0.92963478	0.687185678	3.586720381
	7.4	0.938606008	4.587900951	0.469303004	0.938606008	0.713539533	3.724272588
	7.6	0.946780342	4.627857051	0.473390171	0.946780342	0.738045006	3.852177293
	7.8	0.954194848	4.664099114	0.477097424	0.954194848	0.760774093	3.970810265
	8	0.96088659	4.696808312	0.480443295	0.96088659	0.781802336	4.080565792
	8.2	0.966892633	4.726165817	0.483446317	0.966892633	0.801207788	4.181851274

W,N,mdl Dimensionless

W,N,mdl	
0	0
0.291178174	0.027450402
0.571672131	0.053893564
0.841681577	0.079348314
1.101406218	0.10383348
1.351045757	0.127367886
1.590799899	0.149970362
1.820868351	0.171659733
2.041450816	0.192454826
2.252747	0.212374468
2.454956607	0.231437487
2.648279344	0.249662708
2.832914913	0.26706896
3.009063022	0.283675068
3.176923374	0.29949986
3.336695674	0.314562163
3.488579628	0.328880803
3.916306475	0.369204134
4.334180335	0.408598588
4.74022808	0.446878152
5.132890176	0.483895804
5.510963253	0.519538097
5.873549838	0.553720423
6.220014376	0.586382867
6.549944838	0.617486585
6.86311924	0.647010649
7.159476493	0.6749493
7.439091077	0.701309561
7.702151068	0.726109162
7.948939118	0.749374749
8.179816025	0.771140335
8.395206582	0.791445969
8.595587411	0.810336582
8.781476543	0.827861011
8.953424515	0.844071158
9.112006803	0.859021274
9.2578174	0.872767357
9.391463408	0.885366642

8.4	0.972250042	4.752352803	0.486125021	0.972250042	0.819070147	4.275082678
8.6	0.976995882	4.775550441	0.488497941	0.976995882	0.835470025	4.360680759
8.8	0.981167217	4.795939904	0.490583609	0.981167217	0.850488352	4.43906793
9	0.984801113	4.813702365	0.492400556	0.984801113	0.864205886	4.510665693
9.2	0.987934633	4.829018996	0.493967317	0.987934633	0.876702808	4.575892557
9.4	0.990604844	4.84207097	0.495302422	0.990604844	0.88805841	4.63516237
9.6	0.992848809	4.853039459	0.496424404	0.992848809	0.898350835	4.688883005
9.8	0.994703594	4.862105636	0.497351797	0.994703594	0.90765689	4.737455347
10	0.996206263	4.869450674	0.498103131	0.996206263	0.916051898	4.781272541
10.2	0.997393881	4.875255746	0.49869694	0.997393881	0.923609597	4.820719448
10.4	0.998303513	4.879702022	0.499151756	0.998303513	0.930402065	4.856172293
10.6	0.998972224	4.882970678	0.499486112	0.998972224	0.936499692	4.887998451
10.8	0.999437078	4.885242884	0.499718539	0.999437078	0.941971151	4.916556373
10.833	0.999496757	4.885534593	0.499748378	0.999496757	0.942818429	4.920978686
11	0.999735141	4.886699813	0.499867571	0.999735141	0.946883414	4.942195607
11.2	0.999903477	4.887522638	0.499951739	0.999903477	0.951301765	4.965256899
11.4	0.999979151	4.887892532	0.499989576	0.999979151	0.955289836	4.986072373
11.6	0.999999228	4.887990668	0.499999614	0.999999228	0.95890965	5.004965752
11.8	1	4.887994442	0.5	1	0.962220929	5.022248753
12	1	4.887994442	0.5	1	0.965264741	5.038135731
12.2	1	4.887994442	0.5	1	0.968063317	5.052742715
12.4	1	4.887994442	0.5	1	0.970636416	5.066172833
12.6	1	4.887994442	0.5	1	0.973002203	5.078520903
12.8	1	4.887994442	0.5	1	0.975177381	5.089874104
13	1	4.887994442	0.5	1	0.977177309	5.100312593
13.2	1	4.887994442	0.5	1	0.979016104	5.109910065
13.4	1	4.887994442	0.5	1	0.98070675	5.118734281
13.6	1	4.887994442	0.5	1	0.982261183	5.126847541
13.8	1	4.887994442	0.5	1	0.983690377	5.134307126
14	1	4.887994442	0.5	1	0.985004423	5.141165702
14.2	1	4.887994442	0.5	1	0.986212598	5.14747169
14.4	1	4.887994442	0.5	1	0.987323432	5.153269614
14.6	1	4.887994442	0.5	1	0.988344767	5.158600405
14.8	1	4.887994442	0.5	1	0.989283814	5.163501702
15	1	4.887994442	0.5	1	0.990147204	5.168008107
15.2	1	4.887994442	0.5	1	0.990941031	5.172151437
15.4	1	4.887994442	0.5	1	0.991670901	5.175960944
15.6	1	4.887994442	0.5	1	0.992341966	5.179463524

9.513560502	0.896877169
9.624729141	0.907357431
9.725591442	0.916866079
9.816768614	0.925461675
9.89887887	0.933202501
9.972535762	0.940146398
10.03834687	0.946350645
10.09691278	0.951871862
10.14882635	0.956765938
10.19467213	0.961087984
10.23502607	0.964892293
10.27045524	0.968232326
10.3015178	0.971160704
10.30626166	0.971607925
10.32876299	0.973729205
10.35273128	0.975988781
10.37395448	0.977989568
10.39295603	0.979780912
10.4102432	0.981410634
10.42613017	0.982908356
10.44073716	0.984285408
10.45416727	0.985551513
10.46651534	0.986715609
10.47786855	0.987785916
10.48830703	0.988769989
10.49790451	0.989674777
10.50672872	0.990506668
10.51484198	0.991271533
10.52230157	0.991974775
10.52916014	0.992621357
10.53546613	0.993215845
10.54126406	0.993762436
10.54659485	0.994264989
10.55149614	0.994727051
10.55600255	0.995151886
10.56014588	0.995542493
10.56395539	0.995901628
10.56745797	0.996231829